



HAL
open science

Biomimetic approaches of cell shape changes: Impact of membrane and actin network properties

Rogério Lopes dos Santos

► **To cite this version:**

Rogério Lopes dos Santos. Biomimetic approaches of cell shape changes: Impact of membrane and actin network properties. Biophysics. Université Paris-Saclay, 2023. English. NNT : 2023UPASF044 . tel-04262170

HAL Id: tel-04262170

<https://theses.hal.science/tel-04262170>

Submitted on 27 Oct 2023

HAL is a multi-disciplinary open access archive for the deposit and dissemination of scientific research documents, whether they are published or not. The documents may come from teaching and research institutions in France or abroad, or from public or private research centers.

L'archive ouverte pluridisciplinaire **HAL**, est destinée au dépôt et à la diffusion de documents scientifiques de niveau recherche, publiés ou non, émanant des établissements d'enseignement et de recherche français ou étrangers, des laboratoires publics ou privés.

Biomimetic approaches of cell shape changes: Impact of membrane and actin network properties

Approches biomimétiques des changements de formes cellulaires : Impact des propriétés de la membrane et des réseaux d'actine

Thèse de doctorat de l'Université Paris-Saclay

École Doctorale n° 571, Sciences Chimiques : Molécules, Matériaux, Instrumentation et Biosystème (2MIB)

Spécialité de doctorat : Physique

Graduate School : Chimie

Référent : Université d'Évry Val d'Essonne

Thèse préparée à l'Unité de Recherche : **LAMBE** (Laboratoire Analyse, Modélisation, Matériaux pour la Biologie et l'Environnement), CNRS - UMR8587 sous la direction de **Clément CAMPILLO**, Maître de conférence

Thèse soutenue à Paris-Saclay, le 17 juillet 2023, par

Rogério LOPES DOS SANTOS

Composition du Jury

Membres du jury avec voix délibérative

Emmanuèle HELFER

Directrice de recherche, CINaM (Marseille)

Présidente

Aurélié BERTIN

Directrice de recherche, Institut Curie (Paris)

Rapportrice

Julien HEUVINGH

Maître de conférences - HDR, ESPCI (Paris)

Rapporteur

Christophe LE CLAINCHE

Directeur de recherche, I2BC (Paris-Saclay)

Examineur

ACKNOWLEDGEMENTS

I would like to express my heartfelt gratitude and appreciation to the following individuals who have played a significant role in the completion of my work:

First of all, many thanks to Cécile Sykes, Camille Simon, Antoine Allard, Julie Plastino, Karine Guevorkian and Clément Campillo for laying the first scientific bricks of this journey. It was an honour to be part of your team.

Izadora, Salma, Maxime, Dorian, Rose and Raphael: Thank you for your constant support and stimulating discussions about nothing and everything. Your diverse perspectives and willingness to share your knowledge have enriched me scientifically and personally.

For Michel, Olek, Guillaume, and Sid, thank you for your insightful comments on my presentations and results during our weekly meetings and for your helpfulness with any technical obstacle I encountered. It was an honour and a pleasure to be part of your team.

Clément, I am deeply grateful for your guidance, mentorship, and unwavering support. Your encouragement and belief in my abilities have been invaluable. I am fortunate to have had such an exceptional mentor who consistently challenged me to achieve my best. I genuinely wish you all the best.

I sincerely thank the esteemed jury members who dedicated their valuable time, expertise, and critical evaluation of my project.

To my dear best friend, Ailine, thank you for being here. Thank you for having welcomed me into your home. I could not have a better starting point for this journey than that. I know I can always count on you. As simple as that.

I am forever grateful to my mother for her unconditional love, unwavering support, and belief in my dreams. Your encouragement, patience, and sacrifices have been the bedrock of my success. Your unwavering faith in me has been my driving force, and I am deeply grateful for everything you have done for me.

Lastly, I want to express my deepest gratitude to my wife for her unwavering support, understanding, and love. Your belief in me, your sacrifices, and your unwavering encouragement with a good dose of truthfulness have been my greatest strength. I know you wish me well, and you have been my rock throughout this journey, and I am forever grateful for your presence in my life. I have the best partner in crime. Um kreb txeu.

CONTENTS

1	Introduction.....	2
2	State of the art: studying cell shape changes using biomimetic systems.....	4
2.1	Biological membranes	4
2.1.1	Structure of biological membranes	4
2.1.2	Membrane physics	9
2.1.3	Biomimetic membrane systems	14
2.2	Actin cytoskeleton	18
2.2.1	Actin structure.....	20
2.2.2	Actin dynamics.....	21
2.2.3	Actin Binding Proteins	23
2.3	Reconstituted membrane-actin systems.....	27
2.3.1	Review 1: Studying actin-induced cell shape changes using Unilamellar Vesicles and reconstituted actin networks.	28
2.3.2	Review 2: Remodelling of membrane tubules by the actin cytoskeleton	41
3	Materials and methods	57
3.1	Buffers ..	57
3.2	Biomimetic membrane systems.....	57
3.2.1	Giant Unilamellar Vesicles preparation	58
3.2.2	Supported membrane nanotubes.....	59
3.3	Reconstituted actin networks	61
3.4	Microscopy techniques	63
3.4.1	Epifluorescence microscopy	63
3.4.2	Stimulated Emission Depletion Microscopy (STED)	63
3.4.3	Atomic Force Microscopy (AFM)	64
3.5	Microfluidic devices	65
4	Results	66
4.1	Phase-separated lipid nanotubes.....	66
4.1.1	Preparation of phase-separated membrane nanotubes.....	66
4.1.2	Probing mechanical properties of phase-separated membrane nanotubes ..	69
4.2	Actin-induced shape changes on GUVs	74
4.2.1	Remodelling of homogeneous GUVs by actin network polymerisation.....	74
4.2.2	Controlling actin network polymerisation on phase-separated GUVs.....	89
4.3	Tracking actin-induced shape changes on GUVs	116
5	Conclusion and perspectives.....	119
6	References.....	123

1 INTRODUCTION

Cells are constantly readapting their shape to achieve biological processes such as migration, intracellular trafficking and division. Such processes require the active remodelling of cell membranes which is fuelled by the dynamics of the actin cytoskeleton (Blanchoin et al. 2014).

Assessing the mechanisms of membrane remodelling by the actin cytoskeleton in the complex environment of the cell interior is very challenging. Indeed, many different types of proteins are implied in these processes. Therefore, reconstituted biomimetic systems are useful as they have the advantage of a biochemically controlled environment. They allow controlling and tuning the biophysical properties of both membranes and reconstituted actin networks. This *in vitro* approach is based on the bottom-up design of biomimetic systems of increasing complexity to understand the role of each element of the biological machinery and their interplay on cell shape changes.

In this work, my objective is to build biomimetic systems comprising phase-separated lipid membranes and actin networks. Indeed, the cell membrane is highly heterogeneous, and these heterogeneities interact with the actin cytoskeleton (Fritzsche et al. 2017). However, the membranes used in biomimetic studies are, in most cases, homogeneous. Only (Liu and Fletcher 2006) used heterogeneous Giant Unilamellar Vesicles that contain lipid domains. They show that the actin network affects lipid domain formation and organisation on GUVs. This result suggested that cells control membrane organisation by readapting their actin cytoskeleton. Nevertheless, the effect of membrane heterogeneities on membrane remodelling by actin remains unclear.

This manuscript is organized as follows. In section 2, I introduce the context of my work: I briefly describe the properties of biological membranes and of the actin cytoskeleton, as observed in biological situations and in reconstituted biomimetic systems. I show how

reconstituted lipid membranes such as Giant Unilamellar Vesicles (GUVs), supported lipid bilayers (SLBs) or membrane nanotubes allied with techniques such as micropipette aspiration (Rawicz et al. 2000), optical tweezers (A. Allard, Valentino, et al. 2020) and Atomic Force Microscopy (AFM) (Lamour et al. 2020) gives access to the physical properties of reconstituted membranes. Moreover, I show the effects of reconstituted actin networks on these membrane models, allowing mimicking some of the shape changes observed *in vivo*. In particular, I participated in two reviews articles summarising the scientific literature on reconstituted GUVs interacting with actin networks (Lopes dos Santos and Campillo 2022) and membrane nanotubes remodelling by actin *in vivo* and *in vitro* (Antoine Allard, Lopes dos Santos, and Campillo 2021).

Section 3 presents all the materials and methods used for this work: namely the preparation of reconstituted membrane systems coupled with actin networks and the observation techniques that I used, such as STED, AFM, and fluorescence microscopy.

Finally, in section 4, I present and discuss my results. First, I studied the mechanics and morphology of phase-separated nanotubes with the AFM. Then, I investigated on GUVs how membrane composition and actin network structure affect membrane remodelling by actin. Furthermore, I developed a system based on GUVs with lipid domains that allows spatial control of the site of actin polymerization, allowing a new degree of control over these biomimetic systems.

2 STATE OF THE ART: STUDYING CELL SHAPE CHANGES USING BIOMIMETIC SYSTEMS

In this section, we will present the elements that control cellular shape changes and, therefore, the main ingredients that we will use in our experiments: membranes and actin

First, we must describe what a cell is. Living organisms are divided into three groups: Bacteria, archaea, and eukaryotes, and all share a common basic unit, the cell. Eukaryotic living organisms are composed of cells with a nucleus and organelles surrounded by selective membranes, which we will describe in detail below. The deoxyribonucleic acid (DNA) molecule inside the nucleus carries all the genetic information indispensable to sustain life. Besides compartmentalising essential elements for cell life, the membranes also participate in many biological functions.

Many of the receptors that trigger cell shape changes and allow cells to probe their external environment are embedded in biological membranes. Depending on the signalling pathway activated (Biyasheva et al. 2004), many biological responses such as endocytosis, exocytosis, lamellipodia or filopodia imply various types of membrane remodelling. Moreover, the actin cytoskeleton plays an essential role in membrane remodelling by applying the forces needed to deform the membrane. It translates into local deformations such as filopodia to probe the environment and endocytosis to uptake external components, or global deformations resulting for instance in cell division. Cell membranes and the actin cytoskeleton are thus major actors of cell life, and I will give more details about both in the following sections.

2.1 BIOLOGICAL MEMBRANES

2.1.1 Structure of biological membranes

Biological membranes are composed of many different types of lipids

(van Meer, Voelker, and Feigenson 2008) that self-assemble in a bilayer and comprise many embedded proteins. Lipids and proteins diffuse in the two-dimensional plane of the membrane. This structure constitutes the so-called "fluid mosaic" model (Singer and Nicolson 1972). Besides, the membranes can be described as thin elastic sheets under tension regarding bending and stretching deformations. We will present these aspects in the following sections.

Composition

Biological membranes are formed of lipids, which form barriers between the internal and external regions isolating intracellular compartments from the cytosol or the whole cell from external medium. However, membranes are semi-permeable to water and small uncharged molecules. Larger molecules and ions rely on membrane pores or channels that passively or actively regulate the passage (Delcour 2009).

Lipids composing membranes are amphiphilic, meaning they have a hydrophilic head and one or more hydrophobic hydrocarbon tails. The most abundant lipids in cell membranes are phospholipids such as phosphatidylcholine (PC), phosphatidylethanolamine (PE) and sphingomyelin (SM). These lipids differ from one another by their polar head composition, as depicted in **Figure 1**. The PC has two hydrocarbon tails linked to a glycerol-phosphate-choline group that forms the polar head. Like PC, the SM has a phosphocholine group and a serine replacing the glycerol present in PC to form the polar head. PE differs from SM by the ethanolamine replacing the choline on its polar head.

The hydrophobic tail also affects the properties of the lipid. Double bonds between carbons in one or both chains of the lipid or unsaturations affect their properties. Saturated tails have no double bonds and, as a result, have straight, unkinked tails. Unsaturated tails have double bonds and, as a result, have kinked tails, as depicted in **Figure 1**. These differences in structure affect the mechanical properties of the membrane, such as the fluidity and lateral organisation of the membrane (Baumgart, Hess, and Webb 2003; Rawicz et al. 2000). Furthermore, the length of the lipid tail also affects

the mechanical properties of the membrane. A thicker membrane is stiffer (Rawicz et al. 2000).

In addition to phospholipids, most cell membranes contain cholesterol, a sterol (van Meer, Voelker, and Feigenson 2008). Smaller in size compared to phospholipids, the cholesterol has a single tail. Its size allows it to insert between phospholipids, and by interacting with them, it can change membrane properties such as phospholipids organisation, membrane fluidity and bending rigidity (Hao, Mukherjee, and Maxfield 2001; Kwik et al. 2003; Silvius 2003; Titushkin and Cho 2006).

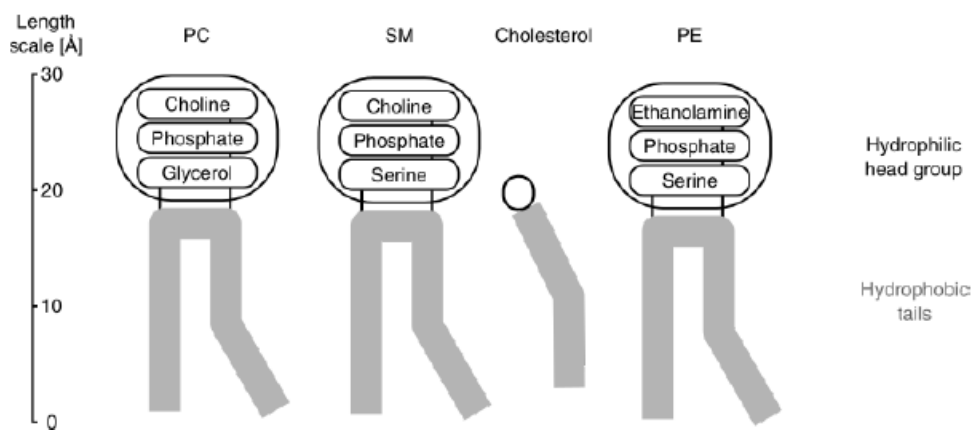


Figure 1: Structure of bilayer components. Three phospholipids: phosphatidylcholine (PC); sphingomyelin (SM) and phosphatidylethanolamine (PE); and cholesterol. All present a hydrophilic polar head and a hydrophobic tail. Adapted from (Alberts et al. 2008).

Lipids self-assembly

In an aqueous environment and due to the energetically unfavourable interaction between the hydrophobic tail and water, phospholipids will “hide” their hydrophobic tail by forming self-assembled structures. Moreover, the lipid geometry dictates the type of structure formed (Israelachvili 2011). In the case of conical lipids, a round structure called

micelle forms, where the hydrophilic head faces the aqueous solution, and the hydrophobic tail is towards the interior. Phospholipids being cylindrical or truncated cones, they spontaneously form bilayers. Due to the energetically unfavourable state, the bilayer closes on itself and tends to form a sealed compartment (**Figure 2**).

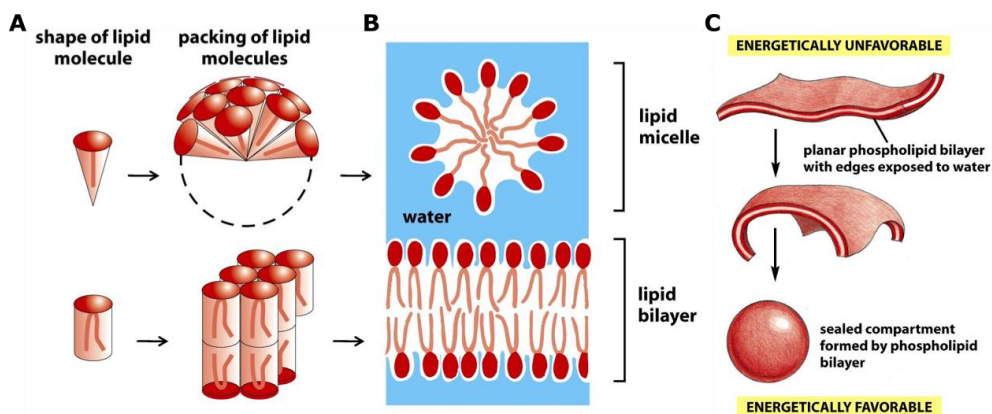


Figure 2: Self-assembly of lipids. Lipid shape (A) defines the structure: micelle or lipid bilayer (B). The latter self-arranges into a vesicle (Alberts et al. 2008)

Membrane fluidity

Lipid bilayers are considered a two-dimensional fluid with the following features:

- Rotational diffusion: Lipids rotate on themselves. The associated diffusion coefficient, D_{rot} is 10^9 rad²/s (Moore, Lopez, and Klein 2001);
- Flipping diffusion: lipids can flip from one monolayer to the other in a timescale of a few hours (McConnell and Kornberg 1971);
- Lateral diffusion: Lipids diffuse laterally within a monolayer, D_{lat} is 1 to 10 $\mu\text{m}^2/\text{s}$ (Filippov, Orädd, and Lindblom 2003).

The diffusion of a lipid depends on the bilayer composition. For instance, D_{lat} decreases upon adding cholesterol (Filippov, Orädd, and

Lindblom 2003). Because of its size, cholesterol inserts into the bilayer and interacts with phospholipids impairing their mobility.

Furthermore, SM possesses longer hydrophobic tails than phosphatidylcholine, and SM membranes are more rigid than PC membranes (Hac-Wydro and Wydro 2007; Niemelä, Hyvönen, and Vattulainen 2004; Tristram-Nagle, Petrache, and Nagle 1998). The SM tend to be more saturated than PC lipids. These effects also favour their segregation from other lipids and, thus, the formation of lipid domains (described in section 2.1.1).

Membrane domains

The early works that led to the idea of the fluid mosaic model mainly implied homogeneous membranes (Singer and Nicolson 1972). (Brown and Rose 1992) showed that detergent-resistant membranes (DRM) were enriched in sphingolipids and cholesterol, implying that cell membranes were heterogeneous. More recent works (Edidin 2003; Nicolson 2014) highlighted the lipid bilayer's heterogeneity and, in particular, the existence of lipid domains called "rafts" (Nicolson and Ferreira de Mattos 2021). Altogether, these works showed that segregated membrane regions driven by preferential interaction between certain lipid classes coexist along the membrane. These domains have functional roles (Kai Simons and Ikonen 1997; K. Simons and Toomre 2000), such as intracellular trafficking (Surma et al. 2011; Kulkarni, Wiemer, and Chang 2022) or by sorting proteins required for the activation of signalling pathways (Rothberg et al. 1990; Shelby et al. 2021).

Moreover, the experiments realised by (Baumgart, Hammond, et al. 2007) showed that giant plasma membrane vesicles (GPMV) formed large lipid domains. GPMVs are isolated after treatment of the cell membrane. They maintain the majority of lipids and membrane proteins when compared to DRM. GPMVs composition is extremely close to cell membranes but lack cytoskeleton. This membrane model is great for observations of a natural membrane, but its composition is not controlled as in a synthetic membrane. Note that the large-scale domains observed in GPMVs are absent in cell membranes, probably

because of the interplay between the membrane and the cytoskeleton.

Synthetic membranes are biochemically controlled. They are prepared from purified lipids and can comprise lipid mixtures exhibiting lipid domains (Ahmed, Brown, and London 1997; Silvius, del Giudice, and Lafleur 1996). Therefore, they are also used to study membrane domains (see section 2.1.3).

2.1.2 Membrane physics

Membrane elasticity

To describe the elasticity of membranes, particularly their stretching and bending properties, membranes are modelled as thin sheets of elastic material. Note that pure lipid membranes have no elastic resistance to shearing (**Figure 3**) because of their fluid nature.

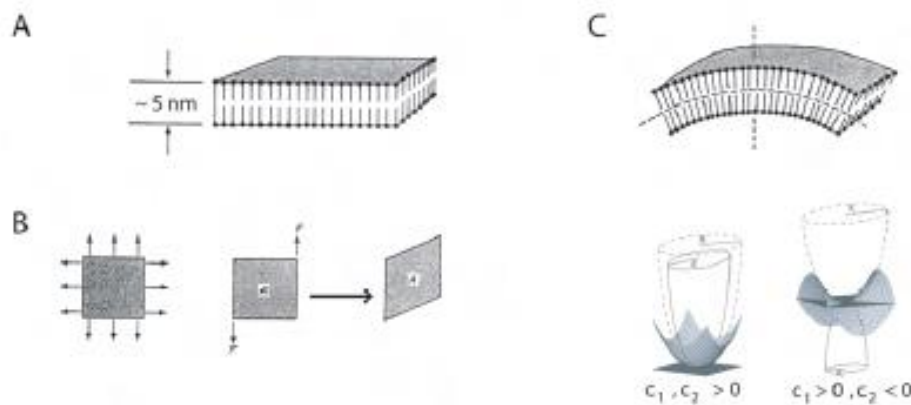


Figure 3: Types of membrane deformation: from flat membrane where no forces are applied (A) to in-plane deformations (B), left: area expansion (stretching), right: shear. Out-of-plane deformations: bending. Lower panel: any out-of-plane deformation is defined by its principal curvatures (C_1 and C_2) that give the mean curvature C . Adapted from (Canham 1970; Girard 2004).

Stretching energy is linked to the relative change in the area of the membrane $\frac{\Delta A}{A}$:

$$E_{stretching} = \chi \frac{\Delta A}{A} \quad (1)$$

Where χ is the stretching modulus, on the order of 0.1 N/m (Helfrich 1973; E. Evans and Rawicz 1990), ΔA is the area variation, and A is the total area of the membrane.

The energy associated with the bending of the membrane writes:

$$E_{bending} = \frac{1}{2} \kappa (C - C_0)^2 \quad (2)$$

Where κ is the membrane bending rigidity, ranging from 10 to 50 $k_B T$ (Bochicchio and Monticelli 2016), depending on the lipid composition of the membrane. Lipid tail unsaturation levels, length (Rawicz et al. 2000) and interactions with other lipid tails (Chakraborty et al. 2020) affect membrane bending rigidity. The mean curvature of the membrane C is defined by the sum $1/R_1 + 1/R_2$, where R_1 and R_2 are the principal radii of curvature of the membrane. The spontaneous curvature C_0 accounts for a curved membrane at rest, if the membrane is flat at rest, $C_0 = 0$. Spontaneous curvature can happen when proteins such as proteins of the Bin/Amphiphysin/Rvs (BAR) superfamily (Gallop et al. 2006; Mesarec et al. 2021; Peter et al. 2004) bind to the membrane.

$$\kappa = K_a h^2 / c_e \quad (3)$$

Finally, another critical parameter to describe membrane mechanics is the mechanical tension in the membrane plane. This parameter is not easy to define; therefore, we will illustrate it through a classical experiment. (E. Evans and Rawicz 1990; Rawicz et al. 2000), among others, used the micropipette aspiration technique on Giant Unilamellar Vesicles, cell-sized spheres of lipid membrane (see section 2.1.3), to probe the response of lipid membrane to an increase in tension. In this micropipette experiment, membrane tension σ can be calculated by applying the Laplace law knowing the pressure difference ΔP between the micropipette interior and exterior and the

vesicle radius R and the pipette radius r (Drury and Dembo 1999):

$$\sigma = \frac{r}{2(1-\frac{r}{R})} \Delta P \quad (4)$$

Two regimes are observed when the GUV membrane is submitted to increasing mechanical tension. A high membrane tension regime, where the relation between tension and area is linear and depends on the stretching modulus χ (**Figure 4 A**). After a few percent of stretching deformation, the membrane ruptures, and the corresponding lysis tension is on the order of 10^{-3} N/m (Evan Evans et al. 2003; Nichol and Hutter 1996). In a low membrane tension regime, the thermal membrane fluctuations are smoothed by increasing membrane tension, and tension and membrane area increase has a logarithmic relation (**Figure 4 B**).

The area increase of the membrane $\Delta A/A$ can be calculated by measuring the geometrical parameters of the vesicle, R , r , and the length of the vesicle aspirated in the micropipette. The contributions of membrane fluctuations, dominated by the bending rigidity, and membrane stretching on the membrane area increase are linked by the so-called Helfrich relation:

$$\alpha = \frac{\Delta A}{A} = \frac{k_B T}{8\pi k} \ln \frac{\pi k^2}{\sigma a^2} + \frac{\sigma}{K_a} \quad (5)$$

This equation shows the logarithmic term accounting for membrane fluctuations and the linear term accounting for membrane stretching. In most situations, particularly in the experiments that we will present in this manuscript, we work in the regime where membrane fluctuations dominate, and we do not consider stretching effects.

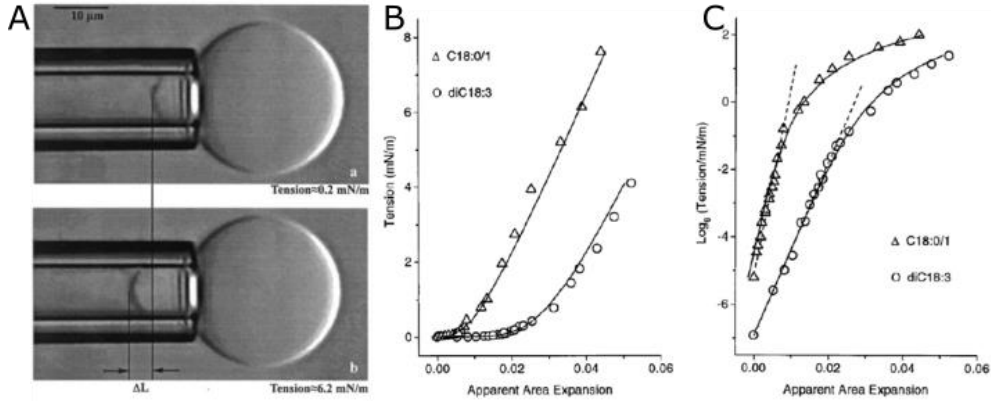


Figure 4: Micropipette aspiration of GUVs illustrating their bending and stretching properties. A: Micrograph of the experiments showing an increase of L for an increased tension. B: Membrane tension versus apparent area expansion, the linear part of the curve corresponds to the elastic regime. C: Semilog plot of tension versus apparent area expansion for the same data as in (A). Linear fits (dashed lines) applied to the range of very low tensions yield the elastic bending moduli, k . Adapted from (Rawicz et al. 2000).

Physics of membrane nanotubes

Inside living cells, many cylindrical structures made of lipid membranes, here called membrane nanotubes, are observed (section 2.3.2). Here, we will briefly present the physics of their formation. These membrane nanotubes form when a lipid membrane is submitted to a point force; *in vivo*, this force can be exerted by various processes summed up on **Figure 5 A**. **Figure 5 B** shows the effect of a point force f exerted on a membrane, here a GUV. Upon increase of the force, the GUV becomes ellipsoidal and when the force is increased up to a critical force f_0 , a membrane nanotube forms and coexists with a quasi-spherical vesicle (Rossier et al. 2003). The free energy of the tube can be written as :

$$F_{tube} = \frac{\pi\kappa}{r}L + 2\pi rL\sigma_m - fL \quad (6)$$

Where L is the tube length, σ_m is the membrane tension, and κ is the bending rigidity of the lipid membrane. The first term accounts for the

bending energy, the second one for the effect of membrane tension and the third one corresponds to the work of the external force. From equation 6, we can obtain the force to maintain the nanotube:

$$f_0 = 2\pi\sqrt{2\sigma_m\kappa} \quad (7)$$

and the equilibrium radius of the nanotube (Hochmuth et al. 1982; Waugh 1982) :

$$r = \sqrt{\frac{\kappa}{2\sigma_m}} \quad (8)$$

The pulling force and the tube radius are therefore linked by :

$$f = \frac{2\pi\kappa}{r} \quad (9)$$

Meaning that for the same radius, the pulling force only depends on the bending rigidity κ and thus the lipid composition. For instance, with typical values of membrane tension ranging from 0.01 to 0.3 mN/m (Gauthier, Masters, and Sheetz 2012; Lieber et al. 2013), the membrane nanotube radius is in the order of tens of nm, and the pulling force is in the order of tens of pN.(9)

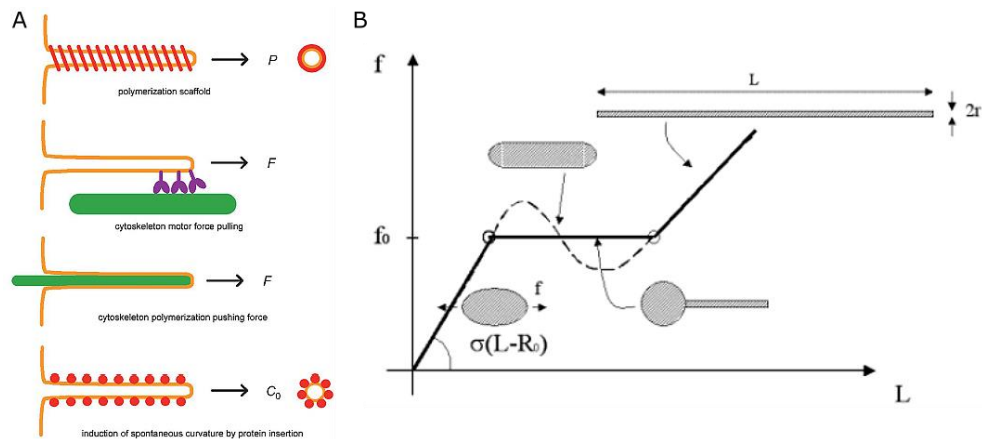


Figure 5: Schematic representation of membrane nanotube formation: A: Various modes of formation *in vivo* (Roux 2013). B: plot of force F versus elongation L of a liposome. At small forces, the liposome has an ellipsoidal shape, and the force is proportional to $L - R_{liposome}$, where $R_{liposome}$ is the initial radius of the liposome. Under strong forces, the shape becomes a "cigar" of length L and radius R . At intermediate force $F = F_0$, we have coexistence between a quasi-spherical liposome and a tether (Rossier et al. 2003).

2.1.3 Biomimetic membrane systems

Artificial membranes are ideal for biochemical and biophysical studies for a few reasons. The biochemically controlled conditions allow the reconstitution of biologically relevant processes in a minimal system with controlled composition. Moreover, mechanical parameters such as bending rigidity and tension can also be tuned. With a bottom-up approach, experiments gain in complexity by adding more building blocks, such as cytoskeleton proteins (presented in 2.2.3), which gives more complexity to biomimetic systems and, thus, mimic more accurately the cellular situation.

In this section, different biomimetic systems that reconstitute biological membranes are presented.

Supported lipid bilayers (SLB)

SLBs are obtained by adhesion and rupture of small vesicles onto a substrate, for example, glass. Lipids D_{lat} and D_{rot} are similar to those of free lipid bilayers due to a thin layer of water (1-2 nm) between the glass and the lipid bilayer. Once attached to a surface, it allows using techniques such as atomic force microscopy (AFM) (Mingeot-Leclercq et al. 2008; Picas, Rico, and Scheuring 2012). Nevertheless, as the membrane of SLBs is attached to a substrate, it gives a strong limitation to this system to study membrane shape changes. It could lead to using another membrane model, liposomes.

Liposomes

As mentioned, a free lipid bilayer closes on itself, forming a vesicle or liposome with various sizes:

- Small unilamellar vesicles (SUV \sim 15-30 nm): prepared by sonication of lipid bilayers films;
- Large unilamellar vesicles (LUV \sim 100-200 nm): extrusion on MLV;
- Giant unilamellar vesicles (GUV \sim 1-100 μ m): prepared by electroformation (Angelova and Dimitrov 1988) inverted emulsion (Pautot, Frisken, and Weitz 2003) or gel swelling (Hoger et al. 2009).

The first two, SUVs and LUVs, are below the diffraction limit of visible light (around 200 nm). Thus, GUVs and GPMVs are suitable for observations by optical microscopy of membrane behaviour. Plus, their size is cell-like, allowing comparisons with cell membrane behaviour and mimicking physical properties of biological membranes such as fluidity and tension. Therefore, GUVs are ideal for biophysical experiments with either the membrane alone or a reconstituted protein at its surface. Membrane thermal fluctuation or membrane deformation induced by proteins are assessed through such systems. For instance, (Helfer et al. 2000) showed that bending rigidity increases when GUVs are surrounded by F-actin, which decreases membrane thermal fluctuations. (Giardini, Fletcher, and Theriot 2003) highlighted

the effect of the actin network stresses capable of propelling GUVs and pulling a membrane nanotube. (Liu et al. 2008a) demonstrate the impact of membrane elasticity on actin networks organisation. These articles will be presented in detail below. (Avalos-Padilla, Georgiev, and Dimova 2021) pointed out the effect of the clustering of ESCRT-III on membrane deformation. (Jahnke et al. 2022) illustrated how the motor activity of myosin can pull membrane nanotubes of tens of micrometres long from GUVs.

Membrane nanotubes

Here, we review the techniques for forming and assessing nanotubes' mechanical properties. The first class of techniques mainly forms a single nanotube with a controlled force. (Borghi, Rossier, and Brochard-Wyart 2003) used glass micro-rods to attach GUVs and form nanotubes by applying a hydrodynamic flow dragging the GUV from the micro-rod. (A. Allard, Valentino, et al. 2020; Cuvelier et al. 2005; V. Heinrich and Waugh 1996; Roy et al. 2020) used optically or magnetically trapped beads to apply a point force on a GUV and form nanotubes as depicted in **Figure 6** A and B. In most cases, the GUV is held by a micropipette which can be used to set the membrane tension. The other class of techniques allows the formation of many nanotubes without measuring the tube force. Nanotubes can be formed by using the force generated by kinesin sliding on microtubules, as shown in **Figure 6** C and D (Imam and Bachand 2019; Koster et al. 2003; Roux et al. 2002) or by the motor activity of myosin (Jahnke et al. 2022). More recently, without using GUVs (Dar, Kamerkar, and Pucadyil 2017; Lamour et al. 2020) pulled membrane nanotubes by applying a hydrodynamic flow to lipids dried on surfaces, as demonstrated in **Figure 6** E. The interest of these techniques is to yield a very high number of nanotubes. Moreover, these nanotubes are attached to the surface, allowing the assessment by AFM of their properties (see section 4.1).

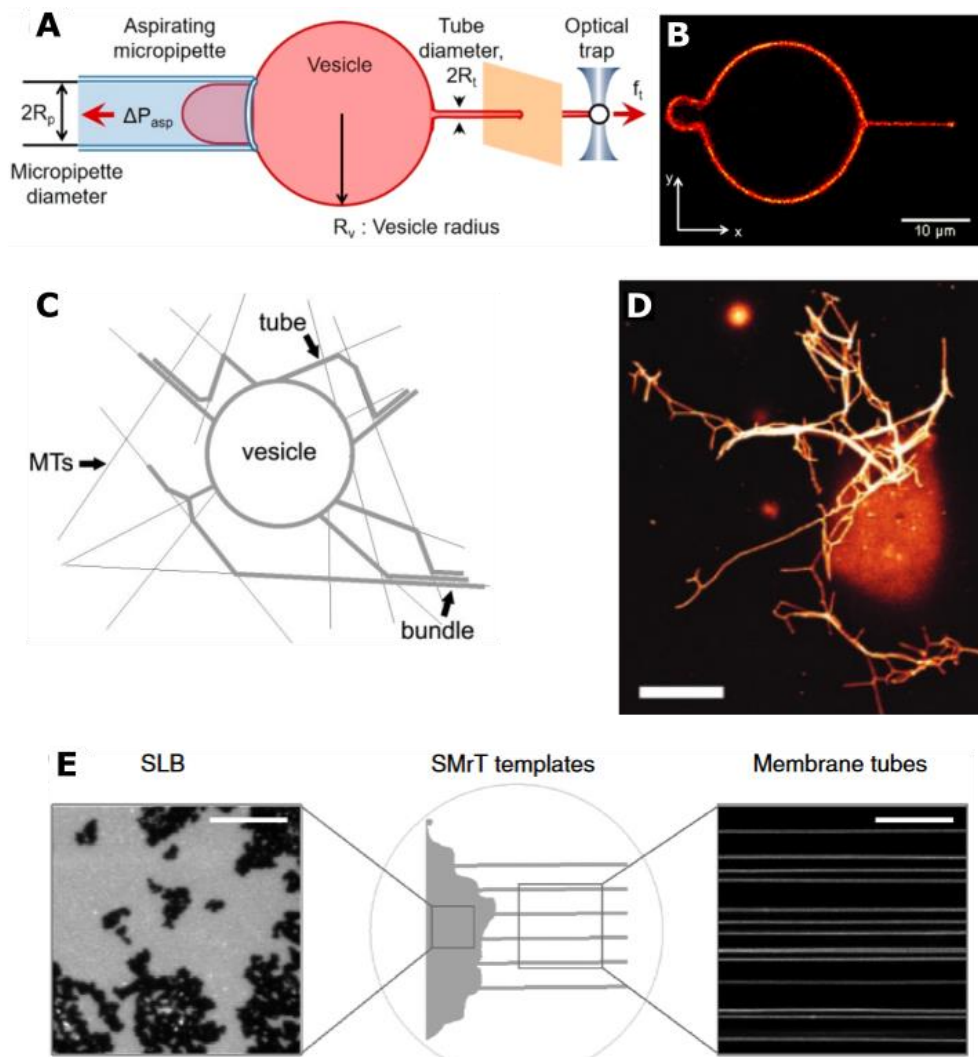


Figure 6: Membrane nanotubes pulling techniques. A: Representation of optical trap experiment. B: Membrane nanotube extrusion as seen in confocal fluorescence imaging (Roy et al. 2020). Representation of tubes pulled from GUV on a surface covered by microtubules (MTs). D: Fluorescence confocal microscopy of EPC tubes pulled from a GUV (Roux et al. 2002). E: schematic of Supported membrane tubes (SMrT) templates showing the supported lipid bilayer (SLB) at source and membrane tubes. Scale bars, 10 μm (Dar, Kamerkar, and Pucadyil 2017).

2.2 ACTIN CYTOSKELETON

The cell shape is maintained by its cytoskeleton and remodelled when needed, as previously mentioned in section 2.1.1. This cytoskeleton comprises three families of filaments: microtubules, intermediate filaments, and actin filaments. All three ensure dynamic and mechanical rearrangements of the cell to execute cellular functions. Nevertheless, actin has been shown to play a crucial role in cell shape changes; therefore, only actin cytoskeleton properties are presented in this section. Depicted in **Figure 7 A** are the different actin structures and the deformation of the plasma membrane that they induce. Note that **Figure 7 B** is the overlay of **A** showing the mechanical profiles of these different actin structures, which gives us an insight into how these structures impact the membrane.

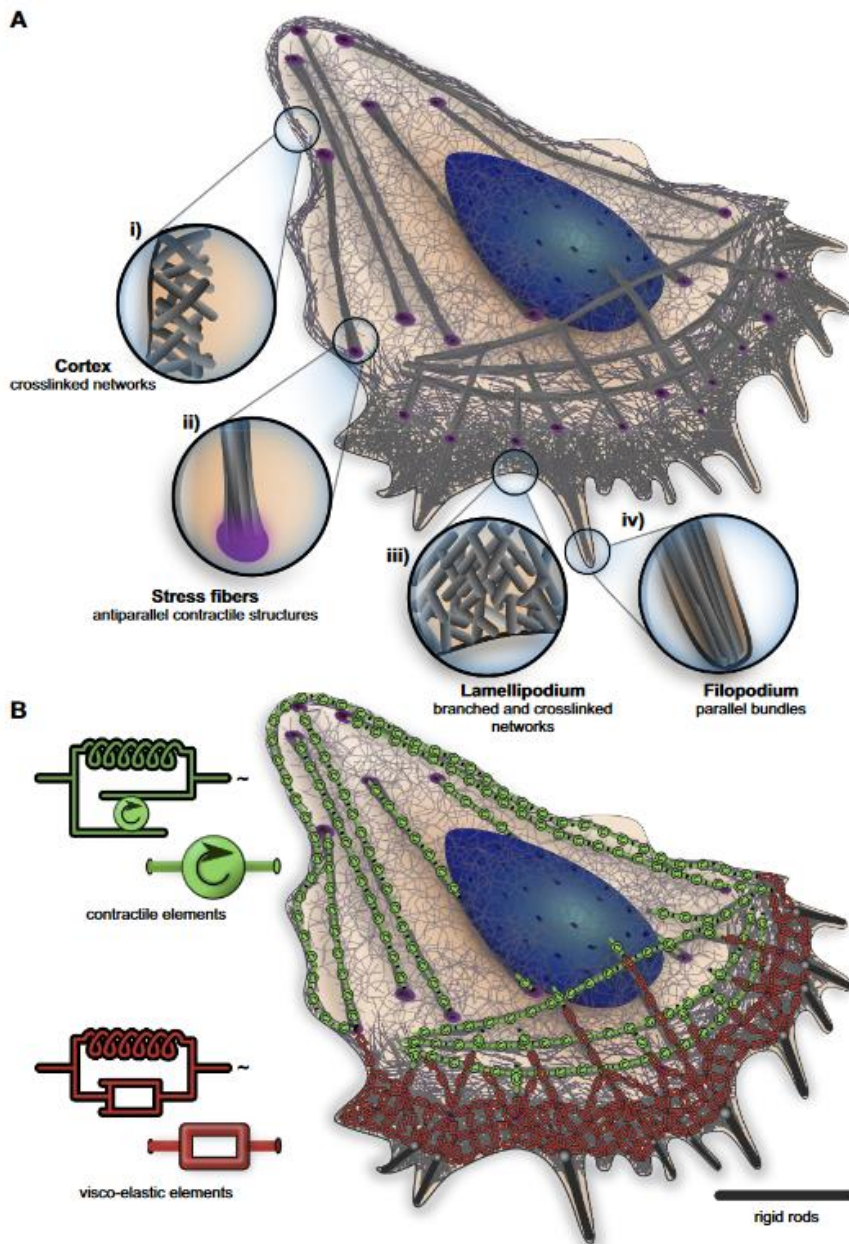


Figure 7: A: schematic representation of the cell with the different architectures indicated: i) the cell cortex; ii) an example of a contractile fibre, the stress fibre; iii) the lamellipodium; and iv) filopodia. The zoom regions highlight the architectural specificities of different regions of the cell. B: overlay of the actin architecture and its mechanical profile. The red rectangles are visco-elastic elements (dashpots) representing the actin network, while the green circles are active springs corresponding to myosin motor activity (Blanchoin et al. 2014).

2.2.1 Actin structure

Actin filaments or F-actin are formed by actin subunits called actin monomers or G-actin (**Figure 8**). The latter is a globular polypeptide chain of 42 kDa and about 57 Å, that can bind to one ATP (adenosine triphosphate) or ADP (adenosine diphosphate) and a divalent cation, magnesium (Mg^{2+}) or calcium (Ca^{2+}), two cofactors essential for actin polymerisation (W Kabsch, Mannherz, and Suck 1985; Wolfgang Kabsch et al. 1990).

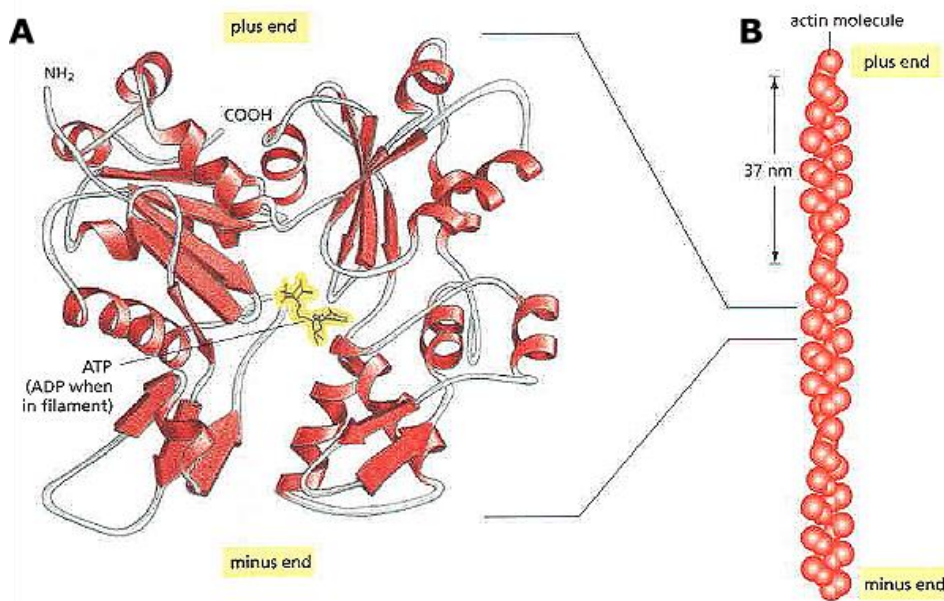


Figure 8: Representation of G-actin and F-actin. (A) G-actin with its central ATP/ADP binding cleft and two binding sites (plus or barbed end and minus or pointed end) for another G-actin. (B) Polarised F-actin is structured as a double-stranded helix presenting a complete twist every 37 nm (Alberts et al. 2008).

2.2.2 Actin dynamics

In the presence of the two cofactors mentioned above and at physiological salt conditions, polymerisation can occur, and its dynamic is composed of several successive steps. First, G-actin monomers spontaneously bind to one another to form a dimer in a polarised way, with the barbed ends pointing in the same direction. However, the link between the two G-actin is weak, and the dimer easily dissociates (Zigmond 1998). This step is called the lag phase before entering the polymerisation phase.

Nucleation

The binding of a third actin monomer stabilises the trimer structure, forming a nucleus that facilitates the binding of other monomers. The nucleation marks the beginning of F-actin elongation.

Elongation

During this phase, new monomers bind, and the oligomers elongate. Monomers assemble and disassemble at the two ends of the filament at different rates. The rate of assembly and disassembly of monomers at each end of the filament to the filament is known as K_{on} and K_{off} , respectively. The K_{on} is inversely proportional to the concentration of free monomers, C , and the K_{off} is constant, with $K_{on}C = K_{off}$. Consequently, during filament growth, the available monomers are incorporated in filaments, and C decreases. This leads to a steady state that corresponds to a critical concentration (C_c) can be calculated :

$$C_c = \frac{K_{off}}{K_{on}} \quad (10)$$

For actin polymerisation to occur, C must be higher than C_c (**Figure 9**). Moreover, due to the differences between K_{on} on the barbed and pointed ends, the C_c is different on each end of the filament. The barbed end C_c is 0.12 μM , and the pointed end C_c is 0.6 μM (Thomas D. Pollard 2016). Therefore, when above C_c , polymerisation prevails over depolymerisation, and the barbed end is the fast-growing end compared to the slower pointed end (T D Pollard 1986). The elongation speed is also controlled by ATP, cations or other proteins (see section

2.2.3).

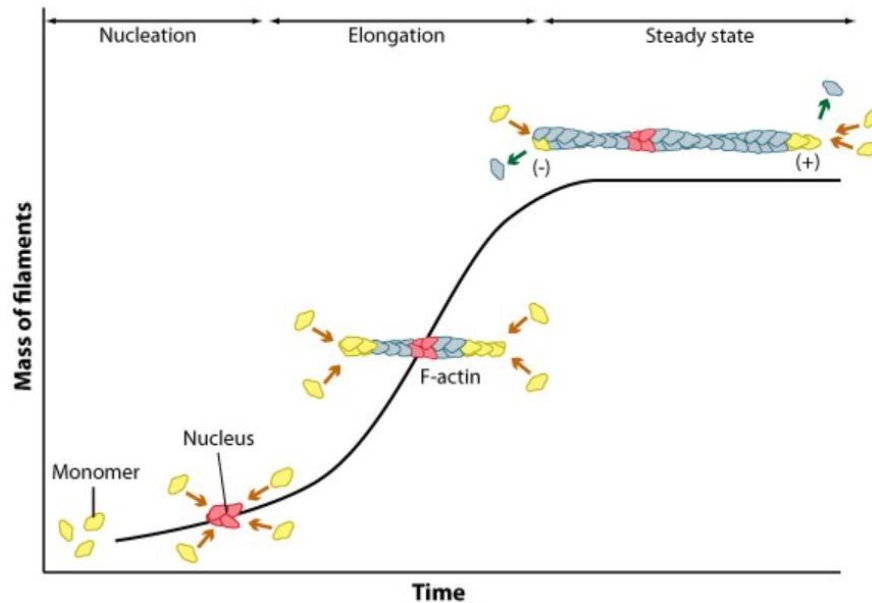


Figure 9: The actin polymerisation sequence from monomers to filaments. All three actin polymerisation phases (nucleation, elongation, and steady-state phase of actin filament assembly) are represented in the histogram showing filament size as a function of polymerisation time (adapted from www.mechanobio.info).

Steady-state

At C_c a plateau phase is reached. The balance between the assembly and disassembly of the filament keeps its length constant. The hydrolysis of ATP into ADP is essential for this phase. G-actin linked to ATP incorporates at the barbed end of the filament. Then, ATP is hydrolysed to become ADP, and the ADP-actin disassembles when it reaches the pointed end of the filament (Fujiwara et al. 2002). Moreover, the difference of the C_c at the two ends of the filament results in the assembly of ATP-actin at the barbed end and disassembly of ADP-actin at the pointed end due to the hydrolysis of ATP that changes the conformation of actin subunit and destabilises actin

interactions (Carlier 1990; Carlier, Pantaloni, and Korn 1986). The two processes occur at an identical rate, creating what is called the “treadmilling of actin” (Wegner 1976).

F-actin has a persistence length (l_p) of 15 μm (Isambert et al. 1995; McCullough et al. 2008), meaning that below l_p , F-actin behaves as a rigid rod, whereas F-actin is flexible at a larger scale.

2.2.3 Actin Binding Proteins

Regulation of F-actin dynamics relies on multiple proteins called actin-binding proteins (ABPs). These ABPs regulate the dynamics of G-actin or F-actin and the structure of actin networks of network structure. These effects are summarised in (**Figure 10**), and we will present in more detail some of the ABPs I use in my experiments.

G-actin regulation

In vivo, G-actin concentration is around 150 - 200 μM for eukaryotic cells (Funk et al. 2019; Thomas D. Pollard, Blanchoin, and Mullins 2000), much larger than the critical concentration for actin polymerisation. However, the cell must maintain a pool of available monomers to form new actin structures dynamically. Proteins regulating G-actin assembly are essential to regulate F-actin formation (**Figure 10**). For instance, the action of proteins, such as profilin, keeps actin in monomeric form.

Profilin is a 14 kDa protein that binds monomeric actin. It complexes with G-actin by its barbed end, leaving the ATP/ADP binding site free (Thomas D. Pollard, Blanchoin, and Mullins 2000). Sterically hindering assembly at the minus end consequently lowers the nucleation probability. Moreover, profilin-actin is favourably bounded to the barbed end of filaments, where profilin rapidly dissociates (Courtemanche and Pollard 2013; Goldschmidt-Clermont et al. 1991), freeing the barbed for the addition of another monomer. (Funk et al. 2019) showed a linear relation between filament elongation speed and actin-profilin concentration when it is below its physiological concentration of 20 μM . A higher concentration leads to the saturation of the elongation speed.

As detailed above, profilin modulates the dynamics of F-actin growth by directly regulating G-actin properties. Regulation at the level of F-actin is also possible by other ABPs.

F-actin regulation

Capping protein (CP) is a heterodimer of 64 kDa that strongly binds ($K_{on}=0.1 - 1$ nM) to the barbed end of the filament. The half-life time of CP dissociation is 30 minutes (Edwards et al. 2014; Schafer, Jennings, and Cooper 1996), which hinders further filament elongation due to the high affinity to actin. Moreover, by controlling F-actin length, it also controls actin network structure. It was shown that shorter filaments create denser actin networks that produce forces to push the membrane (Iwasa and Mullins 2007; Kawska et al. 2012).

High-order actin network

The nucleation of filaments relies on some proteins, such as the Arp2/3 complex or formins, resulting in different actin structures. Arp2/3 forms branched networks, while formins form parallel bundles of F-actin (**Figure 10**).

The Arp2/3 complex, or actin-related protein complex, is a 54 kDa protein composed of seven subunits and has structural similarities with actin (Machesky et al. 1994). For instance, it can bind and act as a cap for the pointed end of F-actin (Mullins, Heuser, and Pollard 1998), but it can laterally bind to F-actin, nucleate a new filament and form an angle of 70° with the first filament (Machesky et al. 1999; Mullins, Heuser, and Pollard 1998; Rouiller et al. 2008). Consequently, Arp2/3 forms a branched actin network. However, Arp2/3 is constitutively inactivated. It requires the action of a nucleating-promoting factor (NPF) or activator. Several proteins can activate Arp2/3. Some of these proteins belong to the Wiskott-Aldrich syndrome protein family (WASp), are localised at the membrane, and share a common C-terminal domain (Espinoza-Sanchez et al. 2018; Rotty, Wu, and Bear 2013) called Verprolin homology-central-acidic region (VCA). The V region binds actin monomers, the acidic or A motif binds and activates Arp2/3, and the central cofilin homology or C region enhances the interactions between V/actin and A/Arp2/3 (Ti et al. 2011). Moreover, the N-terminal of the VCA domain contains a proline-rich domain

(PRD) that binds profilin-actin, rendering it available for the barbed end of the filament (Bieling et al. 2018). This work used a constitutively active VCA, detailed in section 3.3.

Other proteins can rearrange the actin cytoskeleton without inducing actin nucleation. Different actin structures can be achieved by the insertion of proteins that bind filaments together in what can be called a cross-linking effect (**Figure 10**).

Crosslinkers

Fascin is a 58 kDa monomeric protein with two actin-binding domains (ABD) at its C-terminal end (Tseng et al. 2001). Its compact form and ABDs allow the bundling of F-actin in parallel. Indeed, the actin bundle formed by fascin are 8 nm apart. Compared to individual F-actin, the actin bundle reaches the stiffness required to push and form membrane structures such as filopodia (Mogilner and Rubinstein 2005; Vignjevic et al. 2006).

Alpha-actinin (or α -actinin) is a 200 kDa anti-parallel homodimer belonging to the spectrin superfamily (Djinović-Carugo et al. 1999; Maruyama and Ebashi 1965). The monomers of actinin have an ABD arranged in an anti-parallel manner. It was shown that the ABD can display variable orientations (Winkler, Lünsdorf, and Jockusch 1997) and thus arrange bonded F-actin in variable orientations and angles (Hampton, Taylor, and Taylor 2007; Meyer and Aebi 1990). Depending on the ABD configuration, bundles and or networks form in the presence of α -actinin.

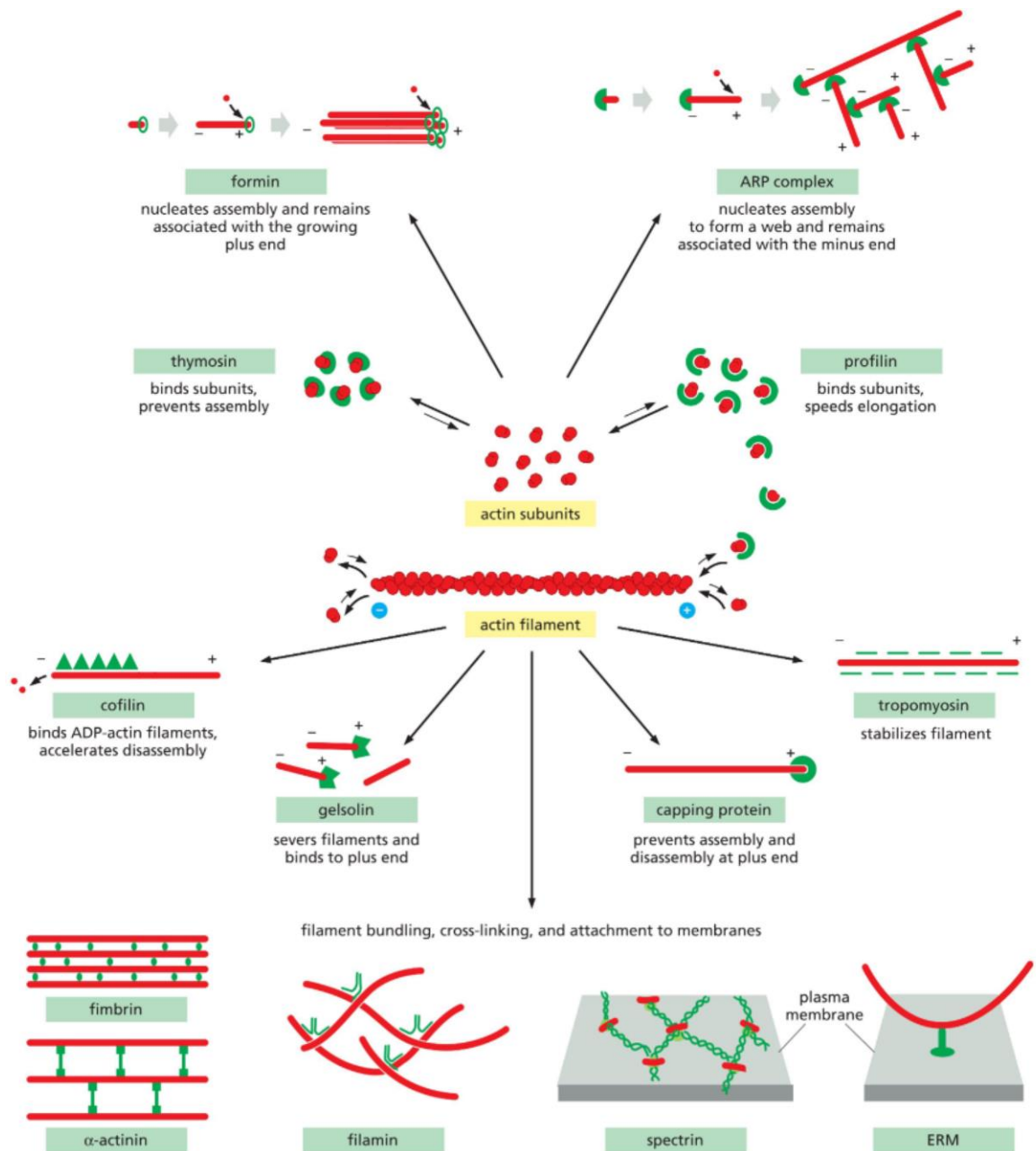


Figure 10: Overview of actin-binding proteins and their functions. Schematic illustration of nucleation, elongation, capping, severing, branching and cross-linking of F-actin (Alberts et al. 2008).

2.3 RECONSTITUTED MEMBRANE-ACTIN SYSTEMS

Membranes and actin on their own represent an entire research field. For example, membrane composition and lipid structures can determine its mechanical properties (Filippov, Orädd, and Lindblom 2003; Häckl, Seifert, and Sackmann 1997; Rawicz et al. 2000). And experiments performed with beads in cellular extracts with a minimal set of purified proteins allowed to identify the proteins needed for actin-induced motility and the forces applied by the actin network (Bernheim-Groswasser et al. 2002; Loisel et al. 1999; Noireaux et al. 2000; van der Gucht et al. 2005).

Below, I present two review articles that I authored, summarising the context of my work. First, I summarise existing works on actin polymerisation on GUVs.

The first review focus on the actin-induced deformations of the membrane rather than the actin-induced motility. Nevertheless, mentioning a few studies on the propulsion of the GUVs by an actin "comet" is important. Indeed, biomimetic systems allow for mimicking the propulsion of pathogens or endosomes inside the cell. Such systems highlighted, for example, the role of Arp2/3 concentrations (Delatour, Helfer, et al. 2008), NPFs mobility (Delatour, Shekhar, et al. 2008) and the detailed forces applied by the actin comet to the GUV (Giardini, Fletcher, and Theriot 2003; Upadhyaya et al. 2003). Our first review presents articles focusing on the actin-membrane interaction and the actin-induced shape changes on GUVs. We sought to highlight how different actin networks result in different membrane deformations.

2.3.1 Review 1: Studying actin-induced cell shape changes using Unilamellar Vesicles and reconstituted actin networks.



Biochemical Society Transactions (2022) 50 1527–1539
<https://doi.org/10.1042/BST20220900>



Review Article

Studying actin-induced cell shape changes using Giant Unilamellar Vesicles and reconstituted actin networks

Rogério Lopes dos Santos¹ and Clément Campillo^{1,2}

¹LAMBE, Université d'Evry Val d'Essonne, CNRS, CEA, Université Paris-Saclay, 91025 Evry-Courcouronnes, France; ²Institut Universitaire de France (IUF), Paris, France

Correspondence: Clément Campillo (clement.campillo@univ-evry.fr)



Cell shape changes that are fuelled by the dynamics of the actomyosin cytoskeleton control cellular processes such as motility and division. However, the mechanisms of interplay between cell membranes and actomyosin are complicated to decipher in the complex environment of the cytoplasm. Using biomimetic systems offers an alternative approach to studying cell shape changes in assays with controlled biochemical composition. Biomimetic systems allow quantitative experiments that can help to build physical models describing the processes of cell shape changes. This article reviews works in which actin networks are reconstructed inside or outside cell-sized Giant Unilamellar Vesicles (GUVs), which are models of cell membranes. We show how various actin networks affect the shape and mechanics of GUVs and how some cell shape changes can be reproduced *in vitro* using these minimal systems.

Introduction

Many biological processes rely on changes in cellular shape. Global changes, for example, in the case of motility and division, and local changes for exo/endocytosis and filopodia formation. The actin cytoskeleton plays a crucial role in such shape changes [1]. It generates polymerization-induced forces deforming the lipid bilayers surrounding the cell and most of its internal compartments by dynamically switching globular 42 kDa actin monomers (G-actin) to polymerized filaments (F-actin). In the cell, many Actin Binding Proteins (ABPs) control actin assemblies dynamics and structure in at least six manners:

- I. By influencing the ability of G-actin to form filaments, such as profilin [2];
- II. By severing actin filaments or preventing their elongation, such as capping proteins (CP);
- III. By nucleating filaments, such as the Actin related protein or Arp2/3 complex [3] and formins. Arp2/3 is a protein complex that, when activated, can nucleate a new filament on the side of a pre-existing filament and thus generate branched networks. Arp2/3 is rich in the lamellipodium of migrating cells, and the polymerization of Arp2/3-nucleated networks generates forces that push the cell membrane forward. Formins nucleate the elongation of bundles of parallel actin filaments [4];
- IV. By regulating the nucleation of filaments by activating the nucleators, for example, WASP (for Wiskott–Aldrich syndrome protein), that regulate F-actin nucleation by activating the Arp2/3 complex [5]. These types of proteins are known as Nucleation Promoting Factors (NPF);
- V. By building higher-order actin-based structures. Such structures are achieved through both cross-linking filaments such as α -actinin [6] and fascin [7] and linking filaments with membranes as proteins of the ezrin-radixin-moesin family [8];

Received: 8 June 2022
Revised: 12 August 2022
Accepted: 22 August 2022

Version of Record published:
16 September 2022

VI. By exerting forces on F-actin. Proteins of the myosin family exert these forces by walking along F-actin using the energy of ATP hydrolysis [9]. Myosin II forms minifilaments that create tension in actin networks by pulling on F-actin.

Within the cell, the diversity of these ABPs leads to the formation and cohabitation of several types of actin-based structures, such as the cortex, stress fibers, or filopodia [1], that reorganize both spatially and temporally in response to internal and external stimuli. Studying these actin-based structures can be problematic in the complex environment of the cell interior, which contains hundreds of proteins potentially interacting with actin. However, a bottom-up strategy based on biomimetic systems can decipher how actin-based structures such as the cortex or filopodia appear, the minimal set of components required for their formation, and their mechanical effects on cell shape. Model systems made of lipid membranes and actin networks reconstituted from purified proteins are helpful to answer these questions since they allow the *in vitro* reconstitution of cellular actin-based structures [10]. Therefore, it is possible to study the physical mechanisms of the formation and maintenance of these structures.

Among membrane models that study the effect of actin dynamics on lipid membranes, Giant Unilamellar Vesicles (GUVs), also called liposomes, are of practical interest as these spheres made of a nanometer-thick bilayer are the size of living cells and can be easily imaged by optical microscopy. Actin can be coupled either to the inside or outside leaflet of the GUVs membrane. In these two configurations, GUV membranes appear flat at the scale of actin networks mesh size, roughly tens of nanometers [11]. Note that the confinement of actin structures can affect membrane shape. Another critical difference is that the inside configuration imposes a finite amount of proteins, contrary to the outside configuration, where this supply is enormous. In this mini-review, we present how actin affects GUVs. In particular, we highlight how these biomimetic systems reproduce *in vitro* some steps of cellular shape changes, thus allowing for the deciphering of their physical mechanisms. We also show how these experiments pave the way for the design of synthetic soft nanomachines inspired by living cells.

We present results by ascending order of complexity in the actin machinery. In most cases, this also corresponds to chronological order. In section I, we present experiments with actin filaments polymerized without nucleators. Then, the same type of filaments in the presence of crosslinkers (section II) and myosin II (section III). Finally, we present examples where nucleators trigger actin polymerization specifically at the GUVs membrane. In each section, we distinguish between assays based on the 'inside' or 'outside' configuration, which can be associated with different preparation techniques (Table 1).

Actin filaments formed without NPFs

The most straightforward assays correspond to actin filaments polymerized without NPFs that are artificially coupled to the outer leaflet or encapsulated in the lumen of GUVs.

Helfer et al. have studied GUVs surrounded by a layer of F-actin connected to their membrane by biotin-streptavidin links (Figure 1A). Optical tweezer microrheology shows that this layer strengthens the GUV membrane. It reduces its transverse thermal fluctuations by increasing its bending rigidity, i.e. the energy to pay to change the curvature of the membrane, from $10 k_B T$ for a lipid membrane to $100\text{--}1000 k_B T$ when the same membrane is coated with actin filaments [12]. Studying in-plane fluctuations of beads attached to the GUV membrane, the authors show that, in the presence of actin filaments, these composite membranes also have a viscoelastic behavior with a 2D shear modulus on the order of 10^{-6} N/m [13]. In contrast, due to their fluidity, there is no elastic resistance to shearing in actin-free lipid membranes. Therefore, these studies show that the actin layer strengthens the GUV membrane by increasing its bending and shearing rigidities.

To encapsulate F-actin, GUVs are formed by electroformation (EF) [14] in a solution containing G-actin (Figure 1B). Then, polymerization is triggered inside the GUVs by Mg^{2+} influx through ionophores inserted in their membrane [15]. Thanks to steric hindrance, PEGylated lipids and cholesterol limit the adsorption of F-actin to the lipid bilayer. In these experiments, F-actin spatial distribution is correlated to the GUV size: in GUVs smaller than $18 \mu\text{m}$, F-actin forms a cortex close to the GUVs membrane, whereas in larger GUVs, actin appears as a 'fuzzy' homogeneous network. Such differences in actin organization are due to a competition between the GUV size and the persistence length (l_p) of F-actin, which is ~ 10 to $17 \mu\text{m}$ [16,17]. These results were among the first to establish that in a GUV larger than l_p , filaments can distribute anywhere,

Table 1 Table summarizing the experimental details of all articles presented in the five sections of the text: inside or outside geometry, GUVs preparation techniques, lipid composition of the GUVs membrane, composition of the actin and actin-related proteins mixture, interaction of the actin structures with the GUVs membranes and effects of the actin on the membrane

Part 1 of 3

	Article	In vs. Out	GUVs Preparation	Lipid composition	Protein mixture	Membrane attachment	Sollicitation/ Deformation
F-actin without NPFs	Helfer et al. [12] Helfer et al. [13]	Out	EF	DOPC PE-Biotin 5%	F-actin (15% biotinylated) with streptavidin	Biotin-streptavidin	Microrheology: actin increases the membrane bending rigidity and adds a viscoelastic response
	Limozin and Sackmann [19]	In	EF	DMPC DMPE-PEG 2.5% Cholesterol 17%	F-actin 2–10 μM α -actinin 0.1–1 μM filamin 100–300 nM	Non-specific	Effect of confinement on F-actin morphology
	Limozin et al. [15]	In	EF	DMPC DMPE-PEG 0–5% Cholesterol 0–37%	F-actin	Non-specific	Effect of confinement on F-actin morphology
F-actin + crosslinkers	Tsai et al. [24]	In	Agarose gel swelling	DOPC PEG-PE 2.5–5% PE-Biotin 0–2.5%	F-actin 12 μM fascin 0.6–2.4 μM	Non-specific	Actin protrusions
	Litschel et al. [25]	In	cDICE	POPC PE-Biotin 1%	G-actin 2–6 μM fascin 66–300 nM	Non-specific	Ring-like formation of bundled actin
	Bashirzadeh et al. [20,26]	In	Modified cDICE	DOPC 70% Cholesterol 30%	G-actin 5 μM fascin 0.5–2.5 μM α -actinin 0.5–1.5 μM	Non-specific	Crosslinked F-actin organization in confined space
F-actin without NPFs + myosin II	Tsai et al. [29]	In	Agarose gel swelling	DOPC 93.8% PEG-DOPE 5% PE-Biotin 1%	G-actin 24–95 μM Myosin 0.12–1.9 μM	Biotin-streptavidin	Actin cortex detachment from membrane
	Takiguchi et al. [28]	In	IE	EPC	F-actin 50–200 μM myosin II 3.8–15 μM	Non-specific	Crosslinking of F-actin by myosins
NPFs at membrane	Liu and Fletcher [35]	Out	EF	DPPC 17.2% DOPC 52.2% Cholesterol 30% Bodipy-TMR-PIP2 0.6%	actin 6 μM N-WASP 390 nM Arp2/3 150 nM	PIP2/N-WASP	Effect of actin on membrane phase transition
	Liu et al. [38]	Out	EF	EPC 75% DOPS 20% PIP2 5%	actin 8.5 μM N-WASP 400 nM Arp2/3 160 nM	PIP2/N-WASP	Filopodia-like protrusions emerging from dendritic networks
	Simon et al. [40,41] Kusters et al. [42] Allard et al. [43]	Out	EF	EPC PE-Biotin 0.1% DGS-Ni 5%	actin 3 μM spVCA 350 nM profilin 3 μM Arp2/3 37 nM CP 0–25 nM	biotin-spVCA	Inward and outward protrusions emerging from dendritic networks; Wrinkled or buckled deformations; Tubule stabilization by actin

Continued

Downloaded from <http://portlandpress.com/biochemtrans/article-pdf/50/5/1527/939000/bst-2022-0900c.pdf> by guest on 24 November 2022

Table 1 Table summarizing the experimental details of all articles presented in the five sections of the text: inside or outside geometry, GUVs preparation techniques, lipid composition of the GUVs membrane, composition of the actin and actin-related proteins mixture, interaction of the actin structures with the GUVs membranes and effects of the actin on the membrane

Part 2 of 3

Article	In vs. Out	GUVs Preparation	Lipid composition	Protein mixture	Membrane attachment	Sollicitation/ Deformation	
Pontani et al. [46]	In	IE	EPC 58% DGS-Ni 5% Cholesterol 37%	G-actin 6.5 mM Arp2/3 0.12 mM Gelsolin 50 nM ADF-cofilin 2 mM Profilin 1 mM VCA-His 0.64 mM	Histidin-nickel	Mimic of the actin cortex	
Wubshet et al. [47]	In	Modified cDICE	DOPC 70% cholesterol 25% DGS-Ni 5%	Actin 5.3 μ M Arp2/3 1 μ M His-VCA 0.5 μ M fascin 10–50%	Histidin-nickel	Protrusion only in the presence of fascin reveals competition with Arp2/3 for G-actin	
Murrell et al. [48]	In	IE	EPC 53% Cholesterol 37% DGS-Ni 10%	G-actin 13 mM Arp2/3 0.24 mM gelsolin 0.1 mM ADF-cofilin 4 mM VCA-His 2.2 mM	Histidin-nickel	Viscous dissipation slows down GUV spreading on adhesive substrates	
Campillo et al. [50] Guevorkian et al. [52]	in	IE/EF	EPC 58–52% DGS-Ni 5–10% Cholesterol 37% PE-Biotin 0.1–1%	Actin 3–13 mM Arp2/3 0.24–0.45 mM VCA-His 2.2–7.8 mM Gelsolin 0–0.1 mM ADF-cofilin 0–4 mM profilin 0–10 mM	Histidin-nickel	Friction induced by membrane nanotube extrusion and lipid diffusion hindered by actin cortex	
Myosin II + branched networks	Carvalho et al. [55]	Out	EF	EPC PE-Biotin 0.1%	Actin 1–3 μ M S-pVCA 100–160 nM profilin 3 μ M Arp2/3 50 nM CP 10–50 nM	biotin-SpVCA	Peeling of actin cortex or GUV squeezing
	Caorsi et al. [57]	out	EF	EPC PE-Biotin 0.1–1%	actin 3 μ M SpVCA 350 nM profilin 3 μ M Arp2/3 35 nM CP 20 nM 50 nM Myosin II	biotin-SpVCA	Myosin motors increase actin cortex tension

Continued

Downloaded from http://portlandpress.com/biochemtrans/article-pdf/50/5/1527/399000/bst-2022-0900c.pdf by guest on 24 November 2022

Table 1 Table summarizing the experimental details of all articles presented in the five sections of the text: inside or outside geometry, GUVs preparation techniques, lipid composition of the GUVs membrane, composition of the actin and actin-related proteins mixture, interaction of the actin structures with the GUVs membranes and effects of the actin on the membrane

Part 3 of 3

Article	In vs. Out	GUVs Preparation	Lipid composition	Protein mixture	Membrane attachment	Sollicitation/ Deformation
Loiseau et al. [59]	In	cDICE	EPC DGS-Ni 0.1–10% PE-Biotin 2.5%	actin 10 μ M His-anilin 0.1–1 μ M Myosin II 0.5–1 μ M	Histidin-nickel	Formation of blebs
Dürre et al. [61]	In	cDICE	EPC DGS-Ni 0.1–10% PE-Biotin 2.5%	actin 3 μ M His-VCA 300 nM Arp2/3 300 nM Profilin 13.5 μ M CP 20–180 nM Myosin II 5 μ M	Histidin-nickel	CP-induced membrane bulging in/out and fission under Myosin II activity
Bashirzadeh et al. [30]	In	Modified cDICE	DOPC 70% Cholesterol 25% DGS-Ni 5%	actin 5 μ M His-VCA 1 μ M Arp 2/3 1 μ M Myosin II 63 nM Fascin 1 μ M α -actinin 0.5 μ M	Histidin-nickel	Blebs formed by branched contractile actomyosin ring

whereas, in a smaller GUV, they stay at the periphery to minimize their bending energy [15]. A detailed study of the mechanism by which confinement affects the structure and mechanics of actin filaments was done in droplets instead of GUVs by Claessens et al. [18].

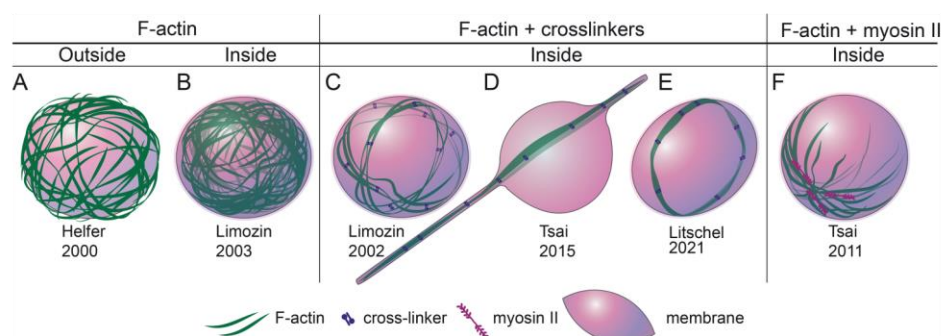


Figure 1. Schematics of biomimetic systems made of GUVs coupled to actin filaments formed without NPFs.

GUVs coupled to F-actin in the outside (A) and inside (B) configurations; GUVs encapsulating F-actin in the presence of crosslinkers (C) α -actinin; (D,E) fascin that induces bundles or rings in the lumen of the GUV (F) GUVs encapsulating F-actin in the presence of myosin II motors.

Actin filaments formed without NPFs in the presence of crosslinkers

In this section, we show how actin filaments polymerized without NPFs in the presence of crosslinkers modulate the structure of the actin network and, in some cases, the GUV shape (Figure 1C–E). To the best of our knowledge, no articles study filaments polymerized without NPFs and crosslinkers on the external membrane of GUVs; we thus discuss papers where filaments and crosslinkers are co-encapsulated. As in the case of section I, the competition between the elasticity of the membrane and that of actin-based structures controls actin organization inside GUVs. In the presence of crosslinkers, the elasticity of actin-based structures varies due to structural differences between crosslinkers, actin to crosslinker ratio (rCA), and the length of the filaments, resulting in a wide variety of actin structures.

When F-actin crosslinked by α -actinin is encapsulated in GUVs (Figure 2C), two different organizations appear depending on the GUV size. At temperatures below 15°C, at which polymerization dynamics are slowed down and bundling formation favored, ring-like structures form in GUVs smaller than 12 μm , whereas spiderweb-like structures form in larger GUVs [19]. In addition, F-actin asters form at the periphery of GUVs larger than 16 μm at the same rCA of 1 : 10, and increasing the rCA does not affect actin organization [20]. However, bundles emerging from the asters are preferentially located at the GUV periphery to minimize bending energy. In the last article, GUVs were formed using an adapted version of the cDICE (continuous droplet interface crossing encapsulation) method [21,22].

In the presence of fascin (Figure 2D), F-actin forms bundles that are able to generate enough force to deform the membrane [23,24]. In GUVs smaller than 8 μm , stiff bundles (rCA = 0.2) form membrane protrusions, whereas soft bundles (rCA = 0.05) have lower bending energy and form ring or web-like organizations [24]. Confinement forces bundles to bend and accumulate at membranes if they are sufficiently long [25] (Figure 2E) or if membrane bending rigidity is high [24]. Moreover, increasing fascin concentration favors bundle to bundle attraction, increasing their overall persistence length and leading to membrane protrusions [26].

Lastly, simultaneous encapsulation of α -actinin and fascin still reveals an effect of the confinement over actin organization as previously described, as well as the competition between fascin and α -actinin for a finite amount of actin filaments, which results in α -actinin significantly impairing the protruding effect of fascin in these conditions [20,26].

Actin filaments formed without NPFs in the presence of myosins II

In this section, we discuss works that observe the effects of co-encapsulating F-actin formed without NPFs together with myosins II. Similar actomyosin networks in the outside configuration have never been reported.

Using the Inverted Emulsion (IE) method [27], Takiguchi et al. encapsulated F-actin and heavy-meromyosin (a fragment of myosin II) in GUVs [28]. The GUVs were of several tens of micrometers, much larger than l_p . F-actin was homogeneously distributed when encapsulated alone, and GUVs were always spherical. However, when heavy-meromyosin and F-actin were encapsulated, the resulting GUVs had non-spherical shapes. The author determined that when actin filaments are crosslinked by heavy-meromyosin, the resulting actin bundles are stiff enough to deform the lipid bilayer.

Other studies have encapsulated F-actin and bipolar myosin II filaments (Figure 2D), able to actively pull on the actin filaments [29]. The F-actin contained biotinylated actin monomers that can attach to the GUV membrane through biotin-streptavidin bonds. The GUVs were formed spontaneously during the hydration in the solution containing the proteins of a hybrid film of agarose and lipids. No external force such as an electric field or centrifugation was applied to form the GUVs. No membrane deformation was observed even if actin was attached via biotin-streptavidin bonds. Still, actin clusters were observed at high myosin II concentration, supposedly because myosin-induced forces ruptured actin-membrane links and condensation of actin filaments in one or few clusters.

To form contractile actomyosin rings, Bashirzadeh et al. [30] encapsulated actin filaments and myosin II in the presence of crosslinkers. They show that the probability of ring formation is higher when the fascin to α -actinin ratio is high and GUV size is smaller than 15 μm . Such conditions seem to impair the formation of protrusions induced by fascin and the formation of asters by α -actinin, as previously shown [20].

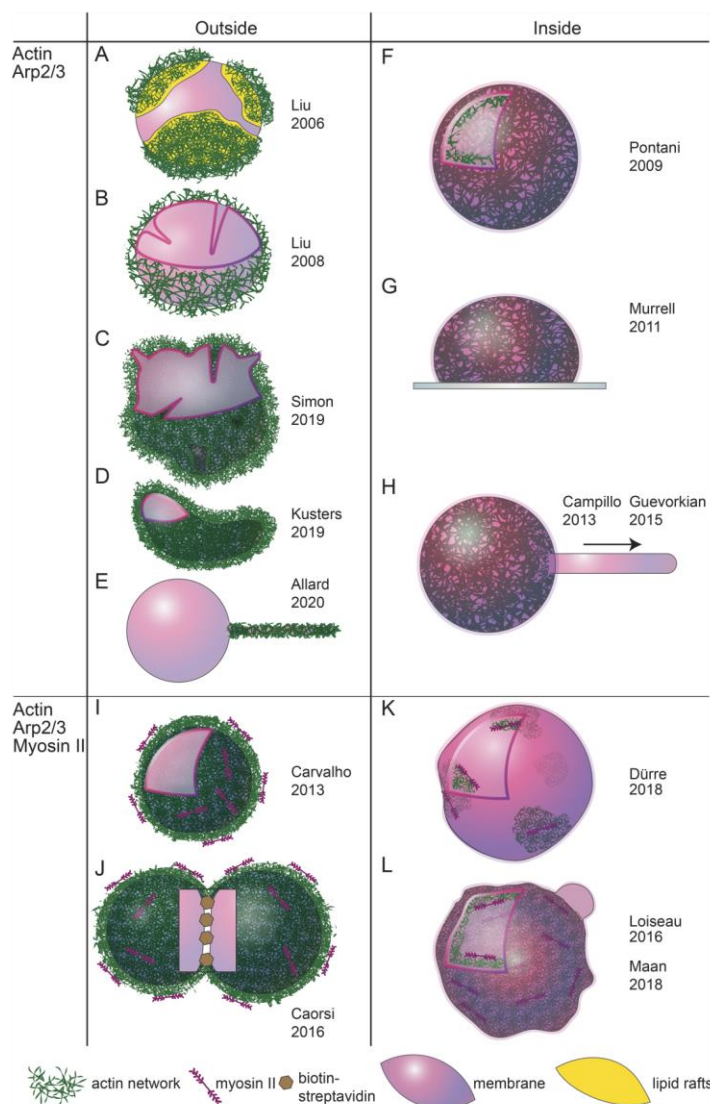


Figure 2. Schematics of biomimetic systems made of GUVs coupled to dynamic F-actin networks nucleated by the Arp2/3 complex.

In the outside configuration: reconstitution of actin-rich membrane domains (A), filopodia-like protrusions (B), filopodia-like protrusions and endocytic pits-like structures (C), global GUV deformation (D), and actin-coated nanotubes (E); In the inside configuration: reconstitution of Arp2/3-generated networks allows forming a cortex-like structure (F); studies on the effect of the cortex on GUV spreading (G) and on membrane dynamics by nanotube pulling experiments (H). Actomyosin networks coupled to the GUV surface (I) or GUVs doublets (J) show myosin-induced shape changes; Encapsulation of Arp2/3 generated actin networks comprising myosin II motors which then induce membrane protrusions (K,L).

Downloaded from <http://portlandpress.com/biochemsoctrans/article-pdf/50/5/1527/3939000/bst-2022-0900c.pdf> by guest on 24 November 2022

Actin network polymerization with NPFs at the membrane

The next step in the reconstitution approach is to mimic the situation observed, for instance, in the cell lamellipodium, where NPFs are attached to the membrane, and actin dynamically polymerizes at the membrane.

Experiments in the ‘outside’ configuration are inspired by works mimicking *in vitro* the actin-induced propulsion of *Listeria* using beads coated with NPFs. When such beads are bathed either in cell extracts or in a minimal mixture of purified actin and regulatory proteins, they are propelled by the forces generated by actin polymerization at their surface. The process starts with filaments nucleation at the bead surface. The nucleation leads to the growth of an actin gel around the bead. As this gel grows from the bead surface, mechanical stresses are accumulated at the gel’s external surface and eventually lead to its rupture. At this point, the symmetry of the system is broken, and the bead is pushed forward by a cylindrical structure made of actin gel, sometimes referred to as an actin ‘comet’ [31]. This ‘bead assay’ was extended to liquid droplets [32] and GUVs coated by NPFs in cell extracts [33,34]. These last experiments have revealed the spatial distribution of polymerization-induced forces at the GUV surface during their propulsion by an actin ‘comet.’ Here, we focus on GUVs bathed in cocktails of pure proteins.

Liu and coworkers [35] used GUVs made of a ternary lipid mixture exhibiting a thermally controlled liquid–liquid phase separation. Below a critical temperature, their membrane segregates between liquid-ordered and liquid disordered domains; over this temperature, the membrane is homogeneous [36]. The actin network shifts the transition temperature of lipid phase separation and influences the spatial distribution of the induced domains (Figure 2A). Because cell membranes are close to phase separation [37], actin networks could contribute to regulating the spatial organization of cell membranes.

The same researchers also showed that branched actin networks polymerizing around GUVs form finger-like protrusions [38] (Figure 2B). In this experiment, there were no crosslinkers inducing bundles as in the articles presented in section II [24,26]. As discussed above, the formation of finger-like protrusion from branched actin networks stems from the balance between membrane and filaments elasticity. When few filaments push against a membrane, the energetic cost for membrane deformation favors gathering these filaments into a single bundle surrounded by a membrane nanotube. In this case, the energy for membrane deformation is reduced. Contrary to a single filament, the forces induced by the polymerization of several parallel filaments can overcome the force required to form such cylindrical membrane tubes, which depends on the membrane bending energy and tension [39]. These results show that membrane elasticity can shape the architecture of actin networks.

Simon et al. [40] showed two types of actin-induced membrane deformations on GUVs using branched Arp2/3-nucleated networks in the presence of profilin and capping protein. They observed membrane tubes pulled toward the GUV exterior and ‘spikes’ toward their interior (Figure 2C). The spikes are observed at low membrane tension and small mesh size of the actin network, while only tubes form for larger tension and mesh size. The tubes, created solely by the retrograde flow induced by actin polymerization from the membrane, share similarities with endocytic bulges even though no curvature-inducing proteins are present. The spikes contain a dendritic network comprising Arp2/3 and CP and are thus very different from the protrusions induced by bundled actin filaments observed in [38]. They form because local heterogeneities in the growth of the actin gel induce a normal pressure acting on the membrane. If such heterogeneity reaches a critical size, it leads to the formation of a spike. The results from [40] clearly show that the same polymerizing dendritic actin network can simultaneously deform membranes in both directions. These deformations in both directions were observed in the ‘inside’ geometry in 2018 in the article by Dürre et al. that will be presented below.

Using the same assay, Simon et al. [41] then investigated how both membrane tension and the presence of CP control shape changes of GUVs. The presence of CP favors membrane deformations for all values of the membrane tension, whereas, without CP, membrane deformations occur only at low membrane tension. In another study [42], these actin gel-covered GUVs were osmotically deflated, leading to global shape changes (Figure 2D). The actin network thickness controls the type of shape changes: for thicknesses higher than 1.5 μm , wrinkles with a wavelength between 5 and 25 μm appear, whereas smaller gel thicknesses lead to large-scale buckling, which results in crescent-shaped GUVs. Wrinkling is favored for thick cortices because buckling implies a strong local deformation of the actin gel, which costs more energy than the formation of wrinkles on all the vesicle surface.

Finally, the same assay was adapted to reconstitute dynamic actin networks at the surface of membrane nanotubes formed from GUVs (Figure 2E) [43]. The objective of this study was to decipher the largely

unknown mechanisms by which actin dynamics contribute to the remodeling of membrane nanotubes inside the cell [44]. During intracellular trafficking, nanotubes are pulled by molecular motors walking on microtubules at the velocity of one micrometer per second. Therefore, to investigate the mechanical stability of actin-coated nanotubes, they were submitted to elongation at this velocity. When the tubes are covered by actin sheaths thicker than 100 nm, they fully stabilize the tubes that cannot be deformed in the range of forces accessible to optical tweezers. Oppositely, thinner actin sheaths break during tube elongation. This breakage results in heterogeneous tubes containing regions covered with actin and regions of bare membrane tubes. The membrane nanotubes are thicker under the actin coat. In contrast, regions devoid of actin have a smaller diameter that relaxes, expanding within minutes. These actin-free regions could provide enough time and the high curvature required for the binding of other proteins that act on tube stability. In addition, Atomic Force Microscopy (AFM) experiments directly probe the effect of the actin coat on tube mechanics and morphology [45] and validate the estimation of the actin sheath diameter presented.

Reassembling a dynamic actin network at the inner surface of a GUV (i.e. in the ‘inside’ configuration) to mimic the cell cortex was an experimental challenge. The process was achieved by preparing GUVs containing the actin machinery in non-polymerizing conditions using the IE technique [46]. A histidine-tagged NPF (VVCA-His) is specifically attached to the inner GUV membrane containing nickel lipids. The authors demonstrated that this NPF induces actin polymerization at the GUV membrane when the inside concentration of salts and ATP is tuned toward polymerization conditions using pores inserted in the membrane (Figure 2F). Membrane protrusions emerge when this type of cortex-containing GUVs is osmotically deflated [47].

The system developed in [46] was then used in several articles as a tool to investigate the mechanical role of the cell cortex in a biomimetic approach. First, [48] studied the spreading of the cortex-containing GUVs on adhesive substrates (Figure 2G). This article showed that a dense and connective actin cortex slows the early stages of the spreading, which highlights the role of viscous dissipation in the cortex at the onset of cell spreading.

The effect of the actin cortex on membrane dynamics has also been probed using membrane nanotube formation (Figure 2H). Nanotubes can be formed with optical tweezers from GUVs held in a micropipette in order to maintain a constant membrane tension. The nanotube length can then be varied to study membrane dynamics [49]. With this assay, [50] showed that the preparation technique of the GUVs, EF or IE, had a more significant effect on membrane dynamics than the presence of an actin cortex. Indeed, GUVs with the same lipid composition formed by these two techniques show no difference in their bending rigidity but a dramatic difference in their membrane friction. In the case of IE-formed GUVs, the membrane dynamics are very close to the ones observed on Giant Plasma Membrane Vesicles extracted from living cells [37]. Surprisingly, the actin network generates only an additional friction force, allowing for the reevaluation of membrane composition and membrane-cortex attachment roles on membrane dynamics. Nanotubes can also be formed by applying a hydrodynamic flow to a GUV attached to a microneedle [51]. With this assay, nanotubes are shorter on GUVs with an actin cortex at the same pulling force than their bare homologs [52], showing that such reconstituted actin cortices mechanically resist lipid movement. Finally, the cortex-containing GUVs have been used to demonstrate the role of actin on the scission of tubules induced by Shiga toxin towards the GUV interior [53]. In the presence of a cortex, these tubules are cut and float freely in the GUV lumen. The hypothesis for this scission is that actin induces nanodomains in the membrane, which could provoke tubule scission because of the energetic cost of domain coexistence, as proposed in [54].

Myosin II effect on polymerized Arp2/3-nucleated actin networks

Myosin II-induced contraction of dendritic actin networks at the external surface of GUVs leads to an increase in the mechanical tension in the network (Figure 2I). This results in either a global crush of the GUV or the peeling of the actin network that collapses on one side of the GUV. The first case is favored by actin-membrane solid attachment, high myosin II concentration, and network cohesiveness [55]. Peeling is a symmetry-breaking event happening when the built-up tension exceeds the critical stress, at which the actin network ruptures [56]. Quantifying the tension in the actomyosin network has been achieved by measuring the contact angle between GUV doublets linked by streptavidin-biotin links [57] (Figure 2J). When actin filaments polymerized without NPF are attached to the doublet surface, its tension remains constant. In contrast, the polymerization of an actin network increases the doublet tension. When myosin II is added, tension increases in both conditions: for

actin filaments polymerized without NPF, it strongly increases with myosin II whereas, for gels, polymerization- and myosin-induced tension synergistically combine to establish a high tension in the actomyosin shell, as it is the case in living cells [58].

Inside GUVs, Loiseau et al. were the first to adapt the cDICE method [21] to form a contractile actomyosin cortex [59] using anillin as a crosslinker and membrane-cortex linker. In this assay, membrane protrusions resembling cellular blebs were observed (Figure 2K). Indeed, myosin II-induced stresses result in the contraction of the cortex and, therefore, lead to an inward pressure that counteracts the outward osmotic pressure. In regions where heterogeneities in the cortex lead to a weaker membrane-cortex attachment, this pressure induces the detachment of the membrane and its blebbing. This biomimetic assay shows *in vitro* the dependence of the blebbing process on the myosin II concentration and membrane-cortex attachment. Similar bleb-like protrusions were observed in the presence of α -actinin and fascin as crosslinkers [30].

Following [59], the same group showed how the actomyosin dynamics affected the spreading of these GUVs on adhesive substrates [60]. The active remodeling of the cortex provides GUVs with an excess membrane area that allows it to sustain the adhesion-induced increase in its membrane tension and prevents it from bursting. Finally, [61] showed that CP controls the shape of the actomyosin cortex (Figure 2L). At low CP concentrations, membrane protrusions towards the exterior appear, whereas concave regions are observed at higher concentrations (60–120 nM). The effect of motors on these membrane deformations is therefore also dependent on the CP concentration: formation of star-like clusters at low CP, actin-rich stable domains at intermediary CP, and fission of membrane protrusions at high CP.

Perspectives

- The studies presented here have shown the minimal components necessary to reconstitute *in vitro* some biological processes observed in cellular experiments. Based on such assays, it is possible to tune the experimental parameters as actin-membrane attachment, actin dynamics, or myosin-induced contractility to precisely decipher each process's physical mechanisms.
- The works presented here show that some processes observed in the cell can be reproduced *in vitro* and mechanical models tested. Examples of such processes are blebbing, membrane tubulation or invagination, cell spreading, and the formation of contractile actomyosin rings that are able to induce membrane constriction.
- An essential aspect of future reconstitution studies would be the control of actomyosin dynamics in space and time. Recall that different actomyosin networks are simultaneously observed inside a living cell, and their dynamics are finely regulated. Therefore, a control on actin polymerization dynamics, motor activity, and membrane structure could be exerted using light-activated compounds (e.g. caged-ATP, blebbistatin), using DNA nanotechnology [62], or other external signals [63]. Such responsive systems would trigger the local assembly of artificial filopodia or blebs and allow for the investigation of how these different actin-based structures compete for actin-monomers or affect the shape of the GUVs.
- As recent studies on living cells have shown how actin networks are interconnected with other cytoskeletal players [64], another critical aspect for future work would be the reconstitution of these crosstalks. Biomimetic studies could play an essential role in investigating this coupling by using model systems; this potential can be seen in [65], where actin and keratin networks are co-encapsulated in GUVs. More generally, other players have to be coupled with cytoskeletal networks, as in [66], where the actin machinery is coupled to ATP production systems. These studies rely on the future development of cutting-edge encapsulation techniques, such as microfluidics [67].

Competing Interests

The authors declare that there are no competing interests associated with the manuscript.

Funding

We acknowledge funding from the French Agence Nationale de la Recherche (ANR-18-CE13-0007-01 awarded to C.C.).

Author contribution

Authors contributed equally.

Acknowledgements

We acknowledge Agnieszka Kawska at IlluScientia.com for the figures illustrations.

Abbreviations

ABPs, actin binding proteins; CP, capping proteins; GUVs, giant unilamellar vesicles; IE, inverted emulsion; NPF, nucleation promoting factors.

References

- 1 Blanchoin, L., Boujemaa-Paterski, R., Sykes, C. and Plastino, J. (2014) Actin dynamics, architecture, and mechanics in cell motility. *Physiol. Rev.* **94**, 235–263 <https://doi.org/10.1152/physrev.00018.2013>
- 2 Pollard, T.D., Blanchoin, L. and Mullins, R.D. (2000) Molecular mechanisms controlling actin filament dynamics in nonmuscle cells. *Annu. Rev. Biophys. Biomol. Struct.* **29**, 545–576 <https://doi.org/10.1146/annurev.biophys.29.1.545>
- 3 Machesky, L.M., Atkinson, S.J., Ampe, C., Vandekerckhove, J. and Pollard, T.D. (1994) Purification of a cortical complex containing two unconventional actins from *Acanthamoeba* by affinity chromatography on profilin-agarose. *J. Cell Biol.* **127**, 107–115 <https://doi.org/10.1083/jcb.127.1.107>
- 4 Romero, S., Clainche, C.L., Didry, D., Egile, C., Pantaloni, D. and Carlier, M.F. (2004) Formin is a processive motor that requires profilin to accelerate actin assembly and associated ATP hydrolysis. *Cell* **119**, 419–429 <https://doi.org/10.1016/j.cell.2004.09.039>
- 5 Machesky, L.M. and Insall, R.H. (1998) Scar1 and the related wiskott–Aldrich syndrome protein, WASP, regulate the actin cytoskeleton through the Arp2/3 complex. *Curr. Biol.* **8**, 1347–1356 [https://doi.org/10.1016/S0960-9822\(98\)00015-3](https://doi.org/10.1016/S0960-9822(98)00015-3)
- 6 Meyer, R.K. and Aebi, U. (1990) Bundling of actin filaments by ct-actinin depends on its molecular length. *J. Cell Biol.* **110**, 12 <https://doi.org/10.1083/jcb.110.6.2013>
- 7 Yamashiro, S., Yamakita, Y., Ono, S. and Matsumura, F. (1998) Fascin, an actin-bundling protein, induces membrane protrusions and increases cell motility of epithelial cells. *Mol. Biol. Cell* **9**, 993–1006 <https://doi.org/10.1091/mbc.9.5.993>
- 8 Bretscher, A., Edwards, K. and Fehon, R.G. (2002) ERM proteins and merlin: integrators at the cell cortex. *Nat. Rev. Mol. Cell Biol.* **3**, 586–599 <https://doi.org/10.1038/nrm882>
- 9 Veigel, C. and Schmidt, C.F. (2011) Moving into the cell: single-molecule studies of molecular motors in complex environments. *Nat. Rev. Mol. Cell Biol.* **12**, 163–176 <https://doi.org/10.1038/nrm3062>
- 10 Lemi re, J., Valentino, F., Campillo, C. and Sykes, C. (2016) How cellular membrane properties are affected by the actin cytoskeleton. *Biochimie* **130**, 33–40 <https://doi.org/10.1016/j.biochi.2016.09.019>
- 11 Kawska, A., Carvalho, K., Manzi, J., Boujemaa-Paterski, R., Blanchoin, L., Martiel, J.L. et al. (2012) How actin network dynamics control the onset of actin-based motility. *Proc. Natl Acad. Sci. U.S.A.* **109**, 14440–5 <https://doi.org/10.1073/pnas.1117096109>
- 12 Helfer, E., Harlepp, S., Bourdieu, L., Robert, J., MacKintosh, F.C. and Chatenay, D. (2000) Microrheology of biopolymer-membrane complexes. *Phys. Rev. Lett.* **85**, 457–460 <https://doi.org/10.1103/PhysRevLett.85.457>
- 13 Helfer, E., Harlepp, S., Bourdieu, L., Robert, J., MacKintosh, F.C. and Chatenay, D. (2001) Viscoelastic properties of actin-coated membranes. *Phys. Rev. E* **63**, 021904 <https://doi.org/10.1103/PhysRevE.63.021904>
- 14 Angelova, M. and Dimitrov, D.S. (1988) A mechanism of liposome electroformation. *Trends Colloid Interface Sci.* **11**, 59–67 <https://doi.org/10.1007/BF0114171>
- 15 Limozin, L., B armann, M. and Sackmann, E. (2003) On the organization of self-assembled actin networks in giant vesicles. *Eur. Phys. J E Soft Matter.* **10**, 319–330 <https://doi.org/10.1140/epje/i2002-10118-9>
- 16 McCullough, B.R., Blanchoin, L., Martiel, J.L. and De La Cruz, E.M. (2008) Cofilin increases the bending flexibility of actin filaments: implications for severing and cell mechanics. *J. Mol. Biol.* **381**, 550–558 <https://doi.org/10.1016/j.jmb.2008.05.055>
- 17 van Mameren, J., Vermeulen, K.C., Gittes, F. and Schmidt, C.F. (2009) Leveraging single protein polymers to measure flexural rigidity. *J. Phys. Chem. B* **113**, 3837–3844 <https://doi.org/10.1021/jp808328a>
- 18 Claessens, M.M.A.E., Bathe, M., Frey, E. and Bausch, A.R. (2006) Actin-binding proteins sensitively mediate F-actin bundle stiffness. *Nat. Mater.* **5**, 748–753 <https://doi.org/10.1038/nmat1718>
- 19 Limozin, L. and Sackmann, E. (2002) Polymorphism of cross-linked actin networks in giant vesicles. *Phys. Rev. Lett.* **89**, 168103 <https://doi.org/10.1103/PhysRevLett.89.168103>
- 20 Bashirzadeh, Y., Redford, S.A., Lorpai boon, C., Groaz, A., Moghimiyanavval, H., Litschel, T. et al. (2021) Actin crosslinker competition and sorting drive emergent GUV size-dependent actin network architecture. *Commun. Biol.* **4**, 1–11 <https://doi.org/10.1038/s42003-021-02653-6>
- 21 Abkarian, M., Loiseau, E. and Massiera, G. (2011) Continuous droplet interface crossing encapsulation (cDICE) for high throughput monodisperse vesicle design. *Soft Matter.* **7**, 4610 <https://doi.org/10.1039/c1sm05239j>

- 22 Bashirzadeh, Y., Wubshet, N., Litschel, T., Schwille, P. and Liu, A.P. (2021) Rapid encapsulation of reconstituted cytoskeleton inside giant unilamellar vesicles. *J. Vis. Exp.* **177**, e63332 <https://doi.org/10.3791/63332>
- 23 Honda, M., Takiguchi, K., Ishikawa, S. and Hotani, H. (1999) Morphogenesis of liposomes encapsulating actin depends on the type of actin-crosslinking. *J. Mol. Biol.* **287**, 293–300 <https://doi.org/10.1006/jmbi.1999.2592>
- 24 Tsai, F.C. and Koenderink, G.H. (2015) Shape control of lipid bilayer membranes by confined actin bundles. *Soft Matter*. **11**, 8834–8847 <https://doi.org/10.1039/C5SM01583A>
- 25 Litschel, T., Kelley, C.F., Holz, D., Adeli Koudehi, M., Vogel, S.K., Burbaum, L. et al. (2021) Reconstitution of contractile actomyosin rings in vesicles. *Nat. Commun.* **12**, 2254 <https://doi.org/10.1038/s41467-021-22422-7>
- 26 Bashirzadeh, Y., Wubshet, N.H. and Liu, A.P. (2020) Confinement geometry tunes fascin-actin bundle structures and consequently the shape of a lipid bilayer vesicle. *Front. Mol. Biosci.* **7**, 610277 <https://doi.org/10.3389/fmolb.2020.610277>
- 27 Pautot, S., Frisken, B.J. and Weitz, D.A. (2003) Production of unilamellar vesicles using an inverted emulsion. *Langmuir* **19**, 2870–2879 <https://doi.org/10.1021/la026100v>
- 28 Takiguchi, K., Yamada, A., Negishi, M., Tanaka-Takiguchi, Y. and Yoshikawa, K. (2008) Entrapping desired amounts of actin filaments and molecular motor proteins in giant liposomes. *Langmuir* **24**, 11323–6 <https://doi.org/10.1021/la802031n>
- 29 Tsai, F.C., Stuhmann, B. and Koenderink, G.H. (2011) Encapsulation of active cytoskeletal protein networks in cell-sized liposomes. *Langmuir* **27**, 10061–10071 <https://doi.org/10.1021/la201604z>
- 30 Bashirzadeh, Y., Moghimiyanavval, H. and Liu, A.P. (2022) Encapsulated actomyosin patterns drive cell-like membrane shape changes. *iScience* **25**, 104236 <https://doi.org/10.1016/j.isci.2022.104236>
- 31 Bernheim-Groswasser, A., Wiesner, S., Golsteyn, R.M., Carlier, M.F. and Sykes, C. (2002) The dynamics of actin-based motility depend on surface parameters. *Nature* **417**, 308–311 <https://doi.org/10.1038/417308a>
- 32 Boukellal, H., Campàs, O., Joanny, J.F., Prost, J. and Sykes, C. (2004) Soft Listeria: actin-based propulsion of liquid drops. *Phys. Rev. E* **69**, 061906 <https://doi.org/10.1103/PhysRevE.69.061906>
- 33 Upadhyaya, A., Chabot, J.R., Andreeva, A., Samadani, A. and van Oudenaarden, A. (2003) Probing polymerization forces by using actin-propelled lipid vesicles. *Proc. Natl Acad. Sci. U.S.A.* **100**, 4521–4526 <https://doi.org/10.1073/pnas.0837027100>
- 34 Giardini, P., Fletcher, D. and Theriot, J. (2003) Compression forces generated by actin comet tails on lipid vesicles. *Proc. Natl Acad. Sci. U.S.A.* **100**, 6493–6498 <https://doi.org/10.1073/pnas.1031670100>
- 35 Liu, A.P. and Fletcher, D.A. (2006) Actin polymerization serves as a membrane domain switch in model lipid bilayers. *Biophys. J.* **91**, 4064–4070 <https://doi.org/10.1529/biophysj.106.090852>
- 36 Veatch, S.L. and Keller, S.L. (2003) Separation of liquid phases in giant vesicles of ternary mixtures of phospholipids and cholesterol. *Biophys. J.* **85**, 3074–3083 [https://doi.org/10.1016/S0006-3495\(03\)74726-2](https://doi.org/10.1016/S0006-3495(03)74726-2)
- 37 Lingwood, D., Ries, J., Schwille, P. and Simons, K. (2008) Plasma membranes are poised for activation of raft phase coalescence at physiological temperature. *Proc. Natl Acad. Sci. U.S.A.* **105**, 10005–10010 <https://doi.org/10.1073/pnas.0804374105>
- 38 Liu, A.P., Richmond, D.L., Maibaum, L., Pronk, S., Geissler, P.L. and Fletcher, D.A. (2008) Membrane-induced bundling of actin filaments. *Nat. Phys.* **4**, 789–793 <https://doi.org/10.1038/nphys1071>
- 39 Heinrich, V. and Waugh, R.E. (1996) A piconewton force transducer and its application to measurement of the bending stiffness of phospholipid membranes. *Ann. Biomed. Eng.* **24**, 595–605 <https://doi.org/10.1007/BF02684228>
- 40 Simon, C., Kusters, R., Caorsi, V., Allard, A., Abou-Ghali, M., Manzi, J. et al. (2019) Actin dynamics drive cell-like membrane deformation. *Nat. Phys.* **15**, 602–609 <https://doi.org/10.1038/s41567-019-0464-1>
- 41 Simon, C., Caorsi, V., Campillo, C. and Sykes, C. (2018) Interplay between membrane tension and the actin cytoskeleton determines shape changes. *Phys. Biol.* **15**, 065004 <https://doi.org/10.1088/1478-3975/aa11ab>
- 42 Kusters, R., Simon, C., Lopes Dos Santos, R., Caorsi, V., Wu, S., Joanny, J.F. et al. (2019) Actin shells control buckling and wrinkling of biomembranes. *Soft Matter*. **15**, 9647–9653 <https://doi.org/10.1039/C9SM01902B>
- 43 Allard, A., Bouzid, M., Betz, T., Simon, C., Abou-Ghali, M., Lemièrre, J. et al. (2020) Actin modulates shape and mechanics of tubular membranes. *Sci. Adv.* **6**, eaaz3050 <https://doi.org/10.1126/sciadv.aaz3050>
- 44 Allard, A., Lopes dos Santos, R. and Campillo, C. (2021) Remodelling of membrane tubules by the actin cytoskeleton. *Biol. Cell* **113**, 329–343 <https://doi.org/10.1111/boc.202000148>
- 45 Lamour, G., Allard, A., Pelta, J., Labdi, S., Lenz, M. and Campillo, C. (2020) Mapping and modeling the nanomechanics of bare and protein-coated lipid nanotubes. *Phys. Rev. X* **10**, 011031 <https://doi.org/https://doi.org/10.1103/PhysRevX.10.011031>
- 46 Pontani, L.L., van der Gucht, J., Salbreux, G., Heuvingh, J., Joanny, J.F. and Sykes, C. (2009) Reconstitution of an actin cortex inside a liposome. *Biophys. J.* **96**, 192–198 <https://doi.org/10.1016/j.bpj.2008.09.029>
- 47 Wubshet, N.H., Bashirzadeh, Y. and Liu, A.P. (2021) Fascin-induced actin protrusions are suppressed by dendritic networks in GUVs. *Mol. Biol. Cell* **32**, 1634–1640 <https://doi.org/10.1091/mbc.E21-02-0080>
- 48 Murrell, M., Pontani, L.L., Guevorkian, K., Cuvelier, D., Nassoy, P. and Sykes, C. (2011) Spreading dynamics of biomimetic actin cortices. *Biophys. J.* **100**, 1400–1409 <https://doi.org/10.1016/j.bpj.2011.01.038>
- 49 Evans, E. and Yeung, A. (1994) Hidden dynamics in rapid changes of bilayer shape. *Chem. Phys. Lipids* **73**, 39–56 [https://doi.org/10.1016/0009-3084\(94\)90173-2](https://doi.org/10.1016/0009-3084(94)90173-2)
- 50 Campillo, C., Sens, P., Köster, D., Pontani, L.L., Lévy, D., Bassereau, P. et al. (2013) Unexpected membrane dynamics unveiled by membrane nanotube extrusion. *Biophys. J.* **104**, 1248–1256 <https://doi.org/10.1016/j.bpj.2013.01.051>
- 51 Borghi, N., Rossier, O. and Brochard-Wyart, F. (2003) Hydrodynamic extrusion of tubes from giant vesicles. *Europhys. Lett.* **64**, 837–843 <https://doi.org/10.1209/epl/2003-00321-x>
- 52 Guevorkian, K., Manzi, J., Pontani, L.L., Brochard-Wyart, F. and Sykes, C. (2015) Mechanics of biomimetic liposomes encapsulating an actin shell. *Biophys. J.* **109**, 2471–2479 <https://doi.org/10.1016/j.bpj.2015.10.050>
- 53 Römer, W., Pontani, L.L., Sorre, B., Rentero, C., Berland, L., Chambon, V. et al. (2010) Actin dynamics drive membrane reorganization and scission in clathrin-independent endocytosis. *Cell* **140**, 540–553 <https://doi.org/10.1016/j.cell.2010.01.010>

- 54 Allain, J.M., Storm, C., Roux, A., Amar, M.B. and Joanny, J.F. (2004) Fission of a multiphase membrane tube. *Phys. Rev. Lett.* **93**, 158104 <https://doi.org/10.1103/PhysRevLett.93.158104>
- 55 Carvalho, K., Tsai, F.C., Lees, E., Voituriez, R., Koenderink, G.H. and Sykes, C. (2013) Cell-sized liposomes reveal how actomyosin cortical tension drives shape change. *Proc. Natl Acad. Sci. U.S.A.* **110**, 16456–16461 <https://doi.org/10.1073/pnas.1221524110>
- 56 Carvalho, K., Lemièrre, J., Faqir, F., Manzi, J., Blanchoin, L., Plastino, J. et al. (2013) Actin polymerization or myosin contraction: two ways to build up cortical tension for symmetry breaking. *Philos. Trans. R. Soc. B Biol. Sci.* **368**, 20130005 <https://doi.org/10.1098/rstb.2013.0005>
- 57 Caorsi, V., Lemièrre, J., Campillo, C., Bussonnier, M., Manzi, J., Betz, T. et al. (2016) Cell-sized liposome doublets reveal active tension build-up driven by acto-myosin dynamics. *Soft Matter*. **12**, 6223–6231 <https://doi.org/10.1039/C6SM00856A>
- 58 Tinevez, J.Y., Schulze, U., Salbreux, G., Roensch, J., Joanny, J.F. and Paluch, E. (2009) Role of cortical tension in bleb growth. *Proc. Natl Acad. Sci. U.S.A.* **106**, 18581–6 <https://doi.org/10.1073/pnas.0903353106>
- 59 Loiseau, E., Schneider, J.A.M., Keber, F.C., Pelzl, C., Massiera, G., Salbreux, G. et al. (2016) Shape remodeling and blebbing of active cytoskeletal vesicles. *Sci. Adv.* **2**, e1500465 <https://doi.org/10.1126/sciadv.1500465>
- 60 Maan, R., Loiseau, E. and Bausch, A.R. (2018) Adhesion of active cytoskeletal vesicles. *Biophys. J.* **115**, 2395–2402 <https://doi.org/10.1016/j.bpj.2018.10.013>
- 61 Dürre, K., Keber, F.C., Bleicher, P., Brauns, F., Cyron, C.J., Faix, J. et al. (2018) Capping protein-controlled actin polymerization shapes lipid membranes. *Nat. Commun.* **9**, 1630 <https://doi.org/10.1038/s41467-018-03918-1>
- 62 Jahnke, K., Weiss, M., Weber, C., Platzman, I., Göpfrich, K. and Spatz, J.P. (2020) Engineering light-responsive contractile actomyosin networks with DNA nanotechnology. *Adv. Biosyst.* **4**, 2000102 <https://doi.org/10.1002/adbi.202000102>
- 63 Perrier, D.L., Vahid, A., Kathavi, V., Stam, L., Rems, L., Mulla, Y. et al. (2019) Response of an actin network in vesicles under electric pulses. *Sci. Rep.* **9**, 8151 <https://doi.org/10.1038/s41598-019-44613-5>
- 64 Bashirzadeh, Y. and Liu, A.P. (2019) Encapsulation of the cytoskeleton: towards mimicking the mechanics of a cell. *Soft Matter*. **15**, 8425–8436 <https://doi.org/10.1039/C9SM01669D>
- 65 Deek, J., Maan, R., Loiseau, E. and Bausch, A.R. (2018) Reconstitution of composite actin and keratin networks in vesicles. *Soft Matter*. **14**, 1897–1902 <https://doi.org/10.1039/C7SM00819H>
- 66 Lee, K.Y., Park, S.J., Lee, K.A., Kim, S.H., Kim, H., Meroz, Y. et al. (2018) Photosynthetic artificial organelles sustain and control ATP-dependent reactions in a protocellular system. *Nat. Biotechnol.* **36**, 530–535 <https://doi.org/10.1038/nbt.4140>
- 67 Weiss, M., Frohnmayer, J.P., Benk, L.T., Haller, B., Janiesch, J.W., Heitkamp, T. et al. (2018) Sequential bottom-up assembly of mechanically stabilized synthetic cells by microfluidics. *Nat. Mater.* **17**, 89–96 <https://doi.org/10.1038/nmat5005>

2.3.2 Review 2: Remodelling of membrane tubules by the actin cytoskeleton

This second review summarise the biological situations in which the actin cytoskeleton remodels membrane tubules. Then, we present the physics behind nanotube formation and the *in vitro* reconstitution experiments that allow us to understand the role of the actin cytoskeleton in membrane nanotube formation, elongation, constriction and scission.

Remodelling of membrane tubules by the actin cytoskeleton

Antoine Allard*^{†‡§}² , Rogério Lopes dos Santos*²  and Clément Campillo*^{1,2} 

*LAMBE, Université d'Évry, CNRS, CEA, Université Paris-Saclay, Évry-Courcouronnes 91025, France, †Sorbonne Université, UPMC, Paris 06, Paris, France, ‡Laboratoire Physico Chimie Curie, Institut Curie, PSL Research University, CNRS UMR168, Paris, France, and §Department of Physics, University of Warwick, Gibbet Hill Road, Coventry CV4 7AL, UK

Inside living cells, the remodelling of membrane tubules by actomyosin networks is crucial for processes such as intracellular trafficking or organelle reshaping. In this review, we first present various *in vivo* situations in which actin affects membrane tubule remodelling, then we recall some results on force production by actin dynamics and on membrane tubules physics. Finally, we show that our knowledge of the underlying mechanisms by which actomyosin dynamics affect tubule morphology has recently been moved forward. This is thanks to *in vitro* experiments that mimic cellular membranes and actin dynamics and allow deciphering the physics of tubule remodelling in biochemically controlled conditions, and shed new light on tubule shape regulation.

In architecture and industrial design, form follows function (Sullivan, 1896). For biological objects, from proteins to organisms, shape and function are intimately related. Living cells modify their shape to achieve biological processes such as division or motility. These shape changes rely on the reorganisation of the actomyosin cytoskeleton, a dynamic network of biopolymers (actin filaments) and molecular motors of the myosin family, which remodel biological membranes (Blanchoin et al., 2014). The actin cytoskeleton comprises at least two types of filaments assemblies: branched actin gels nucleated by the Arp2/3 complex and actin bundles nucleated by Formins. The Arp2/3 complex forms new actin filaments that emerge from a pre-existing filament with an angle of 70°. In the cell, Arp2/3 complex gels are found in the lamellipodium, the cortex and in endocytic patches (Mullins et al., 1998). Formins sit at the polymerising end of filaments and stimulate their parallel elongation forming structures in cells like filopodia or microvilli (Watanabe et al., 2014; Evangelista et al., 2003), among others. Changes

in the actin cytoskeleton structure resulting from the type of filament nucleation results in different mechanisms of force production and therefore different types of membrane deformation. The actin cortex, an actin-rich region close to the plasma membrane, comprising myosin motors, and linked to the membrane through Ezrin-Radixin-Moesin (ERM) proteins (Maniti et al., 2013), is an important player for membrane remodelling. Its dynamics plays an important role in global cell shape changes, as the ones implied in cell motility, but also in local shape changes implied in endocytosis.

This review focuses on the actomyosin driven remodelling of a particular type of membrane structures, hereby called 'membrane tubules'. They are cylinders made of a lipid bilayer, with a radius of tens of nanometres and a length up to micrometres. Tubular membrane structures are found all over the cell (Figure 1) and can be classified according to their lifetime (Roux, 2013). On the one hand, some are stable tubular structures, such as mitochondria or some regions of the endoplasmic reticulum (ER). If they can undergo dynamic rearrangements, they stay globally cylindrical over time. Hereafter, we call such cases 'structural tubules' (section *Structural Tubules*). On the other hand, some tubules are 'transient', like

¹To whom correspondence should be addressed (email: clement.campillo@univ-evry.fr)

²These authors contributed equally to this work.

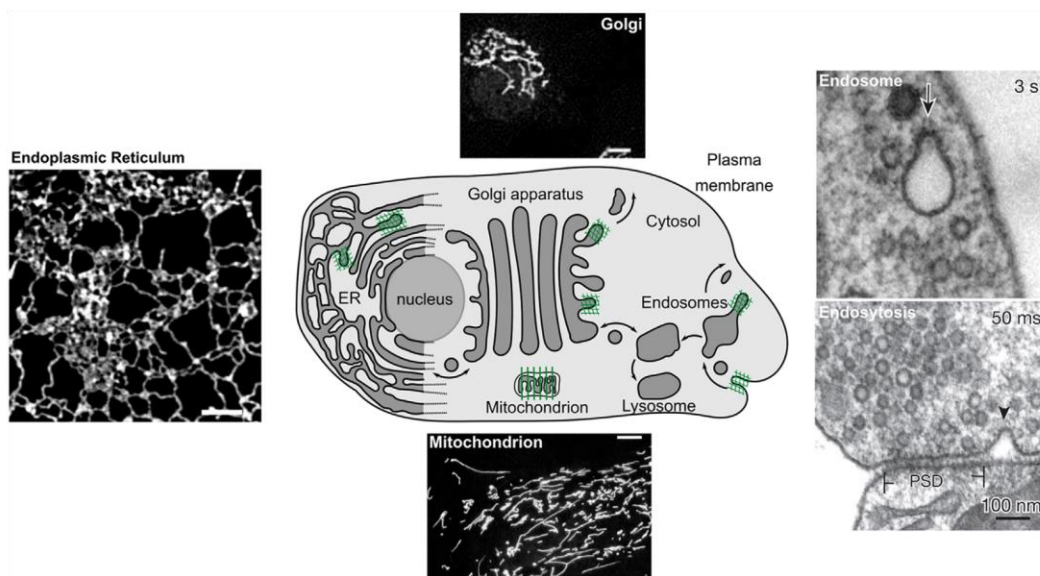
Key words: Actin, Membrane, Tubule, Vesicle trafficking.

Abbreviations: AFM, Atomic Force Microscopy; ALR, Autophagic Lysosome Reformation; ATP, Adenosine TriPhosphate; CIE, Clathrin-Independent Endocytosis; CME, Clathrin-Mediated Endocytosis; DRP1, Dynamin-Related Protein 1; ER, Endoplasmic Reticulum; ERM, Ezrin-Radixin-Moesin; TGN, Trans-Golgi Network

This is an open access article under the terms of the Creative Commons Attribution License, which permits use, distribution and reproduction in any medium, provided the original work is properly cited.

Figure 1 | Remodelling of membrane tubules by actin dynamics in eukariotic cells

(Centre) Scheme of a cell. Because the endoplasmic reticulum extends all over the cell, it is drawn partially. (Endoplasmic reticulum) Tubular ER in the periphery of a COS-7 cell expressing Sec61 β , an ER membrane marker. Scale bar: 2 μ m. Reprinted from (Nixon-Abell et al., 2016). (Golgi) Immunofluorescence confocal image of RPE-1 cells labelled for the Golgi protein GMAP210. Note the characteristic ribbon-like shape of the Golgi apparatus and its position close to the nucleus. Scale bar: 10 μ m. Reprinted from (Egea et al., 2015). (Endosome and Endocytosis) Electron micrographs showing buds (black arrowheads) on an endosome and via ultra-fast endocytosis. PSD: postsynaptic density. Reprinted from (Watanabe et al., 2014). (Mitochondrion) Mitochondrion in a portion of a living cell stained with rhodamine 123. Scale bar: 10 μ m. Reprinted from (Chen, 1988).

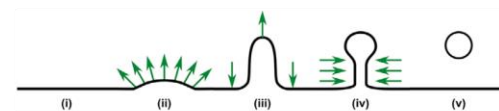


the ones extruded from the plasma membrane or the Golgi apparatus for intracellular trafficking, in which membranes intermittently deform into vesicular or tubular carriers (section *Transient Tubules*). Last, some 'intermediate' cases exist: endosomes and melanosomes are examples of organelles with a permanent tubular region from which carriers are dynamically pulled out (section *Intermediate Tubular Structure*). In all of these cases, the evolution of a tubule follows the steps depicted in Figure 2: an initially flat membrane (i), undergoes budding (ii), then this bud is pulled out and elongated (iii), potentially constricted (iv) and finally scissioned (v).

In this review, we highlight the role of actin in the dynamics of membrane tubules with the eyes of physicists. Indeed, if the role of the microtubule cytoskeleton in the elongation of membrane tubules has

Figure 2 | Actin effect on the fate of membrane tubules

The membrane (black) is deformed over time by forces produced by the actin cytoskeleton (green arrows). The time sequence is as follows: (i) flat, (ii) budding, (iii) tubulation, (iv) constriction and (v) scission.



been widely documented (Gurel et al., 2014; Terasaki et al., 1986; Egea et al., 2015; Delevoye et al., 2014; Du et al., 2016), we show here that actin dynamics also have a crucial role in membrane tubules formation, elongation and scission. It is crucial

to understand this interaction between actin and lipid tubules to fully describe the mechanisms of cell trafficking and remodelling. Indeed, this question is also of therapeutic importance, as it is clear that intracellular traffic deregulation, namely because of actin dynamics perturbation, is a hallmark of cancer progression (Mosesson et al., 2008). For instance, some human tumours exhibit an unusual expression of proteins (e.g., HIP1, HIP1R or cortactin) which coordinate endocytic sites remodelling by the actin cytoskeleton. Therefore, links between cancer and endocytosis, or more generally tubule remodelling, through the perturbation of the actin cytoskeleton, may be the subject of further therapeutic approaches and motivates this digest of the state of the art. In sections *Structural Tubules*, *Transient Tubules* and *Intermediate Tubular Structure*, we present *in vivo* experiments that clearly demonstrate actin-induced remodelling of structural, transient and intermediate tubules, respectively, showing the ubiquitous role of actin in tubule dynamics. In particular, we explore the mechanical role of actin in the steps depicted in Figure 2. Then, in section *Physics of Membrane Tubule Remodelling*, we describe the physical mechanisms that explain membrane tubule morphology changes by the action of cytoskeletal forces, by comparing the forces required to deform membranes with the ones generated by actin polymerisation. Finally, we show that biomimetic systems help to unravel the physical mechanisms underlying membrane tubule remodelling by actin. The advantage over *in vivo* situation is that physical and biochemical parameters can be tuned to test the validity of quantitative models and help to understand the experiments on living cells (section *In Vitro Tubule Remodelling by Actin*).

Structural tubules

Endoplasmic reticulum

The outer nuclear envelope and the ER enclose a single space called the ER lumen that takes 10% of the cell volume. The ER membrane accounts for half of the cellular membranes. Briefly, this organelle is essential for protein and lipid syntheses. In particular, it produces lipids and transmembrane proteins inserted inside lipid bilayers. The ER delivers proteins by producing transport vesicles addressed to the Golgi apparatus. It forms an interconnected membranous network made of flattened sheets (cisternae) and

tubules spreading over the cytosol (Park and Blackstone, 2010). The diameter of these tubules lies in the range of 30–100 nm (Gurel et al., 2014), whereas their length is in the 0.5–2 μm range (Perkins et al., 2020).

The role of microtubules in the maintenance of the dynamic tubular structure of the ER in mammals has been widely documented (Terasaki et al., 1986; Gurel et al., 2014). Oppositely, in yeast, microtubules have little effect on ER tubule dynamics (Prinz et al., 2000). Generally, filamentous actin (or F-Actin) colocalises with the ER, and the ER dynamics are influenced by Arp2/3 complex nucleated actin networks (Prinz et al., 2000; Griffing, 2010; Lynch et al., 2011). The formation of tubules from the ER and the control of their length (elongation and retraction) is driven by the actomyosin cytoskeleton (Sparkes et al., 2009; Griffing, 2010) (Figure 3(i)). While these tubules do not undergo scission, the presence of actin maintains the ER sheet–tubule balance and affect their dynamics (Joensuu et al., 2014). Strikingly, the ER tubule network fluctuates less when actin is depolymerised (Prinz et al., 2000). This implies that actin polymerisation actively increases the fluctuations of such tubules. Altogether, these suggest that remodelling and maintenance of sheet–tubule balance in ER rely on branched actin networks that stabilise the morphology of ER sheets. Networks mediated by formins also associate with ER/mitochondrion and ER/endosome contacts (Figures 3(ii) and 3(iii)). While the role of such networks is debated (Chhabra et al., 2009), it has been reported that formin-mediated actin networks are involved for mitochondrial fission and endosome remodelling, as described later in sections *Mitochondrion* and *Endosomes*

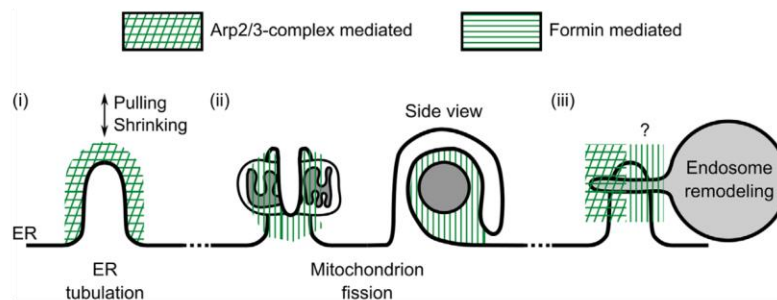
Mitochondrion

Mitochondria produce the energy (adenosine triphosphate) required to ensure cellular functions can occur. They are double-membrane-enclosed organelles that represent about a fifth of the cell volume and a third of its membrane surface (Alberts et al., 2002). Mitochondria have the shape of elongated cylinders, typically 1 μm long with a diameter of 150–300 nm. These dimensions may, however, vary between cell lines (Hatch et al., 2014).

Mitochondria undergo fusion or fission to meet the metabolic needs of the cell or to ensure their

Figure 3 | Actin is involved during endoplasmic reticulum (ER) remodelling

(i) Actin polymerisation, mediated by the Arp2/3 complex, drives tubules growth outward from the ER and control their retraction.
 (ii) The ER tubules and mitochondrion interact at the future mitochondrial fission site, thanks to formin-mediated actin networks.
 (iii) Tubules from the ER and tubular endosomes interact with actin. While branched Arp2/3 nucleated networks are involved in endosome remodelling, the role of formin-mediated networks remains to be deciphered.



proper sharing between daughter cells during cell division. Mitochondrial fission is an example of actin-dependent tubular remodelling, even if the physical mechanisms at play are unclear. The known elements of this process are depicted in Figure 3(ii). Fission occurs at ER/mitochondrion contact sites, where mitochondria are surrounded by tubules formed from the ER (Korobova et al., 2013, 2014). Arp2/3 complex and formin mediated actin networks, together with myosins, are recruited at these sites and induce mitochondrion constriction (Korobova et al., 2013; Ji et al., 2015; Moore et al., 2016; Schiavon et al., 2020). The role of actin polymerisation or myosin contraction forces on this constriction and its precise role on mitochondrial fission remains to be elucidated. Completion of mitochondrial scission requires an additional protein, dynamin-related protein 1 (Drp1). It has been reported *in vitro* that Drp1 had a high affinity with actin, suggesting that the presence of actin could induce its recruitment at mitochondrial fission site (Ji et al., 2015). Ultimately, Drp1 itself radially constricts and cuts the mitochondrion (Hatch et al., 2014).

Transient tubules

Transient tubules are ubiquitously involved in intracellular transport, which encompasses all the cellular processes involving exchanges of material between the membrane-delimited compartments of the cell: cellular organelles and plasma membrane. Their

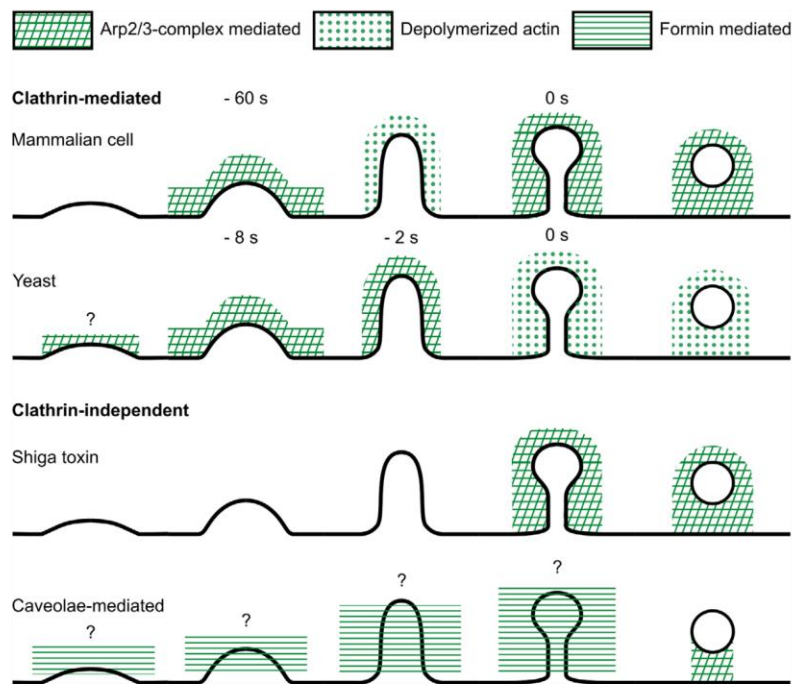
formation follows the time sequence previously described, which ends with the release of a transport vesicle that will be carried through the cell. Such transporters gather proteins and lipids needed for the targeted region and vary in composition, size and shape (Ratamero and Royle, 2019). Most transporters are spherical but some can have a tubular shape (Martinez-Menarguez, 2013). At a given enclosed volume, a tube has a higher surface area than a sphere. Consequently, the tubular geometry favours lipid bilayer enrichment in transmembrane proteins, while spherical vesicles efficiently transport water soluble molecules.

Endocytosis

Endocytosis refers to the internalisation of molecules from outside of the cell by the formation of a membrane vesicle. The cell has several ways to invaginate the membrane for endocytosis. It either relies on clathrin, a protein that coats the membrane and initiates its curvature at the endocytic site ('clathrin-mediated endocytosis' or CME, sections *Clathrin-Mediated Endocytosis in Mammalian Cells* and *Clathrin-Mediated Endocytosis in Yeast*) or is clathrin-independent ('clathrin-independent endocytosis' or CIE) as in the case of Shiga toxin endocytosis (section *Endocytosis of Shiga Toxin*) or caveolin-mediated endocytosis (section *Caveolae-Mediated Endocytosis*). In the following, we describe the role of actin during these processes. In addition, one key player that controls

Figure 4 | Actin is involved during endocytosis

Summary of the role of actin in several types of endocytosis: clathrin-mediated (mammals and yeast) and clathrin-independent (Shiga toxin and caveolae-mediated endocytosis). Endocytosis is based on budding, tubulation, constriction and fission. In the presence of clathrin, the timing indicates the time that precedes fission. A question mark indicates that the involvement of actin remains to be determined. Localisation of actin is indicative.



endocytosis is the local tension, which can be due to both pure lipid membrane tension and to membrane–cortex attachment (Hochmuth et al., 1996; Boulant et al., 2011; Shin et al., 2018; Mundy et al., 2002).

Clathrin-mediated endocytosis in mammalian cells

It takes 1–5 min to go from invagination to fission, relying on the cooperation of numerous proteins (Yoshida et al., 2018) (Figure 4). The budding mainly results from the clathrin coat. However, electron microscopy images show that a dense branched actin network is present before tubulation and forms a collar-like actin patch that surrounds the bud (Collins et al., 2011). The orientation of the filaments suggests that the actin network produces compressive forces applied towards the bud. In a later

time, during tubule maturation, depolymerisation of actin occurs until a new actin assembly is again required 1 min before completion of the fission (see first row, Figure 4). Therefore, actin polymerisation may be involved in producing compressive forces that enable scission. In addition, bent actin filaments have been observed close to the neck, this could be a way to store elastic energy that would later contribute to tubule constriction (Akamatsu et al., 2020).

Clathrin-mediated endocytosis in yeast

Several proteins cooperate to provide, in a short period of time (about 10 s), the necessary force to counteract the high hydrostatic pressure: pressure ~ 10 atm = 1 MPa, membrane tension ~ 0.5 mN/m and pulling force ~ 1 μ N for endocytosis (Minc et al.,

2009; Basu et al., 2014; Lemièrre and Berro, 2018; Dmitrieff and Nédélec, 2016). Endocytosis in yeast strictly relies on the assembly of a highly dynamic branched actin network (Gachet and Hyams, 2005; Goode et al., 2015) (Figure 4, second row) and both inhibition of actin polymerisation and stabilisation of filaments with jasplakinolide inhibits endocytosis (Ayscough, 2000; Kaksonen et al., 2003; Aghamohammadzadeh and Ayscough, 2009).

Endocytosis starts with the arrival of coat proteins, including clathrin and its adaptors with actin-binding domains (Skruzny et al., 2012). This step prepares the site for the assembly of a branched actin network (Figure 4). At a late stage of the coating, about 8 s before fission, it is still unclear whether actin dynamics help the formation of the initial bud (Goode et al., 2015). Data indicates that inhibition of actin polymerisation with latrunculin A prevents membrane bending at the endocytic site (Kukulski et al., 2012; Picco et al., 2015), while immunofluorescence images suggest that membrane bending precedes actin network assembly (Idrissi et al., 2012). It was suggested that membrane curvature appears only when the membrane and the actin polymerisation are coupled by clathrin adaptors at the tip of the invagination (Picco et al., 2018).

During tubule elongation, nucleation and polymerisation of new branched filaments at the plasma membrane drive tubule elongation thanks to actin-linking proteins, such as epsin, which couples F-actin and the tip (Sirotkin et al., 2010; Kaksonen et al., 2003). Tubule elongation ends 2 s before fission, up to a tubule length of 140 nm and a tip radius of 7–40 nm (Picco et al., 2018). Then, the actin network reorganises, it extends its volume, F-actin severing increases and the polymerisation rate is reduced (Chen and Pollard, 2013; Picco et al., 2015; Sirotkin et al., 2010). This reorganisation drives fission and internalisation of a vesicle (Kaksonen et al., 2005, 2003).

Endocytosis of Shiga toxin

The endocytosis of the bacterial Shiga toxin is an example of clathrin-independent endocytosis (Figure 4, third row). The first step of this process is the induction of tubular membrane invaginations towards the cell interior (Romer et al., 2007). Actin networks are not required for the formation and elongation of these tubules, while their scission is actin dependent. In-

deed, tubule formation is due to the imposition of a local negative curvature to the membrane by the binding of the toxin, without contribution of actin dynamics. Oppositely, tube scission is clearly actin dependent, as inhibition of actin polymerisation leads to the accumulation of stable and longer tubules. To explain this scission mechanism, it has been proposed that actin dynamics were triggering the formation of lipids nanodomains in the membrane, that could lead to tubule scission (Romer et al., 2010). This hypothesis emerges from two results: On one hand, actin affects the phase behaviour of lipid domains in model membranes (Liu and Fletcher, 2006), on the other hand, the presence of domains favours tubule scission because of the energetic cost of boundaries between domains (Roux et al., 2005; Allain et al., 2004). This suggests that actin polymerisation could favour the formation of lipid nanodomains in the membrane and thus indirectly induce membrane scission.

Ultrafast clathrin-independent endocytosis

While most evidence shows that tubule remodelling during endocytosis relies on the presence of a dense branched actin network able to produce substantial forces, some cells internalise cargoes thanks to formin-mediated actin bundles (Soykan et al., 2017; Shin et al., 2018). For instance, neurotransmission in mice is based on the fusion of synaptic vesicles followed by two types of endocytosis: slow CME of synaptic vesicle proteins with a time of about 1–10 s and ultrafast CIE that rapidly recycles synaptic vesicles within 100 ms (Soykan et al., 2017). In particular, tubule fission during CIE is associated with formin-mediated actin bundles, coupled with myosin II, rather than mediated by the Arp2/3 complex.

Caveolae-mediated endocytosis

Caveolae-mediated endocytosis involves invaginations formed by the transmembrane protein caveolin, that pinches off cholesterol-rich microdomains serving as reservoirs when the plasma membrane is stretched (Conner and Schmid, 2003; Bastiani and Parton, 2010; Sinha et al., 2011). This type of endocytosis leads to the internalisation of small vesicles with a diameter of about 50–60 nm (Conner and Schmid, 2003). Caveolae-mediated endocytosis is Arp2/3 complex independent and the endocytic sites associate with actin stress fibres (Rohlich

Remodelling of membrane tubules by the actin cytoskeleton

and Allison, 1976; Echarri et al., 2012; Echarri and Del Pozo, 2015) (Figure 4). For example, the virus SV40 hijacks the endocytic pathway to enter the cell. More specifically, this virus induces a breakdown of actin stress fibres to promote virus entry through caveolae-mediated endocytosis (Pelkmans et al., 2002). Last, an actin patch emerges to form an actin tail that propels the enclosed virus from the endocytic site. While actin is unquestionably present, its mechanical role during this form of endocytosis remains to be elucidated.

Transport from the Golgi apparatus

The morphology of the Golgi apparatus is highly variable among living systems, ranging from isolated tubules to stacked compartments (Egea et al., 2013). For eukaryotes, one cisterna faces the ER to trade material, the medial stacks sort proteins for correct addressing, while the last cisterna, the trans-Golgi network (TGN), faces the plasma membrane. The latter redirects vesicles towards different cell locations, such as the plasma membrane or endosomes. The study of the interaction between actin and the Golgi apparatus is challenging because of its proximity to the nucleus, a region abundant in proteins, including actin (Gurel et al., 2014). Besides, the microtubule cytoskeleton plays an important role in maintaining the shape and dynamics of the Golgi apparatus, as reviewed in (Egea et al., 2015). In particular, microtubules and microtubules-associated motors control the formation and fusion of tubular structures from the Golgi. Here, we restrict to the effect of actin dynamics on the fate of membrane tubules.

ER–Golgi apparatus exchanges require activation of the Arp2/3 complex (Campellone et al., 2008). The induced branched actin network polymerises on the Golgi apparatus and is then involved in vesicle secretion from the TGN (Chen et al., 2004; Almeida et al., 2011). There is no evidence that actin is able to induce the budding while the Arp2/3 complex defect inhibits elongation of tubules (Almeida et al., 2011). A burst of actin, associated with several types of myosins near the Golgi, precedes fission events, suggesting the role of actomyosin dynamics during constriction and scission (Delestre-Delacour et al., 2017; Brownhill et al., 2009; Miserey-Lenkei et al., 2017; Almeida et al., 2011). Furthermore, it has been proposed that the association of actin might affect Golgi functions by spatially segregating its se-

cretory activities to some given membrane regions, others being inhibited by the presence of actin that impairs membrane remodelling. The detailed physical mechanisms remain to be elucidated (Egea et al., 2015).

Intermediate tubular structures

Endosomes

The endosomes (from early to late) are the intermediates between organelles that send (Golgi, plasma membrane) and the ones that receive (Golgi, lysosome or plasma membrane) transport vesicles. An early endosome has a tubular-vesicular shape and is often located at the periphery of the cell to sort proteins coming from the plasma membrane. Some proteins are redirected back to the plasma membrane for recycling, while remaining early endosomes mature to form late endosomes. The late endosome is a hub that sorts proteins towards TGN or lysosomes (section *Lysosomes*).

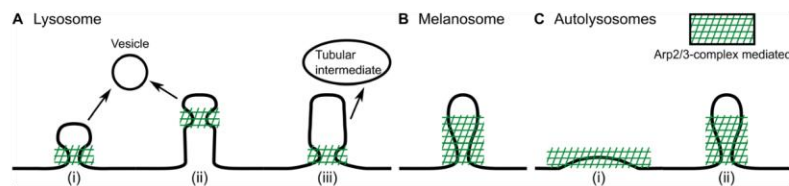
The nucleation of branched actin networks appears at the contact site between endosomal and ER tubules (Figure 3(iii)) (Rowland et al., 2014; Dong et al., 2016). Branched actin networks are involved in the maintenance of endosome morphology, as observed by knocking out the activation of the Arp2/3 complex (Gomez et al., 2012). However, its knockdown increases both endosomal membrane tubulation and fission defects (Derivery et al., 2009; Gomez and Billadeau, 2009; Duleh and Welch, 2010). F-actin networks stabilise the morphology of endosomes, which might help initiate a membrane tubule, while microtubule associated-molecular motors further elongate these tubules (Delevoeye et al., 2014) that eventually undergo fission thanks to the actin cytoskeleton.

Lysosomes

'Lysosome' is a term that includes numerous organelles, such as endolysosomes, phagolysosomes and autolysosomes, which all have different functions (Saffi and Botelho, 2019). In general, lysosomes degrade cargoes from endocytosis or autophagy. They are spherical organelles with an acidic lumen where molecules are digested. Transmembrane proteins ensure the passage of the digested products back towards the cytosol. The lysosomes also differ in shape: they can have either a vesicular or a 10 μm -long tubular shape (Chow et al., 2002). The lysosomes

Figure 5 | Actin is involved in lysosome, melanosome and autolysosome remodelling

(A) The membrane of a parent lysosome can undergo membrane deformation to form a bud (i) or a tubule (ii and iii). They may undergo fission to release a vesicular (i and ii) or tubular (iii) intermediate. Adapted from (Saffi and Botelho, 2019). (B) Branched actin networks might play a role in tubule remodelling during the recycling pathway from melanosomes. Adapted from (Ripoll et al., 2018). (C) During autolysosome reformation, a branched actin network facilitates (i) budding and (ii) tubulation of the autolysosome. Adapted from (Dai et al., 2019).



are first remodelled by clathrin, which provides the initial membrane curvature required to form a bud that later undergoes fission into a vesicle or is elongated into a tubule (Sridhar et al., 2013; Saffi and Botelho, 2019) (Figure 5A). Therefore, as for endosomal tubules, *in vivo* experiments show that extrusion, constriction and fission of lysosomal tubules might depend on branched actin dynamics, whereas microtubule associated-molecular motors elongate these tubules. The physical mechanisms of actomyosin induced endosomal tubules remain to be explored.

Melanosomes

Melanosomes share common properties with endosomes and lysosomes (Marks et al., 2013). Similar to endosomes, they are hubs for endocytic cargoes, serve as a storage for melanin pigments and recycle proteins and lipids via tubule carriers. Tubulation itself might occur without the need of actin, while constriction and fission at the neck are mediated by myosin VI, a non-conventional myosin that walks on actin filaments towards their minus end, and rely on the presence of a branched actin network rather than formin-mediated actin filaments (Ripoll et al., 2018) (Figure 5B). Both depletion of the activator of the Arp2/3 complex and inhibition of the branched actin network assembly affect the neck constriction, and thus increase fission defects.

Autolysosomes

The autophagy pathway allows degradation of intracellular contents—such as proteins, organelles or foreign bodies—first encapsulated in an autophago-

some that ultimately fuses with lysosomes (Yu et al., 2018). The last step of autophagy consists in autophagic lysosome reformation, during which budding, pulling of micrometre-sized tubules and fission of their tip occur successively (Munson et al., 2015; Yu et al., 2010) (Figures 5C(i) and 5C(ii)). The overall process is similar to CME: clathrin initiates budding (Rong et al., 2012), molecular motors walking on microtubule tracks pull the invagination (Du et al., 2016) while dynamin induces tubule fission (Schulze et al., 2013). The presence of a branched actin network localised at the base of the invagination is required for autolysosome tubulation and might facilitate its initiation (Dai et al., 2019). The role of actin during the remaining steps is still unexplored.

Physics of membrane tubule remodelling

To understand what could be the physical effect of actin dynamics in the examples of tubules remodelling presented before, let us start by estimating the maximal force generated by a single polymerising actin filament (Kovar and Pollard, 2004). The rigidity of an actin filament is the product of its persistence length L_p by the thermal energy, $k_B T \times L_p \sim 6.10^{-26} \text{ N m}^2$ where k_B is the Boltzmann constant, T the temperature, and $L_p \sim 15 \mu\text{m}$ (Isambert et al., 1995). Then, the force to buckle a filament F is proportional to this rigidity and inversely proportional to the filament length L : $F = \pi^2 k_B T \times L_p / L$. Buckling of a one-side attached filament has been experimentally observed for a filament of $L \sim 1 \mu\text{m}$ in length (Kovar and Pollard,

2004). Therefore, the maximal force generated by a single actin filament can be estimated to 1 pN.

The force at the tip of finger-like cell protrusions (filopodia) has been measured with micropipette suction and optical tweezers experiments at 10–50 pN (Peskin et al., 1993; Hochmuth et al., 1996; Shao and Hochmuth, 1996). The force at the protruding edge of the lamellipodia, measured by traction force microscopy, is much larger: 10–200 nN (Harris et al., 1980; Lee et al., 1994; Oliver et al., 1995). Altogether, this shows that the assembly of various actin networks enable cells to exert forces in the range of 10–200 pN on cell membranes.

Besides, the physics of lipid bilayers can be characterised in our context by two parameters: their bending modulus κ and tension σ . In cells, the bending modulus lies in the range of 10–50 $k_B T$, where $k_B T$ is the thermal energy, therefore the membrane is subjected to intense thermal fluctuations, while the membrane tension varies from 10 to 300 $\mu\text{N/m}$ (Gauthier et al., 2012; Lieber et al., 2013; Batchelder et al., 2011). In the context of tubule formation, membranes deform following the previously described sequence. The first step, tubule initiation, corresponds to the budding of a flat membrane to a curved bulge. The energy per unit area required to bend a flat membrane sheet is given by $e_b = 2\kappa/R^2$ where R is the curvature radius of the bulge (Helfrich, 1973). Consequently, for $R = 100$ nm, the maximal energy per unit area associated to bending is $e_b = 0.04$ pN/nm. Then, the maximal force to bend the membrane over a height of R is $F_b = e_b \times R = 4$ pN. This force is thus comparable to the force generated by a single actin filament of 1 pN. Therefore, few polymerising filaments in a gel can generate sufficient forces to induce a membrane bulge.

After budding, tubulation occurs if a force f is further applied on the bulge. After an overshoot force for tubule initiation (Derényi et al., 2002), the free energy of the tubule reads:

$$F_{\text{tubule}} = \frac{\pi\kappa}{R_t}L + 2\pi R_t L \sigma - fL \quad (1)$$

where L is the tubule length and R_t its radius. This free energy is composed of three terms that respectively describe the bending energy, the effect of tension and the mechanical work of the external force. This last expression allows calculating the equilib-

rium tubule radius R_0 and force f_0 of the tubule, that are related by (Waugh and Hochmuth, 1987) and (Derényi et al., 2002):

$$f_0 = 2\pi\sqrt{2\kappa\sigma} = \frac{2\pi\kappa}{R_0} \quad (2)$$

These relations link the tubule radius R_0 with its mechanical properties (bending modulus and membrane tension). Taking the values given above allows tubule radii in the range 8–100 nm and leads to forces in the 2–160 pN range. Therefore, several polymerising filaments are sufficient to elongate a membrane tubule by pulling at its tip, provided that its tension is not too large (Simon et al., 2019).

Once the tubule is formed, it can be affected by polymerisation of proteins, such as dynamin, leading to its constriction. Whether actin can induce the same polymerisation force remains to be explored. In the situation where this polymerisation applies a pressure P_a on the tubule surface, its free energy becomes (Roux et al., 2010):

$$F_{\text{tubule}} = \frac{\pi\kappa}{R_0}L + 2\pi R_0 L \sigma + P_a \pi R^2 L \quad (3)$$

In this equation, the bending modulus term tends to increase the tubule radius, while both membrane tension and positive actin polymerisation pressure will decrease it. There is, thus, a critical radius $R_c = 2\sigma/P_a$ at which these two compressive effects are equal. To estimate the polymerisation pressure P_a in the case of actin, we consider that each filament exerts a force of 1 pN on a surface $\xi^2 = (50 \text{ nm})^2$, which is the characteristic actin network mesh size (Pontani et al., 2009; Kawaska et al., 2012), yielding a pressure of $P_a = 10^3$ Pa. The actin pressure contribution will overtake the one of membrane tension for radii $R_0 \gg R_c = 20\text{--}400$ nm. Therefore, actin alone would be dominant for large membrane tubules, which are still in the range of few actin network mesh size. Potentially, the local compression of the tubule could help with its scission and, thus, the release of a transporter.

Besides its direct role in force generation, actin may also induce indirect forces, through friction (Allard et al., 2020a; Campillo et al., 2013; Guevorkian et al., 2015; Borghi and Brochard-Wyart, 2007). During the overall process of tubule formation, lipids flow from the flat membrane towards the tubule. Since the cell membrane is highly coupled with

abundant transmembrane proteins and connected with the underlying actin cortex, lipid mobility is hindered, which affect the dynamics of tubule extrusion. The presence of such a friction could ultimately lead to the scission of tubules under elongation (Simunovic et al., 2017). As previously described, there is experimental evidence of the role of actin in one or several steps of membrane tubule remodelling *in vivo* (sections *Structural Tubules*, *Transient Tubules* and *Intermediate Tubular Structure*). Due to the complexity of the processes involved in cells, deciphering the mechanical role of actin in tubule remodelling is difficult. The use of *in vitro* systems is thus an appealing alternative.

***In vitro* tubule remodelling by actin**

Assessing the role of actin *in vivo* can be complex because of its numerous vital functions (division, migration, etc.). Thus, modifying the actin cytoskeleton to determine its effect on a particular process can induce perturbations on others. Therefore, the physical mechanisms by which actin affects tubule morphology are challenging to elucidate in the complex environment of the cell interior. Moreover, the nanometric size of tubules, comparable with the typical mesh size of actin networks (~30–50 nm; Kawaska et al., 2012), adds an additional difficulty. In order to reduce this complexity, *in vitro* systems present the advantage of a controlled biochemical environment and enable nano- imaging and mechanically probing the tubules, opening the way to decipher the mechanical role of actin in tubule remodelling.

Historically, biomimetic experiments based on actin polymerisation at the surface of micrometric objects could first reproduce actin-based motility on: hard beads (Loisel et al., 1999; Cameron et al., 1999; Noireaux et al., 2000; Bernheim-Groswasser et al., 2002), liquid droplets (Boukellal et al., 2003; Trichet et al., 2008) or giant liposomes larger than 10 μm (Upadhyaya et al., 2003; Giardini et al., 2003). While new polymerisation occurs at the bead or droplet surface where Arp2/3 complex activators are located, elastic stresses build up in the actin network (Noireaux et al., 2000). These stresses induce the network rupture and actin forms a tail that propels the object forward.

In liposome experiments, polymerisation activators are coupled to lipid heads. These experiments recapitulate some steps of tubule evolution depicted

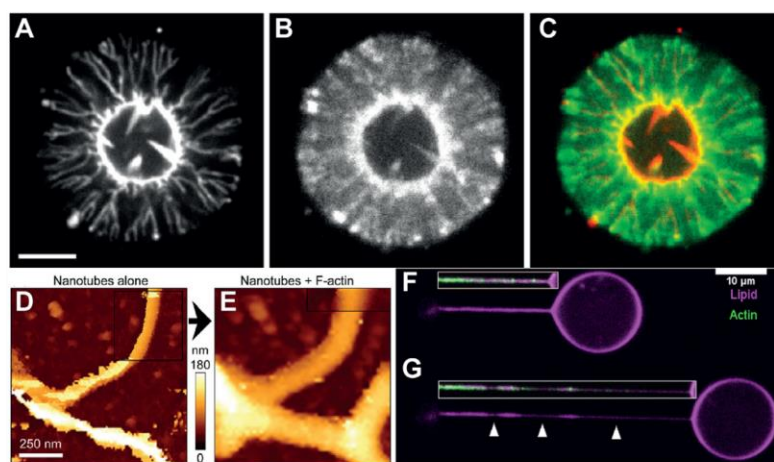
in Figure 2. During the formation of an actin tail propelling liposomes bathed in cytoplasmic extract, a large tubule was first observed at the centre of the tail (Giardini et al., 2003).

Liposomes bathed in the cytosol of HEK cells exhibit many tubules (Anitei et al., 2017). To explain their extrusion and elongation, the authors propose the following mechanism: clathrin induces membrane budding and tubule elongation remains dependent on the mechanical action of the actin network. Recently, liposomes covered by a polymerisation activator, and bathed in a minimal cocktail of pure proteins exhibit two types of membrane protrusion (Simon et al., 2019): ‘spikes’ towards the liposome interior, reminiscent of filopodia, and tubules towards their exterior (Figures 6A–6C). These tubules are very similar to the ones observed by (Anitei et al., 2017) in cell extracts, showing that budding and tubule elongation can successfully happen in the absence of membrane-bending proteins, only because of actin polymerisation dynamics. Interestingly, membrane tension controls the type of protrusion: spikes form only at low tension, whereas tubules always appear. Altogether, these results highlight the crucial role of actin in tubule formation, and its ability to form tubules independently without the help of motors or membrane bending proteins. Inward and outward protrusions were also observed when actin polymerises at the inner surface of liposomes, and depend on the presence of capping proteins (Dürre et al., 2018). Furthermore, when non-muscle myosin II is added, fission of inward membrane deformations was observed.

Additionally, the mechanics and morphology of preformed membrane tubules are affected by the presence of branched actin networks (Figures 6D and 6E). Atomic force microscopy (AFM) nanomapping of tubules before and after actin polymerisation at their surface allows direct observation of a ~ 100 nm sheath of actin that surrounds the tubule and increases its effective rigidity (Lamour et al., 2020). Using optical tweezers, tubules surrounded by an actin sheath can mechanically be probed by mimicking tubule elongation *in vivo* under the action of molecular motors (Allard et al., 2020a). In this case, the fate of the tubule depends on the actin amount: A sleeve thicker than a few hundreds of nanometres is unable to deform and such a sheath of actin stabilises the entire tubule, in length and radius, while at smaller

Figure 6 | *In vitro* systems to study the effect reconstituted actin networks on membrane nanotubes

(A–C) Confocal observations of inwards (spikes) and outwards (tubules) protrusions induced by the growth of a branched actin network on initially spherical vesicles. Membrane is observed in **A**, capping protein in **B** and merge in **C**, scale bar 5 μm . Reproduced from (Simon et al., 2019). (D and E) AFM imaging of bare preformed tubules on a glass substrate before (D) and after actin polymerisation (E). Reproduced from (Lamour et al., 2020). (F and G) Confocal images before (F) and after (G) pulling a preformed tubule held by an optical tweezer, revealing local changes in tubule radius due to lipid mobility hindrance by the presence of the actin cytoskeleton (arrows). See (Allard et al., 2020a) for more details.



sleeve thicknesses, pulling on the membrane tubule allows tearing the surrounding actin sleeve. Discontinuous tubule regions appear and smaller tubule radii are observed in portions where the actin sleeve is absent (Figures 6F and 6G). This heterogeneity stems from lipids flow hindrance under the actin sleeve. When maintained for several minutes, the tubule radius homogenises along its length. Inside the cell, actin may provide enough time and curvature geometries for the binding of remodelling proteins that act on tubule stability/instability (Morlot et al., 2012). Finally, the actin sheath damps the thermal fluctuations of the tubule (Allard et al., 2020b). In these studies, tubule scission by actin dynamics were never observed and may rely on other parameters such as the lipid composition or the presence of molecular motors.

Conclusion

The role of actin is crucial during all steps of tubule remodelling, namely membrane budding, tubule

elongation, constriction and scission. Many *in vivo* examples presented in sections *Structural Tubules*, *Transient Tubules* and *Intermediate Tubular Structure* show that actin dynamics are implied in all stages of tubule formation and destabilisation, in a variety of physiological contexts. The general importance of the actin-microtubule crosstalk (Pimm and Henty-Ridilla, 2021) highlights the unelucidated question of the relative importance of actin and microtubule-induced tubulation. We have shown that microtubule-associated motors were mainly involved in the elongation of tubules, as in the case of the Golgi apparatus, or in the long-range transport of transport intermediates after tubule scission, in endocytosis for instance. Nevertheless, we have also highlighted that actin and microtubules were both necessary to maintain the dynamical shape of the ER notably, showing that they could have synergistic or redundant roles that are still unclear. In processes, as tubulation from the Golgi, actin and microtubules affect different steps of tubules formation, raising the question of how the timing of actin and microtubule-related

steps are orchestrated. Besides, we show in section *Physics of Membrane Tubule Remodelling*, based on simple considerations of membrane tubule and actin biophysics, that actin dynamics are theoretically able to bud, elongate and constrict membrane tubules. Finally, in section *In Vitro Tubule Remodelling by Actin*, we detail that *in vitro* experiments are powerful to decipher the mechanics of tubule remodelling. In particular, they clearly show that actin alone can initiate budding and elongation of membrane tubules (Simon et al., 2019). Actin polymerisation on formed tubules induces their stabilisation, whereas scission could have been expected from *in vivo* experiments. To go further in the biomimetic approach and closer to the cellular situation, the effect of other players has to be further investigated *in vitro*, in particular complex membrane compositions and motor proteins. A combination of top-down and bottom-up approaches promises exciting experiments for future years.

Funding

We acknowledge funding from the French Agence Nationale de la Recherche (ANR- 18-CE13-0007-01 awarded to C.C.) and the Fondation pour la Recherche Médicale, Grant No. FDT201904007966. All authors contributed to writing the paper.

Acknowledgements

We thank Cécile Sykes, Guillaume Lamour and Steve Williams for reading and commenting our manuscript.

Conflict of interest statement

The authors have declared no conflict of interest.

References

- Aghamohammadzadeh, S. and Ayscough, K. R. (2009). Differential requirements for actin during yeast and mammalian endocytosis. *Nat. Cell Biol.*, **11**(8), 1039–1042
- Akamatsu, M., Vasan, R., Serwas, D., Ferrin, M. A., Rangamani, P. and Drubin, D. G. (2020). Principles of self-organization and load adaptation by the actin cytoskeleton during clathrin-mediated endocytosis. *Elife*, **9**
- Alberts, B., Johnson, A., Lewis, J., Raff, M., Roberts, K. and Walter, P. (2002). *Molecular Biology of the Cell*. New York: Garland Science
- Allain, J.-M., Storm, C., Roux, A., Amar, M. B. and Joanny, J.-F. (2004). Fission of a multiphase membrane tube. *Phys. Rev. Lett.*, **93**(15), 158104
- Allard, A., Valentino, F., Sykes, C., Betz, T. and Campillo, C. (2020a). Fluctuations of a membrane nanotube covered with an actin sleeve. *Phys. Rev. E*, **102**:052402. <https://doi.org/10.1103/PhysRevE.102.052402>
- Allard, A., Bouzid, M., Betz, T., Simon, C., Abou-Ghali, M., Lemiere, J., Valentino, F., Manzi, J., Brochard-Wyart, F., Guevorkian, K., Plastino, J., Campillo, C. and Sykes, C. (2020b). Actin modulates shape and mechanics of tubular membranes. *Sci. Adv.*, **6**(17), eaaz3050
- Almeida, C. G., Yamada, A., Tenza, D., Louvard, D., Raposo, G. and Coudrier, E. (2011). Myosin 1b promotes the formation of post-golgi carriers by regulating actin assembly and membrane remodelling at the trans-golgi network. *Nat. Cell Biol.*, **13**(7), 779–789
- Anitei, M., Stange, C., Czupalla, C., Niehage, C., Schuhmann, K., Sala, P., Czogalla, A., Pursche, T., Coskun, U., Shevchenko, A. and Hoflack, B. (2017). Spatiotemporal control of lipid conversion, actin-based mechanical forces and curvature sensors during clathrin/ap-1-coated vesicle biogenesis. *Cell Rep.*, **20**(9), 2087–2099
- Ayscough, K. R. (2000). Endocytosis and the development of cell polarity in yeast require a dynamic f-actin cytoskeleton. *Curr. Biol.*, **10**(24), 1587–1590
- Bastiani, M. and Parton, R. G. (2010). Caveolae at a glance. *J. Cell Sci.*, **123**(22), 3831–3836
- Basu, R., Munteanu, E. L. and Chang, F. (2014). Role of turgor pressure in endocytosis in fission yeast. *Mol. Biol. Cell*, **25**(5), 679–687
- Batchelder, E. L., Holloper, G., Campillo, C., Mezanges, X., Jorgensen, E. M., Nassoy, P., Sens, P. and Plastino, J. (2011). Membrane tension regulates motility by controlling lamellipodium organization. *Proc. Natl. Acad. Sci. U.S.A.*, **108**(28), 11429–11434
- Bernheim-Groswasser, A., Wiesner, S., Golsteyn, R. M., Carlier, M.-F. and Sykes, C. (2002). The dynamics of actin-based motility depend on surface parameters. *Nature*, **417**(6886), 308–311
- Blanchoin, L., Boujemaa-Paterski, R., Sykes, C. and Plastino, J. (2014). Actin dynamics, architecture and mechanics in cell motility. *Physiol. Rev.*, **94**(1), 235–263
- Borghi, N. and Brochard-Wyart, F. (2007). Tether extrusion from red blood cells: integral proteins unbind- ing from cytoskeleton. *Biophys. J.*, **93**(4), 1369–1379
- Boukellal, H., Plastino, J., Noireaux, V. and Sykes, C. (2003). Propelling soft objects. *C. R. Phys.*, **4**(2), 275–280
- Boulant, S., Kural, C., Zeeh, J.-C., Ubelmann, F. and Kirchhausen, T. (2011). Actin dynamics counteract membrane tension during clathrin-mediated endocytosis. *Nat. Cell Biol.*, **13**(9), 1124–1131
- Brownhill, K., Wood, L. and Allan, V. (2009). Molecular motors and the golgi complex: staying put and moving through. *Semin. Cell Dev. Biol.*, **20**(7), 784–792
- Cameron, L. A., Footer, M. J., Van Oudenaarden, A. and Theriot, J. A. (1999). Motility of acta protein- coated microspheres driven by actin polymerization. *Proc. Natl. Acad. Sci. U.S.A.*, **96**(9), 4908–4913
- Campellone, K. G., Webb, N. J., Znameroski, E. A. and Welch, M. D. (2008). Whamm is an arp2/3 complex activator that binds microtubules and functions in er to golgi transport. *Cell*, **134**(1), 148–161
- Campillo, C., Sens, P., Köster, D., Pontani, L.-L., Lévy, D., Bassereau, P., Nassoy, P. and Sykes, C. (2013). Unexpected membrane dynamics unveiled by membrane nanotube extrusion. *Biophys. J.*, **104**(6), 1248–1256
- Chen, J.-I., Lacomis, L., Erdjument-Bromage, H., Tempst, P. and Stamnes, M. (2004). Cytosol-derived proteins are sufficient for arp2/3 recruitment and arf/coatomer-dependent actin polymerization on golgi membranes. *FEBS Lett.*, **566**(1–3), 281–286
- Chen, L. B. (1988). Fluorescent labeling of mitochondria. *Methods Cell Biol.*, **29**, 103–123

- Chen, Q. and Pollard, T. D. (2013). Actin filament severing by cofilin dismantles actin patches and produces mother filaments for new patches. *Curr. Biol.*, **23**(13), 1154–1162
- Chhabra, E. S., Ramabhadran, V., Gerber, S. A. and Higgs, H. N. (2009). Inf2 is an endoplasmic reticulum-associated formin protein. *J. Cell Sci.*, **122**(9), 1430–1440
- Chow, A., Toomre, D., Garrett, W. and Mellman, I. (2002). Dendritic cell maturation triggers retrograde mhc class ii transport from lysosomes to the plasma membrane. *Nature*, **418**(6901), 988–994
- Collins, A., Warrington, A., Taylor, K. A. and Svitkina, T. (2011). Structural organization of the actin cytoskeleton at sites of clathrin-mediated endocytosis. *Curr. Biol.*, **21**(14), 1167–1175
- Conner, S. D. and Schmid, S. L. (2003). Regulated portals of entry into the cell. *Nature*, **422**(6927), 37–44
- Dai, A., Yu, L. and Wang, H.-W. (2019). Whamm initiates autolysosome tubulation by promoting actin polymerization on autolysosomes. *Nat. Commun.*, **10**(1), 1–14
- Delestre-Delacour, C., Carmon, O., Laguerre, F., Estay-Ahumada, C., Courel, M., Elias, S., Jeandel, L., Rayo, M. V., Peinado, J. R., Sengmanivong, L., Gasman, S., Coudrier, E., Anouar, Y. and Montero-Hadjadj, M. (2017). Myosin 1b and f-actin are involved in the control of secretory granule biogenesis. *Sci. Rep.*, **7**(1), 1–13
- Delevoe, C., Miserey-Lenkei, S., Montagnac, G., Gilles-Marsens, F., Paul-Gilloteaux, P., Giordano, F., Waharte, F., Marks, M. S., Goud, B. and Raposo, G. (2014). Recycling endosome tubule morphogenesis from sorting endosomes requires the kinesin motor kif13a. *Cell Rep.*, **6**(3), 445–454
- Derényi, I., Jülicher, F. and Prost, J. (2002). Formation and interaction of membrane tubes. *Phys. Rev. Lett.*, **88**(23), 238101
- Derivery, E., Sousa, C., Gautier, J. J., Lombard, B., Loew, D. and Gautreau, A. (2009). The arp2/3 activator wash controls the fission of endosomes through a large multiprotein complex. *Dev. Cell*, **17**(5), 712–723
- Dmitrieff, S. and Nédélec, F. (2016). Amplification of actin polymerization forces. *J. Cell Biol.*, **212**(7), 763–766
- Dong, R., Saheki, Y., Swarup, S., Lucast, L., Harper, J. W. and de Camilli, P. (2016). Endosome-er contacts control actin nucleation and retromer function through vap-dependent regulation of pi4p. *Cell*, **166**(2), 408–423
- Du, W., Su, Q. P., Chen, Y., Zhu, Y., Jiang, D., Rong, Y., Zhang, S., Zhang, Y., Ren, H., Zhang, C., Wang, X., Gao, N., Wang, Y., Sun, L., Sun, Y. and Yu, L. (2016). Kinesin 1 drives autolysosome tubulation. *Dev. Cell*, **37**(4), 326–336
- Duleh, S. N. and Welch, M. D. (2010). Wash and the arp2/3 complex regulate endosome shape and trafficking. *Cytoskeleton*, **67**(3), 193–206
- Dürre, K., Keber, F. C., Bleicher, P., Brauns, F., Cyron, C. J., Faix, J. and Bausch, A. R. (2018). Capping protein-controlled actin polymerization shapes lipid membranes. *Nat. Commun.*, **9**(1), 1–11
- Echarri, A. and Del Pozo, M. A. (2015). Caveolae-mechanosensitive membrane invaginations linked to actin filaments. *J. Cell Sci.*, **128**(15), 2747–2758
- Echarri, A., Muriel, O., Pavin, D. M., Azegrouz, H., Escolar, F., Terron, M. C., Sanchez-Cabo, F., Martinez, F., Montoya, M. C., Llorca, O. and del Pozo, M. A. (2012). Caveolar domain organization and trafficking is regulated by abl kinases and mdia1. *J. Cell Sci.*, **125**(13), 3097–3113
- Egea, G., Serra-Peinado, C., Salcedo-Sicilia, L. and Gutiérrez-Martínez, E. (2013). Actin acting at the golgi. *Histochem. Cell Biol.*, **140**(3), 347–360
- Egea, G., Serra-Peinado, C., Gavilan, M. P. and Rios, R. M. (2015). Cytoskeleton and golgi-apparatus interactions: a two-way road of function and structure. *Cell Health Cytoskeleton*, **7**:37–54
- Evangelista, M., Zigmund, S. and Boone, C. (2003). Formins: signaling effectors for assembly and polarization of actin filaments. *J. Cell Sci.*, **116**(13), 2603–2611
- Gachet, Y. and Hyams, J. S. (2005). Endocytosis in fission yeast is spatially associated with the actin cytoskeleton during polarised cell growth and cytokinesis. *J. Cell Sci.*, **118**(18), 4231–4242
- Gauthier, N. C., Masters, T. A. and Sheetz, M. P. (2012). Mechanical feedback between membrane tension and dynamics. *Trends Cell Biol.*, **22**(10), 527–535
- Giardini, P. A., Fletcher, D. A. and Theriot, J. A. (2003). Compression forces generated by actin comet tails on lipid vesicles. *Proc. Natl. Acad. Sci. U.S.A.*, **100**(11), 6493–6498
- Gomez, T. S. and Billadeau, D. D. (2009). A fam21-containing wash complex regulates retromer-dependent sorting. *Dev. Cell*, **17**(5), 699–711
- Gomez, T. S., Gorman, J. A., Artal-Martinez de Narvajias, A., Koenig, A. O. and Billadeau, D. D. (2012). Trafficking defects in wash-knockout fibroblasts originate from collapsed endosomal and lysosomal networks. *Mol. Biol. Cell*, **23**(16), 3215–3228
- Goode, B. L., Eskin, J. A. and Wendland, B. (2015). Actin and endocytosis in budding yeast. *Genetics*, **199**(2), 315–358
- Griffing, L. R. (2010). Networking in the endoplasmic reticulum. *Biochem. Soc. Trans.* **38**(3), 747–753
- Guevorkian, K., Manzi, J., Pontani, L.-L., Brochard-Wyart, F. and Sykes, C. (2015). Mechanics of biomimetic liposomes encapsulating an actin shell. *Biophys. J.*, **109**(12), 2471–2479
- Gurel, P. S., Hatch, A. L. and Higgs, H. N. (2014). Connecting the cytoskeleton to the endoplasmic reticulum and golgi. *Curr. Biol.*, **24**(14), R660–R672
- Harris, A. K., Wild, P. and Stopak, D. (1980). Silicone rubber substrata: a new wrinkle in the study of cell locomotion. *Science*, **208**(4440), 177–179
- Hatch, A. L., Gurel, P. S. and Higgs, H. N. (2014). Novel roles for actin in mitochondrial fission. *J. Cell Sci.*, **127**(21), 4549–4560
- Helfrich, W. (1973). Elastic properties of lipid bilayers: theory and possible experiments. *Zeitschrift für Naturforschung C*, **28**(11–12), 693–703
- Hochmuth, F., Shao, J.-Y., Dai, J. and Sheetz, M. P. (1996). Deformation and flow of membrane into tethers extracted from neuronal growth cones. *Biophys. J.*, **70**(1), 358–369
- Idrissi, F.-Z., Blasco, A., Espinal, A. and Gell, M. I. (2012). Ultrastructural dynamics of proteins involved in endocytic budding. *Proc. Natl. Acad. Sci. U.S.A.*, **109**(39), E2587–E2594
- Isambert, H., Venier, P., Maggs, A. C., Fattoum, A., Kassab, R., Pantaloni, D. and Carlier, M.-F. (1995). Flexibility of actin filaments derived from thermal fluctuations. effect of bound nucleotide, phalloidin and muscle regulatory proteins. *J. Biol. Chem.*, **270**(19), 11437–11444
- Ji, W.-K., Hatch, A. L., Merrill, R. A., Strack, S. and Higgs, H. N. (2015). Actin filaments target the oligomeric maturation of the dynamin gtpase drp1 to mitochondrial fission sites. *Elife*, **4**:e11553
- Joensuu, M., Belevich, I., Ramo, O., Nevzorov, I., Vihinen, H., Puhka, M., Witkos, T. M., Lowe, M., Vartiainen, M. K. and Jokitalo, E. (2014). Er sheet persistence is coupled to myosin 1c-regulated dynamic actin filament arrays. *Mol. Biol. Cell*, **25**(7), 1111–1126
- Kaksonen, M., Sun, Y. and Drubin, D. G. (2003). A pathway for association of receptors, adaptors and actin during endocytic internalization. *Cell*, **115**(4), 475–487
- Kaksonen, M., Toret, C. P. and Drubin, D. G. (2005). A modular design for the clathrin- and actin-mediated endocytosis machinery. *Cell*, **123**(2), 305–320
- Kawska, A., Carvalho, K., Manzi, J., Boujemaa-Paterski, R., Blanchoin, L., Martiel, J.-L. and Sykes, C. (2012). How actin network dynamics control the onset of actin-based motility. *Proc. Natl. Acad. Sci. U.S.A.*, **109**(36), 14440–14445

- Korobova, F., Ramabhadran, V. and Higgs, H. N. (2013). An actin-dependent step in mitochondrial fission mediated by the er-associated formin inf2. *Science*, **339**(6118), 464–467
- Korobova, F., Gauvin, T. J. and Higgs, H. N. (2014). A role for myosin ii in mammalian mitochondrial fission. *Curr. Biol.*, **24**(4), 409–414
- Kovar, D. R. and Pollard, T. D. (2004). Insertional assembly of actin filament barbed ends in association with formins produces piconewton forces. *Proc. Natl. Acad. Sci. U.S.A.*, **101** (41), 14725–14730
- Kukulski, W., Schorb, M., Kaksonen, M. and Briggs, J. A. (2012). Plasma membrane reshaping during endocytosis is revealed by time-resolved electron tomography. *Cell*, **150**(3), 508–520
- Lamour, G., Allard, A., Pelta, J., Labdi, S., Lenz, M. and Campillo, C. (2020). Mapping and modeling the nanomechanics of bare and protein-coated lipid nanotubes. *Phys. Rev. X*, **10**(1), 011031
- Lee, J., Leonard, M., Oliver, T., Ishihara, A. and Jacobson, K. (1994). Traction forces generated by locomoting keratocytes. *J. Cell Biol.*, **127**(6), 1957–1964
- Lemière, J. and Berro, J. (2018). Adaptation of actin dynamics and membrane tension control for yeast endocytosis. *bioRxiv*, 342030
- Lieber, A. D., Yehudai-Resheff, S., Barnhart, E. L., Theriot, J. A. and Keren, K. (2013). Membrane tension in rapidly moving cells is determined by cytoskeletal forces. *Curr. Biol.*, **23**(15), 1409–1417
- Liu, A. P. and Fletcher, D. A. (2006). Actin polymerization serves as a membrane domain switch in model lipid bilayers. *Biophys. J.*, **91**(11), 4064–4070
- Loisel, T. P., Boujemaa, R., Pantaloni, D. and Carlier, M.-F. (1999). Reconstitution of actin-based motility of listeria and shigella using pure proteins. *Nature*, **401**(6753), 613–616
- Lynch, C. D., Gauthier, N. C., Biais, N., Lazar, A. M., Roca-Cusachs, P., Yu, C.-H. and Sheetz, M. P. (2011). Filamin depletion blocks endoplasmic spreading and destabilizes force-bearing adhesions. *Mol. Biol. Cell*, **22**(8), 1263–1273
- Maniti, O., Carvalho, K. and Picart, C. (2013). Model membranes to shed light on the biochemical and physical properties of ezrin/radixin/moesin. *Biochimie*, **95**(1), 3–11
- Marks, M. S., Heijnen, H. F. and Raposo, G. (2013). Lysosome-related organelles: unusual compartments become mainstream. *Curr. Opin. Cell Biol.*, **25**(4), 495–505
- Martinez-Menarguez, J. A. (2013). Intra-golgi transport: roles for vesicles, tubules and cisternae. *ISRN Cell Biol.*, 2013(4200)
- Minc, N., Boudaoud, A. and Chang, F. (2009). Mechanical forces of fission yeast growth. *Curr. Biol.*, **19**(13), 1096–1101
- Miserey-Lenkei, S., Bousquet, H., Pylypenko, O., Bardin, S., Dimitrov, A., Bressanelli, G., Bonifay, R., Fraisier, V., Guillou, C., Bougeret, C., Houdusse, A. and Goud, B. (2017). Coupling fission and exit of rab6 vesicles at golgi hotspots through kinesin-myosin interactions. *Nat. Commun.*, **8** (1), 1–13
- Moore, A. S., Wong, Y. C., Simpson, C. L. and Holzbaur, E. L. (2016). Dynamic actin cycling through mitochondrial subpopulations locally regulates the fission-fusion balance within mitochondrial networks. *Nat. Commun.*, **7**(1), 1–13
- Morlot, S., Galli, V., Klein, M., Chiaruttini, N., Manzi, J., Humbert, F., Dinis, L., Lenz, M., Cappello, G. and Roux, A. (2012). Membrane shape at the edge of the dynamin helix sets location and duration of the fission reaction. *Cell*, **151**(3), 619–629
- Mosesson, Y., Mills, G. B. and Yarden, Y. (2008). Derailed endocytosis: an emerging feature of cancer. *Nat. Rev. Cancer*, **8**(11), 835–850
- Mullins, R. D., Heuser, J. A. and Pollard, T. D. (1998). The interaction of arp2/3 complex with actin: nucleation, high affinity pointed end capping and formation of branching networks of filaments. *Proc. Natl. Acad. Sci. U.S.A.*, **95**(11), 6181–6186
- Mundy, D. I., Machleidt, T., Ying, Y.-S., Anderson, R. G. and Bloom, G. S. (2002). Dual control of caveolar membrane traffic by microtubules and the actin cytoskeleton. *J. Cell Sci.*, **115**(22), 4327–4339
- Munson, M. J., Allen, G. F., Toth, R., Campbell, D. G., Lucocq, J. M. and Ganley, I. G. (2015). mtor activates the vps34-uvrag complex to regulate autolysosomal tubulation and cell survival. *EMBO J.*, **34**(17), 2272–2290
- Nixon-Abell, J., Obara, C. J., Weigel, A. V., Li, D., Legant, W. R., Xu, C. S., Pasolli, H. A., Harvey, K., Hess, H. F., Betzig, E., Blackstone, C. and Lippincott-Schwartz, J. (2016). Increased spatiotemporal resolution reveals highly dynamic dense tubular matrices in the peripheral er. *Science*, **354**(6311), aaf3928
- Noireaux, V., Golsteyn, R., Friederich, E., Prost, J., Antony, C., Louvard, D. and Sykes, C. (2000). Growing an actin gel on spherical surfaces. *Biophys. J.*, **78**(3), 1643–1654
- Oliver, T., Jacobson, K. and Dembo, M. (1995). Traction forces in locomoting cells. *Cell Motil. Cytoskeleton*, **31**(3), 225–240
- Park, S. H. and Blackstone, C. (2010). Further assembly required: construction and dynamics of the endoplasmic reticulum network. *EMBO Rep.*, **11**(7), 515–521
- Pelkmans, L., Puñtner, D. and Helenius, A. (2002). Local actin polymerization and dynamin recruitment in sv40-induced internalization of caveolae. *Science*, **296**(5567), 535–539
- Perkins, H., Ducluzaux, P., Woodman, P. G., Allan, V. J. and Waigh, T. A. (2020). Network organisation and the dynamics of tubules in the endoplasmic reticulum. *bioRxiv*
- Peskin, C. S., Odell, G. M. and Oster, G. F. (1993). Cellular motions and thermal fluctuations: the brownian ratchet. *Biophys. J.*, **65**(1), 316–324
- Picco, A., Mund, M., Ries, J., Nedelec, F. and Kaksonen, M. (2015). Visualizing the functional architecture of the endocytic machinery. *Elife*, **4**:e04535
- Picco, A., Kukulski, W., Manenshijn, H. E., Specht, T., Briggs, J. A. and Kaksonen, M. (2018). The contributions of the actin machinery to endocytic membrane bending and vesicle formation. *Mol. Biol. Cell*, **29**(11), 1346–1358
- Pimm, M. L. and Henty-Ridilla, J. L. (2021). New twists in actin-microtubule interactions. *Mol. Biol. Cell*, **32**(3), 211–217
- Pontani, L.-L., Van der Gucht, J., Salbreux, G., Heuvingsh, J., Joanny, J.-F. and Sykes, C. (2009). Reconstitution of an actin cortex inside a liposome. *Biophys. J.*, **96**(1), 192–198
- Prinz, W. A., Grzyb, L., Veenhuis, M., Kahana, J. A., Silver, P. A. and Rapoport, T. A. (2000). Mutants affecting the structure of the cortical endoplasmic reticulum in *saccharomyces cerevisiae*. *J. Cell Biol.*, **150**(3), 461–474
- Ratamero, E. M. and Royle, S. J. (2019). Calculating the maximum capacity of intracellular transport vesicles. *BioRxiv*, 555813
- Ripoll, L., Heiligenstein, X., Hurbain, I., Domingues, L., Figon, F., Petersen, K. J., Dennis, M. K., Houdusse, A., Marks, M. S., Raposo, G. and Delevoeye, C. (2018). Myosin vi and branched actin filaments mediate membrane constriction and fission of melanosomal tubule carriers. *J. Cell Biol.*, **217**(8), 2709–2726
- Rohlich, P. and Allison, A. (1976). Oriented pattern of membrane-associated vesicles in fibroblasts. *J. Ultrastruct. Res.*, **57**(1), 94–103
- Romer, W., Berland, L., Chambon, V., Gaus, K., Windschiegel, B., Tenza, D., Aly, M. R., Fraisier, V., Florent, J.-C., Perrais, D., Lamaze, C., Raposo, G., Steinem, C., Sens, P., Bassereau, P. and Johannes, L. (2007). Shiga toxin induces tubular membrane invaginations for its uptake into cells. *Nature*, **450**(7170), 670–675
- Romer, W., Pontani, L.-L., Sorre, B., Rentero, C., Berland, L., Chambon, V., Lamaze, C., Bassereau, P., Sykes, C., Gaus, K. and Johannes, L. (2010). Actin dynamics drive membrane reorganization and scission in clathrin-independent endocytosis. *Cell*, **140**(4), 540–553

- Rong, Y., Liu, M., Ma, L., Du, W., Zhang, H., Tian, Y., Cao, Z., Li, Y., Ren, H., Zhang, C., Li, L., Chen, S., Xi, J., Yu, L. (2012). Clathrin and phosphatidylinositol-4, 5-bisphosphate regulate autophagic lysosome reformation. *Nat. Cell Biol.*, **14**(9), 924–934
- Roux, A. (2013). The physics of membrane tubes: soft templates for studying cellular membranes. *Soft Matter*, **9**(29), 6726–6736
- Roux, A., Cuvelier, D., Nassoy, P., Prost, J., Bassereau, P. and Goud, B. (2005). Role of curvature and phase transition in lipid sorting and fission of membrane tubules. *EMBO J.*, **24**(8), 1537–1545
- Roux, A., Koster, G., Lenz, M., Sorre, B., Manneville, J.-B., Nassoy, P. and Bassereau, P. (2010). Membrane curvature controls dynamin polymerization. *Proc. Natl. Acad. Sci. U.S.A.*, **107** (9), 4141–4146
- Rowland, A. A., Chitwood, P. J., Phillips, M. J. and Voeltz, G. K. (2014). Er contact sites define the position and timing of endosome fission. *Cell*, **159**(5), 1027–1041
- Saffi, G. T. and Botelho, R. J. (2019). Lysosome fission: planning for an exit. *Trends Cell Biol.*
- Schiavon, C. R., Zhang, T., Zhao, B., Moore, A. S., Wales, P., Andrade, L. R., Wu, M., Sung, T.-C., Dayn, Y., Feng, J. W., Quintero, O. A., Shadel, G. S., Grosse, R. and Manor, U. (2020). Actin chromobody imaging reveals sub-organellar actin dynamics. *Nat. Methods*, **17**(9), 917–921
- Schulze, R. J., Weller, S. G., Schroeder, B., Krueger, E. W., Chi, S., Casey, C. A. and McNiven, M. A. (2013). Lipid droplet breakdown requires dynamin 2 for vesiculation of autolysosomal tubules in hepatocytes. *J. Cell Biol.*, **203**(2), 315–326
- Shao, J.-Y. and Hochmuth, R. M. (1996). Micropipette suction for measuring piconewton forces of adhesion and tether formation from neutrophil membranes. *Biophys. J.*, **71**(5), 2892–2901
- Shin, W., Ge, L., Arpino, G., Villarreal, S. A., Hamid, E., Liu, H., Zhao, W.-D., Wen, P. J., Chiang, H.-C. and Wu, L.-G. (2018). Visualization of membrane pore in live cells reveals a dynamic-pore theory governing fusion and endocytosis. *Cell*, **173**(4), 934–945
- Simon, C., Kusters, R., Caorsi, V., Allard, A., Abou-Ghali, M., Manzi, J., Di Cicco, A., Lévy, D., Lenz, M., Joanny, J.-F., Campillo, C., Plastino, J., Sens, P. and Sykes, C. (2019). Actin dynamics drive cell-like membrane deformation. *Nat. Phys.*, **15**(6), 602–609
- Simunovic, M., Manneville, J.-B., Renard, H.-F., Evergren, E., Raghunathan, K., Bhatia, D., Kenworthy, A. K., Voth, G. A., Prost, J., McMahon, H. T., Johannes, L., Bassereau, P. and Callan-Jones, A. (2017). Friction mediates scission of tubular membranes scaffolded by bar proteins. *Cell*, **170** (1), 172–184
- Sinha, B., Koster, D., Ruez, R., Gonnord, P., Bastiani, M., Abankwa, D., Stan, R. V., Butler-Browne, G., Vedie, B., Johannes, L., Morone, N., Parton, R. G., Raposo, G., Sens, P., Lamaze, C. and Nassoy, P. (2011). Cells respond to mechanical stress by rapid disassembly of caveolae. *Cell*, **144** (3), 402–413
- Sirotkin, V., Berro, J., Macmillan, K., Zhao, L. and Pollard, T. D. (2010). Quantitative analysis of the mechanism of endocytic actin patch assembly and disassembly in fission yeast. *Mol. Biol. Cell*, **21**(16), 2894–2904
- Skruzny, M., Brach, T., Ciuffa, R., Rybina, S., Wachsmuth, M. and Kaksonen, M. (2012). Molecular basis for coupling the plasma membrane to the actin cytoskeleton during clathrin-mediated endocytosis. *Proc. Natl. Acad. Sci. U.S.A.*, **109**(38), E2533–E2542
- Soykan, T., Kaempf, N., Sakaba, T., Vollweiler, D., Goerdeler, F., Puchkov, D., Kononenko, N. L. and Haucke, V. (2017). Synaptic vesicle endocytosis occurs on multiple timescales and is mediated by formin-dependent actin assembly. *Neuron*, **93**(4), 854–866
- Sparkes, I., Runions, J., Hawes, C. and Griffing, L. (2009). Movement and remodeling of the endoplasmic reticulum in nondividing cells of tobacco leaves. *Plant Cell*, **21**(12), 3937–3949
- Sridhar, S., Patel, B., Aphkzava, D., Macian, F., Santambrogio, L., Shields, D. and Cuervo, A. M. (2013). The lipid kinase pi4kiii β preserves lysosomal identity. *EMBO J.*, **32**(3), 324–339
- Sullivan, L. (1896). The tall office building artistically considered. *Lippincotts Magazine*, 403–409
- Terasaki, M., Chen, L. B. and Fujiwara, K. (1986). Microtubules and the endoplasmic reticulum are highly interdependent structures. *J. Cell Biol.*, **103**(4), 1557–1568. ISSN 0021-9525. <https://doi.org/10.1083/jcb.103.4.1557>
- Trichet, L., Sykes, C. and Plastino, J. (2008). Relaxing the actin cytoskeleton for adhesion and movement with ena/vasp. *J. Cell Biol.*, **181**(1), 19
- Upadhyaya, A., Chabot, J. R., Andreeva, A., Samadani, A. and van Oudenaarden, A. (2003). Probing polymerization forces by using actin-propelled lipid vesicles. *Proc. Natl. Acad. Sci. U.S.A.*, **100**(8), 4521–4526
- Watanabe, S., Trimbuch, T., Camacho-Pérez, M., Rost, B. R., Brokowski, B., Söhl-Kielczynski, B., Felies, A., Davis, M. W., Rosenmund, C. and Jorgensen, E. M. (2014). Clathrin regenerates synaptic vesicles from endosomes. *Nature*, **515**(7526), 228–233
- Waugh, R. E. and Hochmuth, R. M. (1987). Mechanical equilibrium of thick, hollow, liquid membrane cylinders. *Biophys. J.*, **52**(3), 391–400
- Yoshida, A., Sakai, N., Uekusa, Y., Imaoka, Y., Itagaki, Y., Suzuki, Y. and Yoshimura, S. H. (2018). Morphological changes of plasma membrane and protein assembly during clathrin-mediated endocytosis. *PLoS Biol.*, **16**(5), e2004786
- Yu, L., McPhee, C. K., Zheng, L., Mardones, G. A., Rong, Y., Peng, J., Mi, N., Zhao, Y., Liu, Z., Wan, F., Hailey, D. W., Oorschot, V., Klumperman, J., Baehrecke, E. H. and Lenardo, M. J. (2010). Autophagy termination and lysosome reformation regulated by mtor. *Nature*, **465** (7300), 942
- Yu, L., Chen, Y. and Tooze, S. A. (2018). Autophagy pathway: cellular and molecular mechanisms. *Autophagy*, **14**(2), 207–215

Received: 1 December 2020; Revised: 25 March 2021; Accepted: 27 March 2021; Accepted article online: 7 April 2021

3 MATERIALS AND METHODS

3.1 BUFFERS

If not specified, all chemicals are purchased from Sigma-Aldrich (St. Louis, Missouri). The buffer for nanotube formation, referred to as NaCl buffer, contains 100 mM NaCl and 20 mM [(4-(2-hydroxyethyl)-1-piperazineethanesulfonic acid) HEPES] at pH 7.4. A second buffer, referred to as TPI (the internal buffer of GUVs) contains 200 mM sucrose, 2 mM Tris in Milli Q water. Then, for actin polymerisation experiments, we used a buffer referred to as TPE (the external buffer of GUVs) that contains 95 mM sucrose, 1 mM Tris, 50 mM KCl, 2 mM MgCl₂, 0.1 mM DTT, 0.02 mg/ml β -casein and 2 mM ATP in Milli Q water. A third buffer, referred to as G-buffer, is used to prepare actin monomers in solution. It contains 2 mM Tris, 0.2 mM CaCl₂, 0.2 mM DTT and 0.2 mM ATP. To avoid ATP denaturation, its addition to TPE or G-buffer is executed on ice. Final buffers are adjusted to 7.4 pH and 200 mOsm. They are stored at -20°C for up to 6 months.

3.2 BIOMIMETIC MEMBRANE SYSTEMS

1,2-dioleoyl-sn-glycero-3-phosphocholine (referred to as DOPC), N-(dodecanoyl)-sphing-4-enine-1-phosphocholine (sphingomyelin, referred to as SM), cholesterol (referred as C) from ovine wool, DSPE-PEG (2000)-Biotin (1,2-distearoyl-sn-glycero-3-phosphoethanolamine-N-[biotinyl(polyethylene glycol) 2000]) (PEG-biotin lipids) and 18:1 DGS-NTA(Ni) (1,2-dioleoyl-sn-glycero-3-[(N-(5-amino-1-carboxypentyl)iminodiacetic acid)succinyl] (Ni-NTA) are obtained from Avanti® Polar Lipids, Inc. (Alabaster, AL). Fluorescent lipids are Texas Red™ r-1,2-dihexadecanoylsn-glycero-3-phosphoethanolamine triethylammonium salt (Texas-Red™ DHPE) and 4,4-Difluoro-5,7-Dimethyl-4-Bora-3a,4a-Diaza-s-Indacene-3-Pentanoic Acid (BODIPY™ FL C5) from ThermoFisher (Waltham, MA).

Figure 11 recapitulates all the lipid compositions used in this work: standard homogenous membranes and ternary lipid mixtures (referred

to as heterogeneous) forming lipid domains. Ternary lipid mixture containing DOPC, cholesterol and sphingomyelin (at a molecular ratio of 2:1:2) are mixed with fluorescent lipids at 0.5% and PEG-biotin at 0.1 % or 3 % to prepare Giant Unilamellar Vesicles (GUV) or nanotubes, respectively. Final lipid mixtures are at 2.5 mg/mL in the organic solvent chloroform/methanol 5:3 (v:v) and stored at -20°C. Lipid mixtures are ready to be deposited on the proper support to form GUVs or lipid nanotubes.

3.2.1 Giant Unilamellar Vesicles preparation

GUVs are prepared using the electroformation technique, adapted from (Angelova and Dimitrov 1988), which consists in rehydrating a dried lipid film under an electric field. The first step is to spread a 10 μ L lipid mixture on the conductive side of two indium tin oxide (ITO)-coated glass slides. A nitrogen stream dries the organic solvent applied for a few seconds. A 1 mm thick PDMS spacer is placed between the two ITO glass slides (conductive sides facing each other), forming a closed chamber, which is then filled with 400 μ L TPI using a 0.75 μ m diameter needle syringe. An alternating current is applied (10 Hz, 1 V RMS) between the two slides for two h. For homogeneous lipid mixtures, this step is performed at room temperature and over the miscibility temperature for heterogeneous lipid mixtures, which is 60°C. GUVs are then collected using the same syringe and conserved at 4°C for up to one week.

Composition	Mol %				
	Homogeneous		Heterogeneous		
Sphingomyelin	-	64.5	42.8	42.8	42.8
Cholesterol	-	34.9	13.8	13.8	13.8
DOPC	99.4	-	42.8	42.8	42.8
DSPE-PEG (2000) Biotin	0.1	0.1	0.1 (3 for nanotubes)		-
DGS-NTA(Ni)	-	-	-	-	1
TexasRed- DHPE	0.5	0.5	0.5	-	0.5
Bodipy-FL-C5	-	-	-	0.1	-

Figure 11: Composition of homogeneous and heterogeneous lipid mixtures used for GUVs or nanotube preparation, including fluorescent lipids and lipids used to bind actin NPF (PEG-biotin and Ni-NTA).

3.2.2 Supported membrane nanotubes

To perform AFM analysis and extract the mechanical properties of lipid nanotubes, the latter must be attached to a surface, as presented later in section 4.1. Thus, we will present here how we coat glass substrates.

Glass functionalisation with streptavidin

For this work, we used 35 mm dishes comprising a 14 mm-diameter uncoated glass well at their centre (MatTek Corporation, Ashland, MA). They avoid using standard 35 mm dishes and thus reduce the amount

of proteins used for actin network reconstitution assays.

Firstly, glass bottom wells are cleaned with ethanol, activated by ozone exposition, and filled with a solution of 94 % methanol, 4 % deionised water, 2 % of 3-aminopropyl-triethoxysilane (APTES, 97 % purity; from Sigma-Aldrich, St. Louis, Missouri) (v:v) and 1 mM acetic acid. After 48 h, a coat of APTES is formed on top of the glass by chemisorption as depicted in **Figure 12**. The glass surface is rinsed with ethanol and dried with a nitrogen stream. Then, a monolayer of streptavidin is grafted on the APTES layer by first immersing the silanised glass in a glutaraldehyde solution (12 % in water), which is rinsed with water after 20 min, and then, for 50 min in a solution of streptavidin (from Sigma-Aldrich) diluted at 5 $\mu\text{g}/\text{mL}$ in PBS. To elute and eliminate non-covalently bound streptavidin, the glass surface is rinsed in the following order with PBS, SDS (0.01 % in water) and deionised water to remove salts. Finally, the surface is dried with a nitrogen stream and kept dry for up to 3 months.

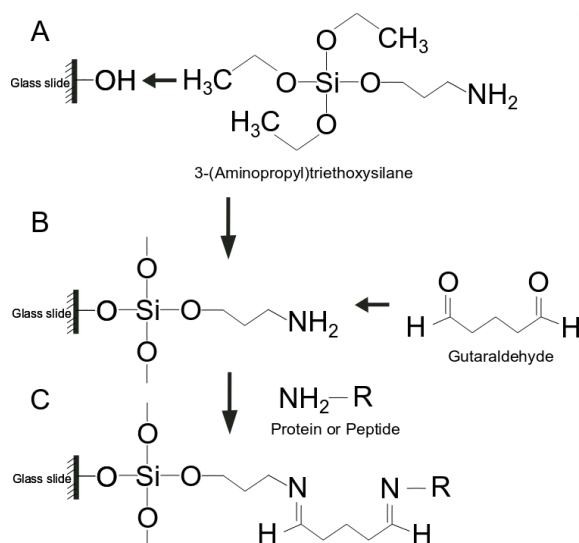


Figure 12: Glass silanisation steps. A: Formation of APTES monolayer on the glass; B: Formation of a covalent bridge by glutaraldehyde (aldehyde groups) between APTES (amine group) and C: Streptavidin (represented by R bonded to an amine group)

Formation of lipid nanotubes

1 μL of the desired lipid mixture at 2 mg/mL is deposited in several droplets of about 0.1 μL on streptavidin-coated glass. The organic solvent is dried with a nitrogen stream. Lipid droplets are rehydrated in 2 mL NaCl buffer at 100 mM. Then, a hydrodynamic flow is manually applied with a 1 mL pipette to form tubes from the lipid deposits. Lipids presenting a PEG-biotin at their polar heads bind to streptavidin, forming supported lipid nanotubes. At last, the chamber is rinsed twice with 2 mL of TPI to remove exceeding floating lipids. Lipid nanotubes are now ready for experiments and microscope observation.

3.3 RECONSTITUTED ACTIN NETWORKS

Porcine Arp2/3, alpha-actinin (rabbit skeletal muscle, >90% pure) and fascin (Wild-Type, Human Recombinant, > 95% pure) are purchased from Cytoskeleton (Denver, CO). Proline-rich domain VCA of human WASP with a streptavidin and histidine tag (S-pVCA-His), mouse $\alpha 1\beta 2$ capping protein and profiling are all purified at UMR 168, PhysicoChimie Curie by John Manzi.

Biotinylated or nickel lipids are used to link the proline-rich domain VCA (pVCA) of human WASP via its streptavidin or histidine tag (S-pVCA-His), respectively, to activate the Arp 2/3 complex and actin polymerisation.

Preparation of actin monomers

For this reconstitution, commercial actin (rabbit skeletal muscle, >99% pure from Cytoskeleton, Denver, CO) and fluorescent actin (Actin, from rabbit muscle, Alexa Fluor™ 488 conjugate, in solution from Thermofisher, Waltham, MA) are mixed at a ratio of 15% in G-buffer at a final concentration of 30 μM of actin monomers and left to depolymerise for 48h. This actin solution is then stored at 4°C for up to 3 weeks.

Actin polymerisation on the GUVs surface

First, we coat the GUV surface comprising biotinylated lipids with the

NPF SpVCA. In an Eppendorf tube, 10 μL of freshly electroformed GUVs are incubated in 350 μM SpVCA for a final volume of 20 μL in TPE for 15 minutes. In a second Eppendorf tube, 5 minutes before SpVCA coating is completed, 15 μL of the actin polymerisation cocktail is prepared in TPE with the following actin-binding proteins (ABP) at the following concentrations: 37 nM Arp2/3, 25 nM capping protein, 3 μM profilin, and 3 μM actin monomers as in (Carvalho et al. 2013). For further experiments, we added α -actinin or fascin at a ratio of $\frac{1}{4}$ for G-actin to the polymerisation solution. Then, 5 μL of SpVCA-coated GUVs are added for actin polymerisation for 15 minutes and finally diluted twice in TPE to stop polymerisation.

Actin polymerisation on nanotubes

The Actin polymerisation protocol on tubes is adapted from the protocol for GUVs. Tubes are attached to the glass-bottom microwells of the Mattek dishes, which volume is 150 μL , and after nanotube formation, the whole dish is filled with 2 mL TPI. Then, TPI is carefully removed, leaving 150 μL at the glass-bottom microwell, and the whole dish is refilled with 2 mL TPE, the suitable buffer for SpVCA coating.

Before SpVCA coating, we remove TPE, leaving 150 μL in the glass-bottom microwell used for incubation. Incubation time is 15 minutes for a final concentration of 800 nM SpVCA in the microwell. After that, non-bounded SpVCA is removed to prevent non-specific actin polymerisation by gently adding 2 mL of TPE in the Mattek well and removing it, leaving 150 μL in the glass-bottom microwell. Then, the actin polymerisation solution at final concentrations of ABPs and actin added into the 150 μL microwell corresponds to the concentrations used for actin polymerisation on GUVs.

3.4 MICROSCOPY TECHNIQUES

3.4.1 Epifluorescence microscopy

Fluorescent images are acquired using a Zeiss inverted microscope with a 63x oil-immersion objective to perform epifluorescence microscopy (GFP filter cube, excitation 470 nm, emission 525 nm; Texas red filter cube: excitation 545–580 nm). Images are collected by AxioCam MRm® camera (Zeiss).

Image analysis are performed with ImageJ software. On the GUVs, the coupled to actin networks following parameters were measured:

- I. size is obtained by fitting an ellipse to the GUV contour,
- II. aspect ratio,
- III. actin tail length

3.4.2 Stimulated Emission Depletion Microscopy (STED)

The principle of STED relies on a donut shape-controlled fluorescence (**Figure 13**). This means that at the central hole, an excitation wavelength activates the fluorochromes, and a second beam induces a ground state around this central area. The constricted activated area is around 20 nm, which makes STED a super resolution microscopy technique.

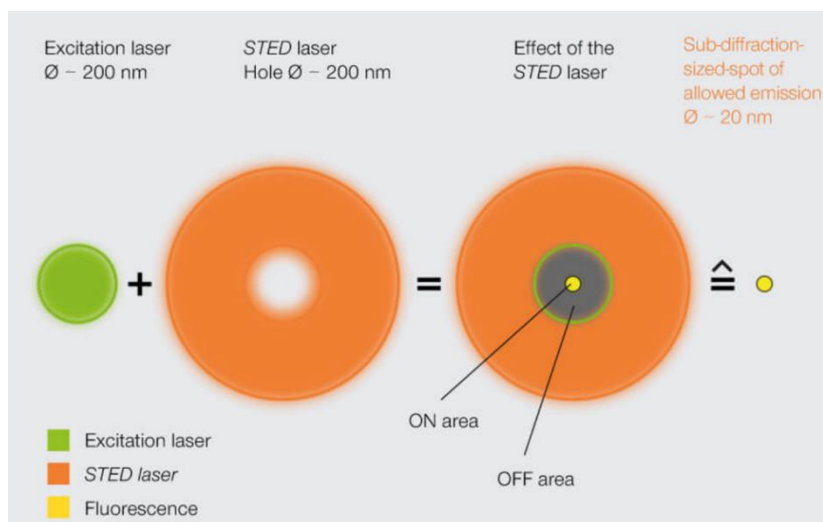


Figure 13: Scheme of STED microscopy principle showing the excitation laser at the centre surrounded by the STED laser, which results in a 20 nm central fluorescence point (<https://abberior.rocks/knowledge-base/how-the-donut-changed-the-world/>).

For STED microscopy assays, abberior STAR RED conjugated to 1,2-dioleoyl-sn-glycero-3-phosphoethanolamine (DOPE) was kindly provided by Frédéric Eghiaian from Abberior instruments. STAR RED is also known as KK114, and a wavelength between 630 – 650 nm can excite it. At 0.2 % STAR RED-DOPE replaced TexasRed-DHPE for STED experiments.

3.4.3 Atomic Force Microscopy (AFM)

For AFM experiments, we used BL-AC40TS-C2 cantilevers (Olympus). The tip apex is in silicon, has a radius of around 8 nm, resonates at about 25 kHz in liquid, and has a spring constant of 0.09–0.12 N/m. We used the Quantitative Imaging™ mode that scans samples recording a force spectroscopy curve in every location.

Our acquisition parameters are as follows: z length of 50-150 nm; vertical tip speed of 10-30 $\mu\text{m/s}$ and the force setpoint at a range of 50-100 pN. The force curves are fitted by $f = \kappa \cdot \delta^2$, where κ corresponds to the local rigidity and δ to the contact point of the tip on the sample.

3.5 MICROFLUIDIC DEVICES

We will see in section 4.2 the need to develop an assay allowing blocking GUVs in microtraps. For this purpose, we used an epoxy microfluidic mould realised by Jacques Fattaccioli's team at CNRS UMR 8640. The microfluidic device printed on PDMS forms a chamber after bonding to a glass slide. The microfluidic device contains designed structures that trap GUVs entering the chamber using a hydrodynamic flow but also allow the further insertion of proteins on the GUVs.

First step: Preparation of PDMS

PDMS is mixed with a curing agent (Sylgard 184) at a mass ratio of 1:10 and degassed under a vacuum pump for about 20 min.

Second step: Printing traps onto PDMS

Once degassed, the PDMS is poured on the epoxy mould and cured at 80°C for at least two hours to obtain a PDMS device with traps (**Figure 31**). Then, the inlet (2.5 mm diameter) and the outlet (0.5 mm diameter) are punched into the solid PDMS device.

Third step: Assembly of the microfluidic device

A glass slide is cleaned with ethanol and dried with a nitrogen stream, and both PDMS and glass slides are treated with air plasma for 30 seconds. PDMS's trap side is turned to the activated glass side and bonded via Si-O-Si links. A gentle pressure is applied to maximise surface contact.

Right after, to prevent further interactions of injected compounds with the PDMS and glass surfaces, we had to passivate the interior of the chamber. We have tried several compounds (see details in section 4.3): Polyvinyl pyrrolidone [poly(N-vinyl-2-pyrrolidone), PVP] at 20% (W:V), PLL-g-PEG at 0,5 mg/ml and Pluronic® F-127, a non-ionic copolymer at 2%(W:V).

4 RESULTS

4.1 PHASE-SEPARATED LIPID NANOTUBES

This section presents the study of phase-separated membrane nanotubes that I prepared and characterised using high-resolution STED and AFM microscopy. I used STED to highlight the morphology of L_o and L_d domains along the nanotubes. Then, I probed their morphology and mechanics by AFM applying the model developed by (Lamour et al. 2020) for homogeneous nanotubes.

So far, only two papers have observed phase-separated nanotubes: (Roux et al. 2005) studied their fission, and (Yuan et al. 2008) showed the light-induced formation of disc-like domains along the nanotubes. The work presented here is the first step towards constructing a biomimetic assay comprising phase-separated nanotubes and actin networks to address the question of tube remodelling by actin dynamics.

4.1.1 Preparation of phase-separated membrane nanotubes

First, we sought to prepare nanotubes using a ternary lipid composition (DOPC/SM/Cholesterol 2/2/1) known to form lipid domains in SLBs and GUVs (Sorre et al. 2009; Veatch and Keller 2003) when the temperature is below the miscibility temperature of 37°C.

We adapted the protocol presented in (Lamour et al. 2020) for homogeneous nanotubes. The nanotubes are formed at a temperature above the miscibility temperature, around 60°C, and then left to cool to room temperature before observation. By epifluorescence microscopy, we observed Liquid disordered (L_d) and Liquid ordered (L_o) domains coexisting along the nanotubes (**Figure 14 A**). These domains are observable and distinguishable by fluorescence microscopy: L_d domains being enriched in fluorescent lipids (Baumgart, Hunt, et al. 2007) appear much brighter than L_o domains. In our experiments,

nanotubes are attached to a glass surface functionalized with streptavidin for AFM experiments, as described in section 3.2.2. In the case of phase-separated nanotubes, the PEG-Biotinylated lipids are segregated in L_o domains (we verified this using GUVs, see section 4.2.2.2). Therefore, the L_o domains are attached to the substrate, and the L_d domains are free. Note that we never observed nanotube fission in our experiments.

Then, we sought to elucidate the structure of these phase-separated nanotubes at a higher resolution. To do so, we imaged the nanotubes using confocal microscopy and STED, and compared the acquired images. In confocal microscopy, the size difference between the domains is hardly distinguishable (**Figure 14 B**), whereas, in STED, we clearly see the morphology difference between L_o and L_d domains, as shown in **Figure 14 C**. To quantify this difference, we drew fluorescence intensity profiles across L_o (blue box in **Figure 14 C**) and L_d (red box in **Figure 14 C**) domains. Characteristic profiles are shown in **Figure 14 D**. For L_o domains, we clearly distinguish the two edges of the nanotube, which appear as two peaks on the fluorescence profile, and thus easily provide a measurement of the nanotube width. For L_d domains, the diameter of the nanotubes is comparable with the resolution of STED (around a few tens of nanometers), the profile thus shows a single intensity peak, and we use the width of this peak at half of its maximum height to evaluate the tube diameter. **Figure 14 E** shows that L_o domains are much wider than L_d domains ($686 \text{ nm} \pm 233 \text{ nm}$ vs. $120 \text{ nm} \pm 34 \text{ nm}$). Knowing the relationship between tube force, tube radius and membrane rigidities (see equation in section 2.1.2) and assuming a force equilibrium between L_o and L_d domains, we can write for phase-separated nanotubes without attachment (Allain et al. 2004; M. Heinrich et al. 2010):

$$f_{L_o} = f_{L_d} \text{ implies } \frac{k_{L_o}}{k_{L_d}} = \frac{\sigma_{L_d}}{\sigma_{L_o}} \text{ or } \frac{k_{L_o}}{r_{L_o}} = \frac{k_{L_d}}{r_{L_d}} \text{ and thus } \frac{k_{L_o}}{k_{L_d}} = \frac{r_{L_o}}{r_{L_d}} = \frac{\sigma_{L_d}}{\sigma_{L_o}} \quad (11)$$

Knowing the values of κ for L_o and L_d domains, 65 and $20 \kappa_B T$, respectively (note that we assume that the segregation of the lipids is total between the domains), L_o domains should be 3.25 times wider than L_d domains for free nanotubes. In our case, the ratio $\frac{r_{L_o}}{r_{L_d}}$ is 5.7,

meaning the nanotubes are much wider than the prediction above (M. Heinrich et al. 2010). As our nanotubes are attached by the L_o domains, these domains are probably not cylindrical. Moreover, as described above, the method used to measure L_d domains diameter provides a rough approximation compared to L_o domains that are measured from one fluorescence intensity peak to another.

In **Figure 14 F**, we followed the previous estimations (Eq.8) to calculate theoretical values of the membrane tension in L_o and L_d domains using $\sigma = \kappa/2r^2$. Each point on the plot represents the tension of the L_o domain as a function of the tension of the L_d domain for one nanotube. A linear fit of our data gives a value for $\frac{\sigma_{L_d}}{\sigma_{L_o}}$ of 3.84 whereas the ratio $\frac{\kappa_{L_o}}{\kappa_{L_d}}$ is 3.25. Nevertheless, the dispersion of points is wide, and no clear trend emerged from this plot.

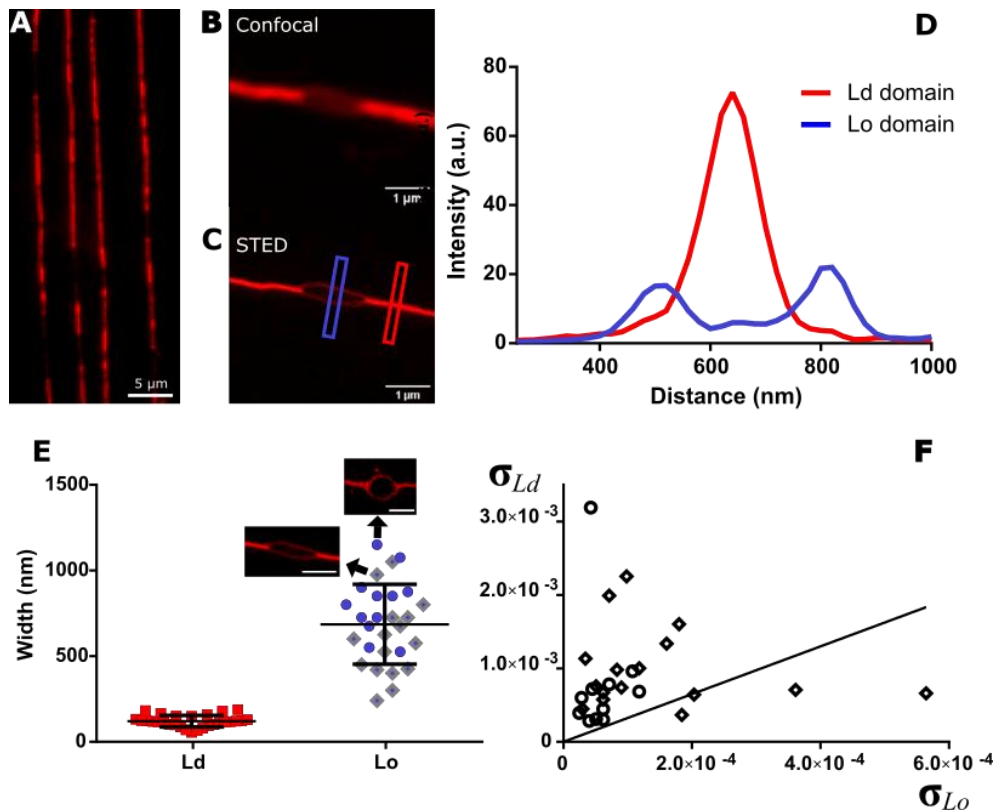


Figure 14: Observation of phase-separated nanotubes. A: epifluorescence microscopy image showing an array of phase-separated nanotubes. B: confocal image of a nanotube vs. C: STED image of the same nanotube clearly show a difference between L_o and L_d domains. D: fluorescence intensity profile from the blue and red boxes in panel C, corresponding to the L_o and L_d domains. E: nanotubes diameter in L_o and L_d domains. Each point represents a nanotube. Square points represent elongated L_o domains as in C, and round points for sphere-like L_o domains. F: nanotube tension calculated from nanotube diameter and bending rigidity. The slope is 3.84 ± 1.15 . $N=3$ independent experiments corresponding to 28 nanotubes.

4.1.2 Probing mechanical properties of phase-separated membrane nanotubes

Phase-separated nanotubes present morphological differences between different domains. Here, we use AFM to acquire

nanomechanical maps of these nanotubes. We follow the approach developed by (Lamour *et al.* 2020), who showed the relationship between the height and the rigidity of homogenous nanotubes using AFM.

First, we image phase-separated nanotubes by fluorescence microscopy to spot boundaries between L_o and L_d domains. Then, we record $1\ \mu\text{m}$ by $1\ \mu\text{m}$ AFM images of these regions using AFM in Quantitative Imaging (QI, from JPK-Bruker) mode. In this imaging mode, the AFM tip is vertically moved in the direction of the sample at each point of the image. During the approach sequence, the tip touches the sample and provides the height of the contact point. Then, the tip indents the sample up to a predefined force called “force setpoint” (**Figure 15 A**). The part of the force curve corresponding to the indentation is fitted by $F = K\delta^2$ with F the force on the tip, and δ the indentation depth to obtain the nanotube rigidity K . Thus, from this sequence, we simultaneously obtain maps of the sample morphology and rigidity (**Figure 15 B**).

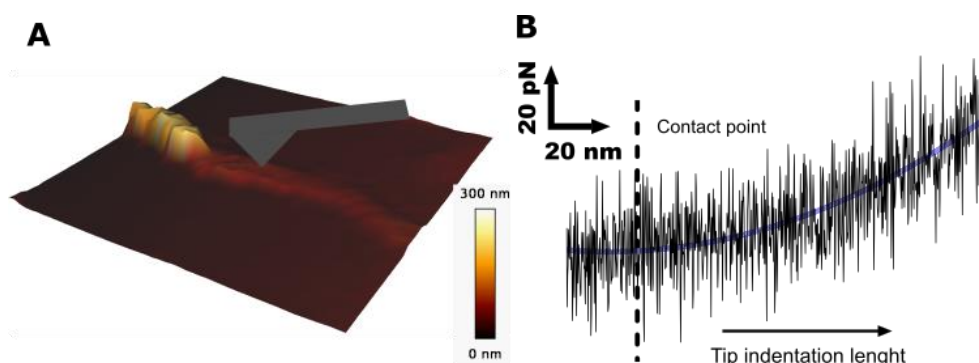


Figure 15: AFM Quantitative imaging of phase-separated nanotube. A: 3D topography image of nanotube composed by L_o and L_d domains over which the AFM cantilever is represented in grey. B: Force-distance curve corresponding to one pixel from a nanotube image.

Figure 16 (A and B) shows topography and rigidity maps of the boundary between two adjacent domains along a single nanotube. In **Figure 16 C**, we draw an intensity profile from the height and rigidity

maps of **Figure 16** A and B. The differences in height and rigidity between the L_o and L_d domains are clearly visible: the L_d domain is smaller and stiffer than the L_o domain. In **Figure 16** D, we gathered the widths and heights of the L_d and L_o domains of our nanotubes. AFM images show that L_d domains appear wider than high, whereas their L_o domains have similar widths and heights. This was also observed by (Lamour *et al.* 2020) for homogeneous nanotubes made of DOPC or SM/Cholesterol. The widths obtained by AFM are close to the value measured on STED images for L_d domains. For L_o domains, the widths are higher than the heights, even if this effect is less pronounced in the AFM measurements.

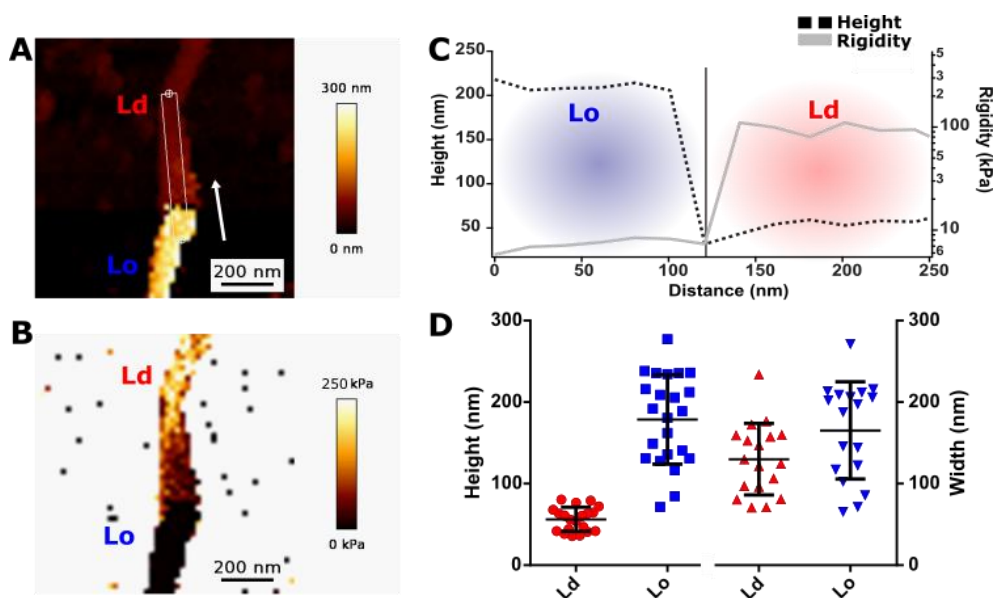


Figure 16: AFM nanomechanical mapping of phase-separated nanotubes. A: Topography map. B: Rigidity map. C: Intensity profile corresponding to the white box in A showing differences in height and rigidity along the nanotube. D: Height vs. Width for a population of nanotubes.

The model developed by (Lamour *et al.* 2020) predicts a power-law relationship between the rigidity of nanotubes and their height. We tested if this model works for the L_d and L_o domains of phase-separated nanotubes.

For all the nanotubes presented in **Figure 14**, we plot in **Figure 17 A** their height (h) vs. rigidity (K) in the L_d and L_o domains. The data corresponding to the two domains of the same nanotube are represented by the same symbol in the histograms of **Figure 17 A** and B. In **Figure 17 A**, a power law dependence between K and height is indeed observed for the L_d (red dots) and L_o (blue dots) domains. The red and blue lines display the predicted trend from (Lamour et al. 2020):

$$K = 22 k^{\frac{3}{2}} (k_B T)^{-\frac{1}{2}} h^{-3} \quad (12)$$

with no adjustable parameter, where κ is the bending rigidity of the membrane. Then, the normalized rigidity:

$$\tilde{K} = \frac{K}{\left[22 k^{\frac{3}{2}} (k_B T)^{-\frac{1}{2}} \right]} \quad (13)$$

is plotted against nanotube height in **Figure 17 B**, and all values collapse on the same master curve as predicted. This shows that the model also accurately predicts the relationship between nanotube rigidity and height in the case of phase-separated nanotubes.

Furthermore, the model provides a prescription to compute the local membrane tension from the rigidity of the nanotube:

$$\sigma = \frac{2}{22^{2/3}} (k_B T)^{1/3} K^{2/3} \quad (14)$$

As a result, for each nanotube, we calculated the distinct tensions of the L_d and L_o domains. These tensions are plotted in **Figure 17** (insert) and show that the calculated tensions in the two domains are coherent with the values of the bending rigidities as predicted by (M. Heinrich et al. 2010) (Eq. 14).

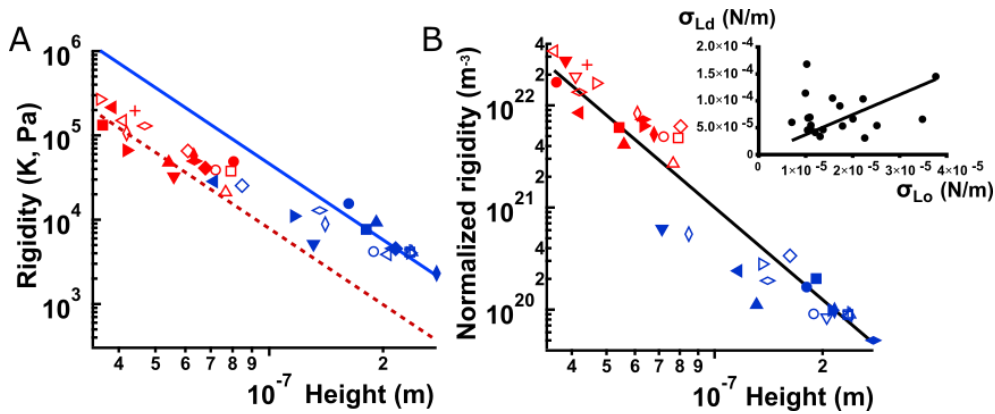


Figure 17: Mechanical properties of phase-separated nanotubes. AFM data of nanotubes represented by different symbols. The L_d and L_o domains of a nanotube are shown as red and blue, respectively. A: nanotube rigidity plotted as a function of the nanotube height. B: normalised rigidity, \tilde{K} vs. nanotube height. Insert: the tension of L_d domain as a function of the tension in the L_o domain. The slope is 3.75 ± 0.40 .

Therefore, we successfully prepared phase-separated nanotubes from mixtures of DOPC, SM and cholesterol. We indeed observed micron-sized domains along the nanotubes, as evidenced by fluorescent images. Using STED microscopy, we directly saw the difference in size between the L_d and L_o domains. Finally, we use AFM to observe these differences in size coupled with differences in local tension. The power-law relationship between nanotube height and nanotube rigidity predicted by (Lamour et al. 2020) for homogeneous nanotubes still works for phase-separated nanotubes. This assay could be used to test the remodelling of phase-separated nanotubes by actin dynamics.

4.2 ACTIN-INDUCED SHAPE CHANGES ON GUVs

In this section, I present my results on the shape changes induced by the polymerisation of an actin network at the surface of GUVs. I will study how these shape changes are affected, first, by membrane mechanics and then by the structure of the actin network. First, we work on GUVs with homogeneous membranes of different bending rigidities and study how they deform in the presence of an Arp2/3-nucleated actin network. Then, we assess the effect of the crosslinkers α -actinin and fascin on these homogeneous GUVs. Finally, I present results on GUVs whose membranes show phase-separated lipid domains coupled with the same types of actin networks: branched Arp2/3 networks, with and without crosslinkers.

4.2.1 Remodelling of homogeneous GUVs by actin network polymerisation

Effect of membrane bending rigidity

First, we consider a biomimetic system composed of homogeneous GUVs. Their membrane is either DOPC or a mixture of sphingomyelin and cholesterol (SMC). These compositions have different bending rigidities, 20 and 65 $k_B T$, respectively (Rawicz et al. 2000; Marsh 2006). We also used these lipids together as a ternary lipid composition to produce phase-separated membranes (sections 4.1.1 and 4.2.2). On these homogeneous GUVs, we polymerise Arp2/3-nucleated branched actin networks (**Figure 18**). For these experiments, we mix the actin cocktail and GUVs preincubated with SpVCA. We let actin polymerise and observe the GUVs after a fixed time of 15 min. This assay is close to the one presented by (Simon et al. 2018), where the GUVs were made of EPC with a bending rigidity of 10 $\kappa_B T$. At this stage, we only change the membrane composition and thus its bending rigidity. The actin cocktail and NPF surface density is identical.

(Simon et al. 2019) showed that inward (“spikes”) and outward (“tubes”) membrane deformations could simultaneously form at the surface of GUVs because of actin polymerisation from the membrane. The type of protrusions observed, tubes or spikes, was controlled by

the interplay between network mesh size and membrane tension; we will return to these results below. In this section, we explore the effect of membrane bending rigidity on the membrane response to actin polymerisation.

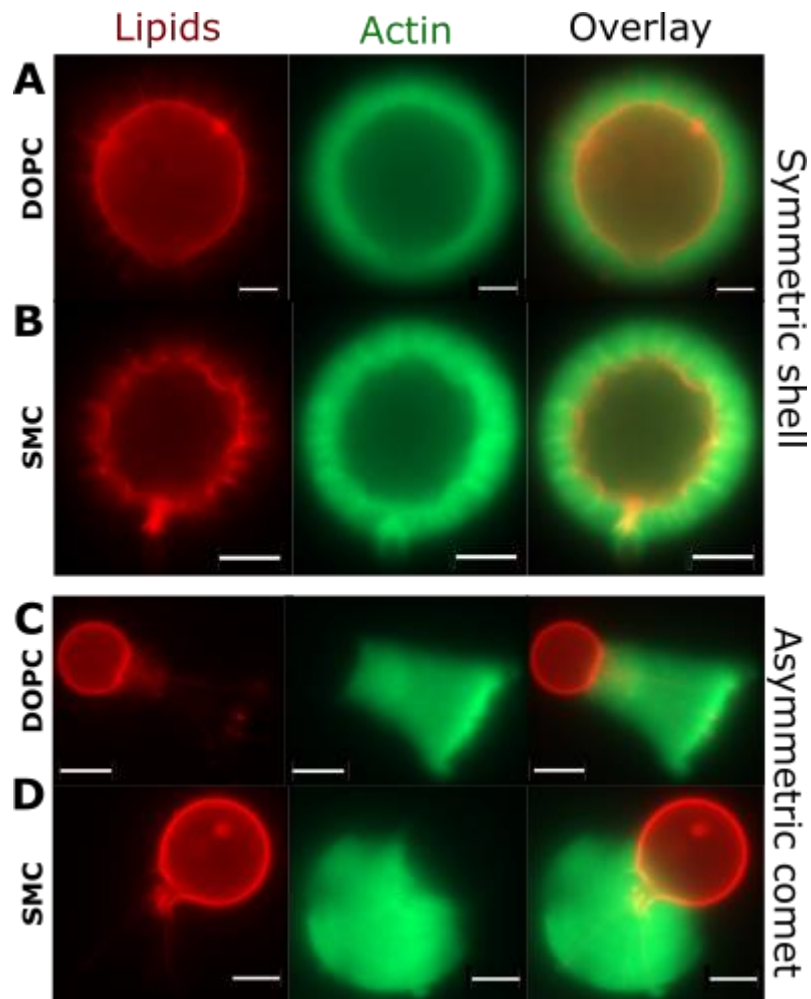


Figure 18: Effect of branched Arp2/3 actin networks polymerised at the surface of homogeneous GUVs with different membrane bending rigidities. The two first rows depict symmetric shells at the surface of DOPC (A) and SMC (B) GUVs. The third and fourth rows show actin comets observed after symmetry breaking on DOPC (C) and SMC (D) GUVs. Epifluorescence images (63x magnification). Scale bar = 5 μm

Figure 18 shows the two types of actin structures observed in experiments on homogenous lipid membranes: a symmetric actin shell (A, B) or an asymmetric actin tail (C, D), usually referred to as a “comet”. From previous experiments performed on beads, droplets, or GUVs, it has been shown that these two actin structures reflect two subsequent steps of actin polymerisation. First, an actin network grows from the GUV surface, forming a homogeneous shell. Then, because of stress accumulation at the surface of the actin shell (van der Gucht et al. 2005), it ruptures, the system breaks its symmetry, and further actin polymerisation generates a comet that propels the GUV (Giardini, Fletcher, and Theriot 2003; Upadhyaya et al. 2003). Let us now characterise the cortices and comets observed in our experiments.

First, we quantify the fraction of shells and comets for DOPC and SMC homogeneous GUVs in **Figure 19** A and B. We also observe some GUVs which display neither clearly actin shells nor comets; we categorise these as “undetermined”. Comets are more frequent than cortices in DOPC GUVs, whereas this tendency is reverted in the case of SMC GUVs. For GUVs with a larger bending rigidity, the probability of breaking the symmetry of the actin cortex is lower.

Then, we examine the case of symmetric actin shells. (Simon et al. 2019) showed that membrane nanotubes were pulled outwards all around the GUVs because of actin polymerisation dynamics. We also observe such tubes in **Figure 18** A and B for DOPC and SMC membranes. Nevertheless, we very frequently observed tubes in shells formed from DOPC membranes (about 75%), which are visible in only 20% of shells in the case of SMC GUVs. Such results seem to indicate that a larger bending rigidity impairs tube formation. (Simon et al. 2019) also reported inward protrusions, “spikes”, when membrane tension was decreased by osmotically deflating the GUVs. As expected, we do not observe such spikes in our experiments as we do not intentionally reduce the membrane tension.

Surprisingly, we observed another feature in the case of SMC membranes only: for almost 40% of the GUVs presenting a symmetric shell, their membrane displays visible micron-scale wrinkles (**Figure 18** B and **Figure 19** B). This effect seems related to the bending rigidity of

the membrane as it is observed only in the GUVs with the stiffest membrane (**Figure 19 C**). We will come back on this below.

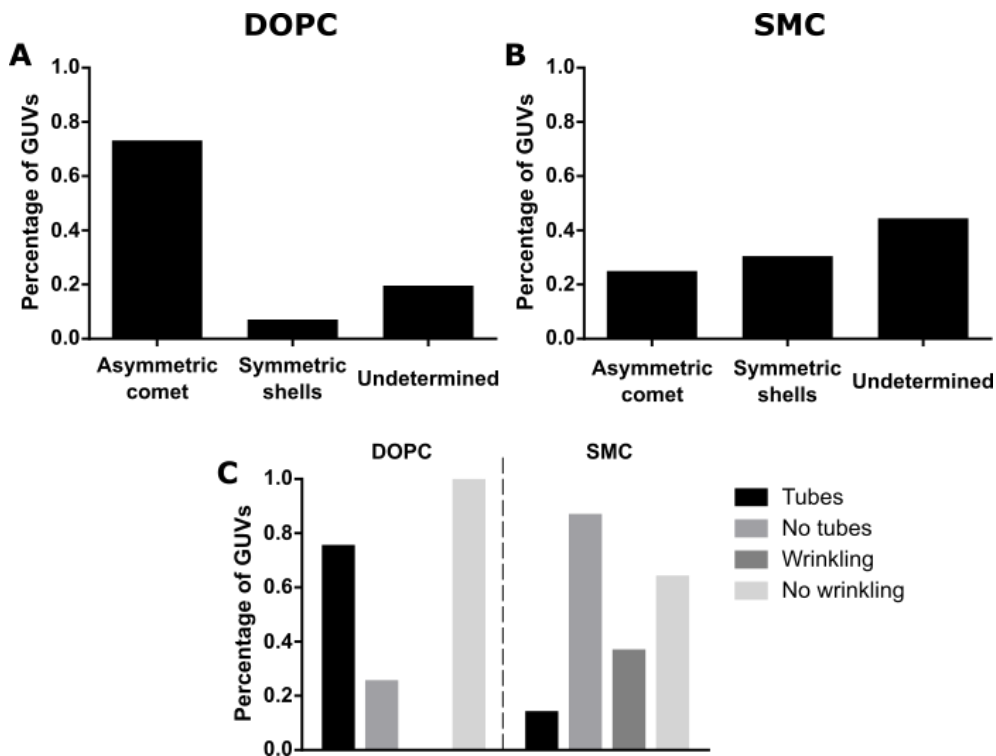


Figure 19: Type of actin structures and membrane deformations formed on homogenous GUVs: asymmetric comets vs. symmetric shells in A and B. C: Effect of membrane composition on shape changes for GUVs with a symmetric shell. Outwards membrane tubes and membrane wrinkling induced by the polymerisation of an Arp2/3 branched actin network shell on DOPC (A) or SMC (B) GUVs. A: DOPC GUVs (112 GUVs from $n=2$ experiments) and B: SMC GUVs (72 GUVs from $n=2$ experiments) GUVs.

Finally, when actin polymerisation induces symmetry breaking of the actin shell (**Figure 18 C and D**), we observe actin comets on one side of the GUVs. Inside the comet, a network of nanotubes is observed at the beginning of the comet (where the GUV was at the onset of the polymerisation), probably corresponding to the tubes pulled in the cortex before symmetry breaking. These tubes appear to coalesce during symmetry breaking and end up in a single nanotube inside the comet, as already observed by (Upadhyaya et al. 2003). In **Figure 20**,

we illustrated this process by choosing GUVs at different stages of the symmetry-breaking sequence, showing the transition from a symmetric shell containing radial nanotubes distributed evenly in the actin network towards an asymmetric comet in which the nanotubes have coalesced.

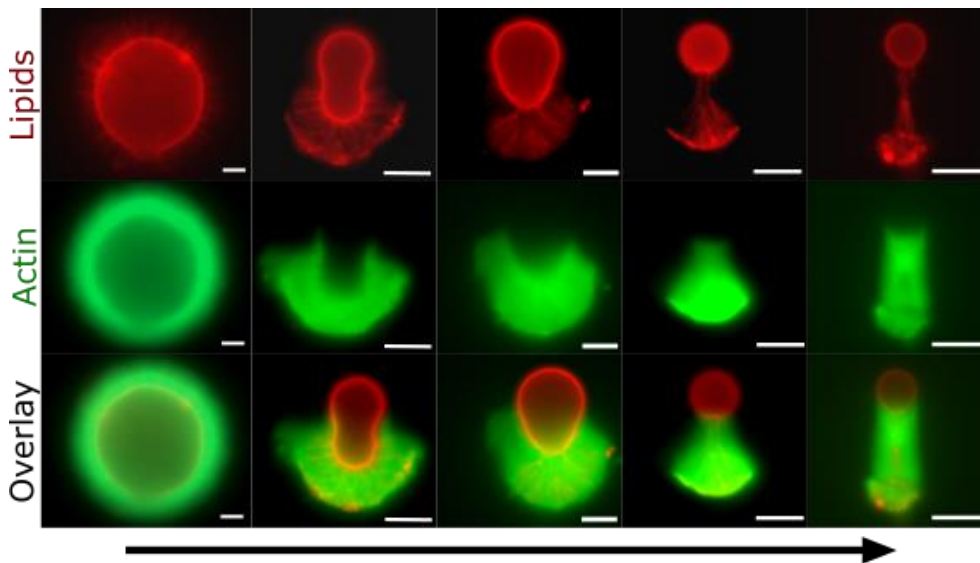


Figure 20: Reconstruction of the sequence of symmetry breaking of an Arp2/3 actin network polymerising around a DOPC GUV. From left to right, we have chosen different GUVs displaying a symmetric actin shell (1st row), GUVs captured during the rupture of the gel (rows 2,3,4) showing how the membrane nanotubes are grouped at the back of the GUVs, and finally, GUV with an actin comet (last row) showing how the tubes have coalesced.

Effect of crosslinkers

Then, we added to our actin cocktail the crosslinker α -actinin or the bundler fascin to modulate the structure of the actin network grown around GUVs. We assess how these network structures modulate DOPC and SMC GUV shape changes.

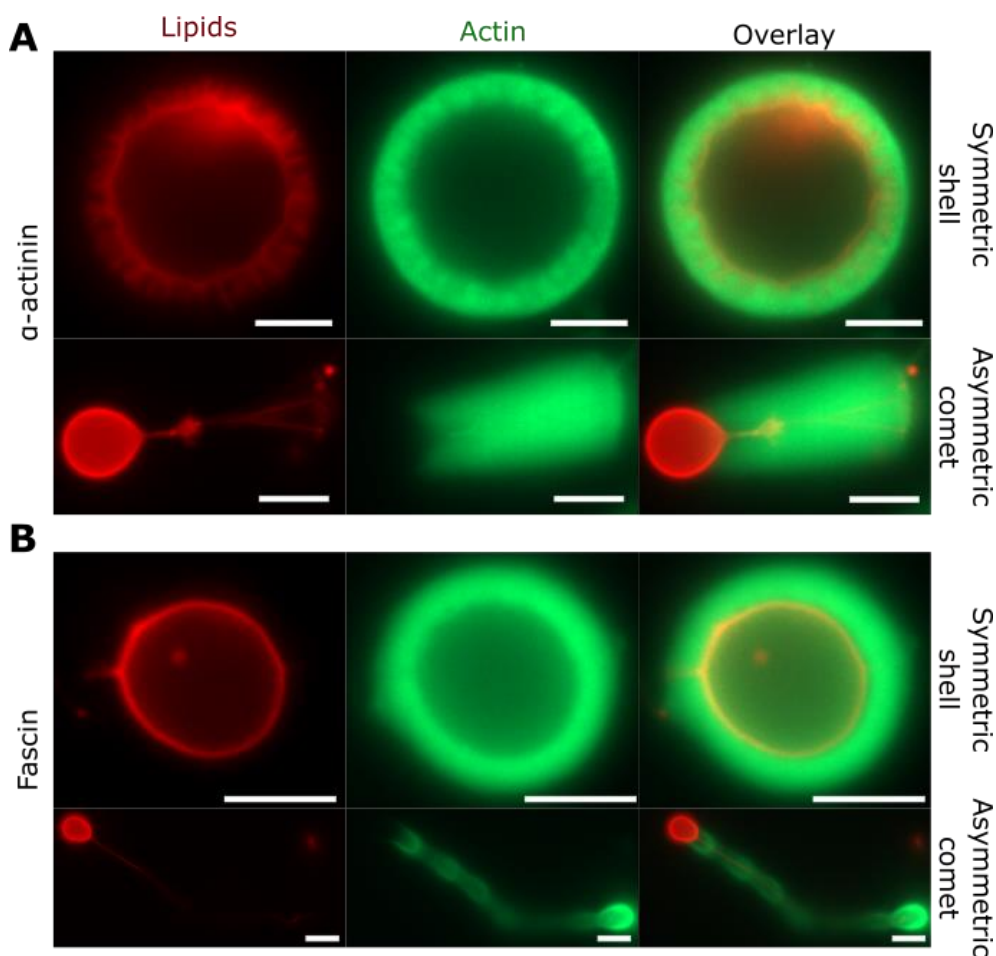


Figure 21: Effect of α -actinin and fascin on branched Arp2/3 actin networks polymerised at the surface of homogeneous GUVs made of DOPC. The two first rows (A) depict symmetric shells and comets in the presence of α -actinin. The third and fourth rows (B), in the presence of fascin. Scale bar = 5 μ m.

As observed in the previous section, we observe two types of actin structures on DOPC membranes (**Figure 21**), symmetric shells or asymmetric comets. As in (**Figure 19 A**), the symmetry-breaking case is more frequent in our experimental system. Adding α -actinin or fascin to Arp2/3 actin networks does not change this tendency (**Figure 22 A**).

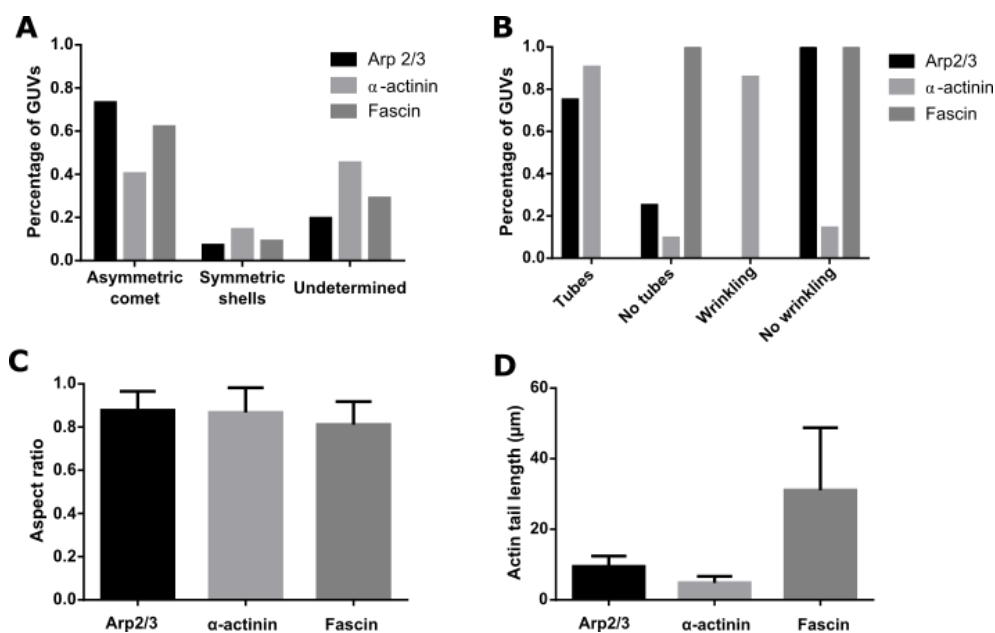


Figure 22: Effect of Arp2/3, α -actinin or fascin on DOPC GUVs. Histograms showing: A: Comets and symmetric shells distribution; B: Percentage of GUVs with a symmetric shell presenting tubes or wrinkled membrane; C: Aspect ratio of symmetry broke GUVs (mean of 10 GUVs in each condition); D: Comet actin tails length (mean of 10 GUVs in each condition). $N=2$; a total of 112, 159 and 100 GUVs of Arp2/3, α -actinin and fascin condition, respectively.

However, in the presence of α -actinin and fascin on DOPC GUVs, the membrane deformations induced by the actin network show strong differences. For symmetric shells, most GUVs display a very large number of tubes at their surface for Arp2/3 alone and Arp2/3 with α -actinin (**Figure 18 A** and **Figure 21 A**, respectively, quantification in **Figure 22 B**). Oppositely, in the presence of fascin, most GUVs display no tubes or only one (**Figure 21 B**, quantification in **Figure 22 B**). The presence of fascin thus impairs the formation of tubes on DOPC membranes. Besides, wrinkles are observed on DOPC membranes only in the presence of α -actinin and not in the case of Arp2/3 and Arp2/3 with fascin (**Figure 22 B**).

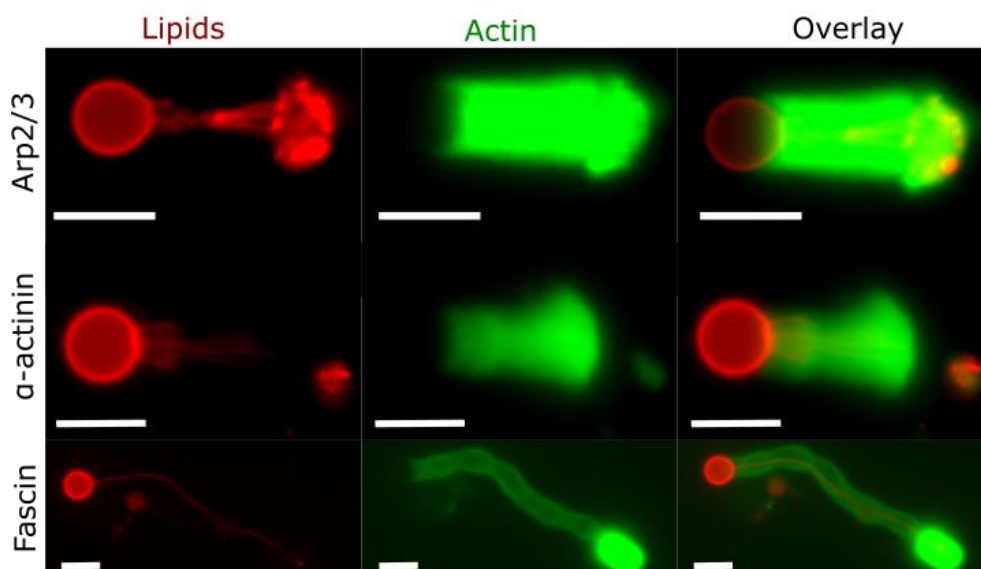


Figure 23: Morphology of asymmetric comets of Arp2/3, α -actinin and fascin formed on DOPC GUVs with three different actin networks: Arp2/3 alone, Arp2/3 with α -actinin or Arp2/3 with fascin. Scale bar = 5 μ m.

Then, we examine the case of comets on DOPC GUVs; whereas comets containing α -actinin have the same length as Arp2/3 comets, fascin induces longer comets (**Figure 23**), and they appear inhomogeneous (**Figure 24 A**). Similar inhomogeneities in the actin density inside comets were already observed by (Bernheim-Groswasser et al. 2002) in an experiment on polystyrene beads covered by VCA in the presence of α -actinin, revealing saltatory movements of the beads. In our experiments, compared to Arp2/3 and α -actinin, in the presence of fascin, the actin tail of an asymmetric comet on DOPC GUV presents fluorescence inhomogeneity (**Figure 24 B**). Note that we have also measured the aspect ratio of the GUV in the presence of a comet, but no significant difference appeared in the three conditions (**Figure 22 C**).

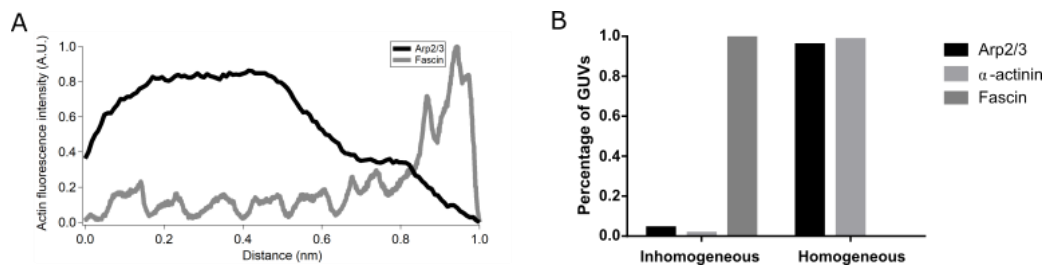


Figure 24: Inhomogeneity in asymmetric actin comets. A: Characteristic fluorescence intensity profiles along Arp2/3 and fascin comets. B: Percentage of GUVs presenting actin "jumps" in the three conditions. $N=2$ experiments; and 82, 64 and 62 of Arp2/3, α -actinin and fascin, respectively.

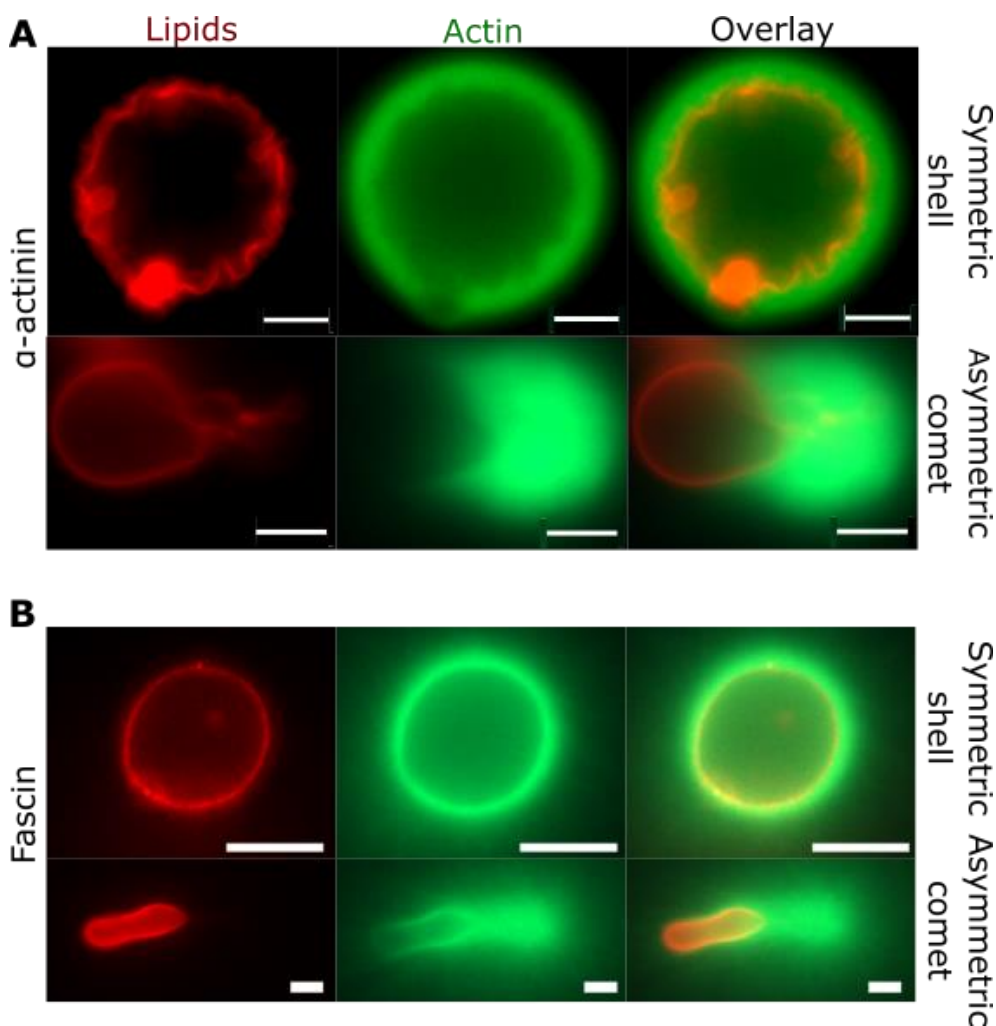


Figure 25: Effect of α -actinin or fascin actin network on SMC GUVs. In the first panel (A), an actin network in the presence of α -actinin results in a symmetric shell or asymmetric comet. In the second panel (B), an actin network in the presence of fascin results in a symmetric shell or asymmetric comet. Scale bar = 5 μ m

Now, we test the effect of α -actinin and fascin on GUVs made of SMC, thus with a larger bending rigidity. **Figure 25** shows that we still observe symmetric shells and asymmetric actin comets when adding α -actinin or fascin (as in **Figure 18 B** and **D**).

When compared to DOPC GUVs, the SMC GUVs seem to favour the formation of symmetric shells (**Figure 19 A** and **B**), and the addition of α -actinin or fascin has no effect on this, as quantified in (**Figure 26 A**).

In symmetric shells polymerised on SMC GUVs in the presence of α -actinin, we observe very strong wrinkling (**Figure 25 A** and **Figure 26 B**) and very few GUVs with tubes, in striking contrast with the case of DOPC GUVs. Note that the large wrinkles differ from the “spikes” observed by (Simon et al. 2019), which were triangular and, in most cases, much longer. GUVs with polymerised symmetric shells in the presence of fascin do not show any deformations, and the GUVs present a smooth surface (**Figure 25 B** and **Figure 26 B**).

In the case of comets, the presence of α -actinin does not affect the length of the comet nor the aspect ratio of the GUV from which the comet emerges compared to the case of Arp2/3-only (**Figure 26 C** and **D**), as shown in (**Figure 18 D**) and (**Figure 25 B**). However, fascin induces longer comets, and the GUVs appear more elongated (**Figure 25 B** and **Figure 26 D**).

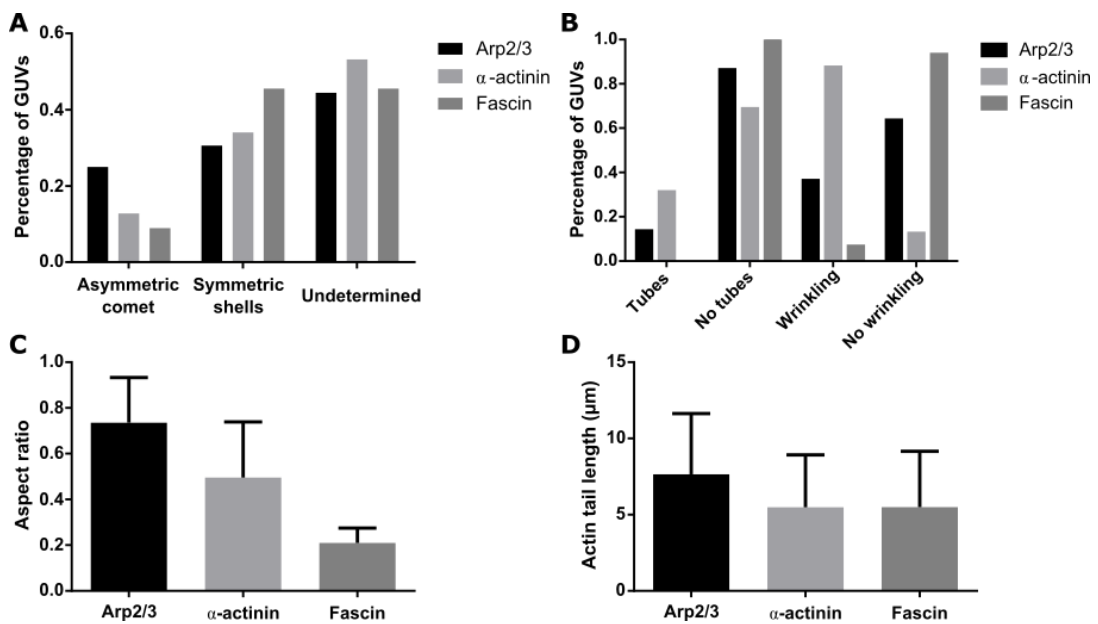


Figure 26: SMC GUVs shape changes under α -actinin or fascin actin network. A: Morphology distribution of SMC GUVs with an Arp2/3 actin network in the presence or not of α -actinin or fascin. B: Percentage of GUVs with a symmetric shell presenting tubes or wrinkled membranes. N=2 experiments; for 72, 47 and 112 GUVs for Arp 2/3, α -actinin and fascin condition, respectively.

Conclusion

We tried to summarise our results in **Figure 27**, and there are three important observations: the effect of the membrane properties, of the actin crosslinker and the actin bundler.

The first effect is due to the bending rigidity. On GUVs polymerised with an Arp2/3 actin network, we observe almost four times more symmetry breaking for DOPC GUVs than for SMC GUVs (**Figure 22 A** vs. **Figure 26 A**), and this trend is still observed when α -actinin or fascin is added. For membrane deformations, we observe about 40% of SMC GUVs with membrane wrinkles and only 15% of GUVs with tubes for SMC GUVs (**Figure 26 B**) in striking contrast with DOPC GUVs, with almost 80% of GUVs presenting tubes and no GUVs with wrinkles (**Figure 22 B**).

The second effect comes from the addition of the crosslinker α -actinin. In this condition, 85% of DOPC GUVs present membrane wrinkling (**Figure 22 B**), and SMC GUVs show a two-fold increase for GUVs presenting membrane wrinkles compared to the Arp2/3-only condition (**Figure 26 B**). For DOPC and SMC GUVs, the crosslinker only slightly increased the number of GUVs presenting tubes.

Finally, in the presence of fascin, DOPC GUVs present longer comets and saltatory traces (**Figure 21 B** and **Figure 22 D**). SMC GUVs squeezed by the comets have a peanut shape (**Figure 25 B**). Concerning membrane deformations, DOPC and SMC GUVs overall have smooth membranes. For SMC GUVs with an actin shell, less than 10% GUVs present membrane wrinkles (**Figure 26 B**) and very few DOPC GUVs present just one tube, as in **Figure 21 B**.

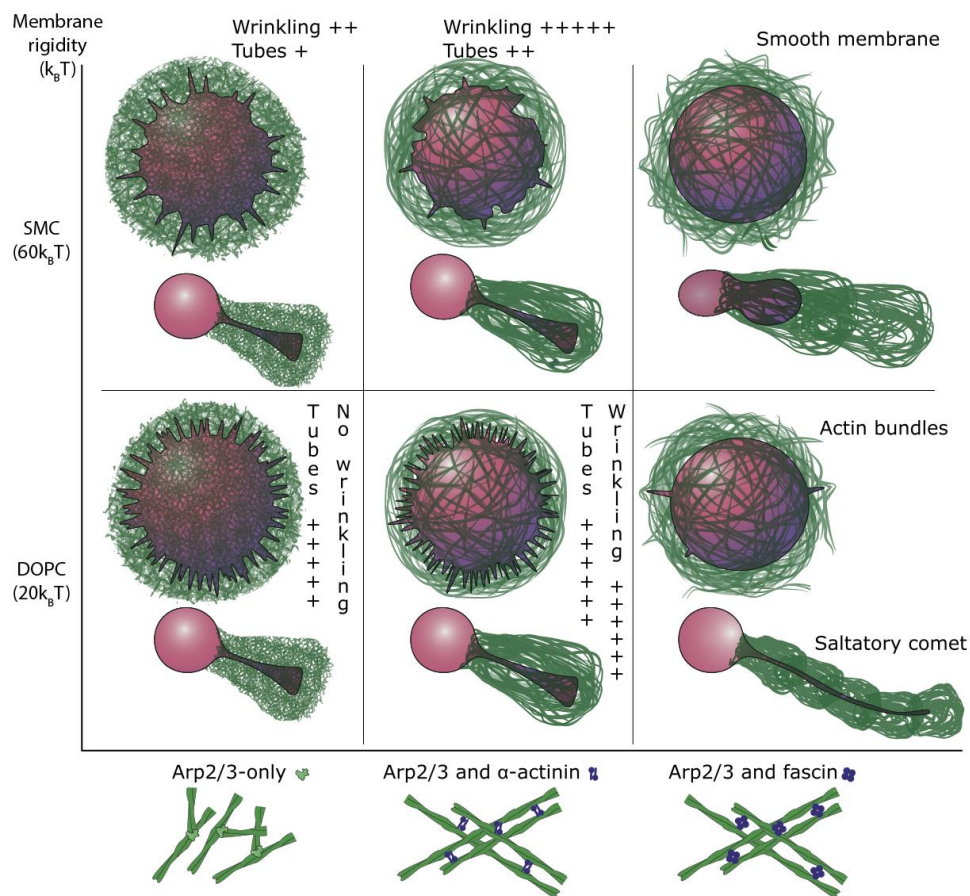


Figure 27: Schematic representation of actin-induced deformations. Low bending rigidity DOPC GUVs vs. higher bending rigidity SMC GUVs. Both tested with Arp2/3-only, α-actinin or fascin. Each condition presents two forms: actin shells and comets.

Tube formation inside actin shells

Our results show an effect of membrane bending rigidity on the formation of nanotubes during cortex growth, as tubes form more frequently on DOPC than on SMC. (Simon et al. 2019) described the formation of tubes by writing a balance between the nanotube formation force and the friction force induced by actin polymerisation. The tube formation force writes:

$$f_{tube} = 2\pi\sqrt{2\kappa\sigma}$$

With κ the bending rigidity and σ the membrane tension. The drag force exerted on the tube by the retrograde flow of actin polymerisation:

$$f_{drag} = 6\pi\eta r_{tube}(v_g - \dot{L})$$

With η the viscosity of the gel, v_g its polymerisation velocity, \dot{L} the velocity of the tube extremity, and the radius of the tube $r_{tube} = \sqrt{\kappa/2\sigma}$. This force cancels when the tube grows at the velocity of the gel polymerisation. To obtain the gel viscosity, the authors started with the estimation of the gel elasticity obtained by (Kroy and Frey 1996) for entangled polymer solutions :

$$E = \frac{k_B T l_p}{\zeta^4}$$

Where l_p is the persistence length of the actin filaments and ζ the mesh size of the network. Then, the gel viscosity is estimated by multiplying this elasticity by a characteristic viscoelastic relaxation time τ_{ve} : $\eta = E\tau_{ve}$ (Margaret L. Gardel et al. 2008; M. L. Gardel et al. 2004). Thus, equating f_{tube} and f_{drag} yields the condition for tube formation :

$$\sigma\zeta^4 < \frac{3}{2} k_B T l_p v_g \tau_{ve}$$

Importantly, this equilibrium does not depend on the membrane bending stiffness; therefore, this model does not explain our observations. This description might be extended to account for two points: first, the drag force on the tube only depends on its radius. This might not reflect reality, as viscous forces along the whole length of the tube could play an important role. The second point is that this model does not consider the friction induced by the linkers between the actin shell and the membrane during tube elongation, which can be very important (Campillo et al. 2013).

Modelling wrinkles in actin shells

We start by recalling the model presented in (Kusters et al. 2019). When GUVs surrounded by a cortex are deflated, buckling appears for thin cortices and wrinkling for thick cortices. We never observe buckling, probably because we do not impose strong volume changes as in (Kusters et al. 2019). Equation 4 in (Kusters et al. 2019) predicts the wavelength of the wrinkles :

$$\lambda = 2\pi \left(\frac{3\kappa}{E} \right)^{1/3}$$

DOPC and SMC membranes have a bending rigidity of 20 and 65 $k_B T$, their λ are 400 and 544nm, respectively. Such a small change could not explain why we do not observe membrane wrinkling on DOPC GUVs

We might observe wrinkling in our case not because of osmotic deflation but because of the actin-induced compression of the GUVs, which could impose a volume change. In this hypothesis, the forces generated by actin with α -actinin are larger and could explain why we observe more wrinkles with the α -actinin network compared to the Arp2/3-only network.

4.2.2 Controlling actin network polymerisation on phase-separated GUVs

This section presents the system I developed to target actin polymerisation on specific parts of phase-separated membranes. We show the different localisations of actin polymerisation, the morphologies and membrane reorganisation induced by actin dynamics. Such a system is the first attempt to mimic compositional heterogeneities of biomembranes observed *in vivo*. We present the results as described in our submitted article and in the additional results (4.2.2.2).

4.2.2.1 Article (under review): *Spatial control of Arp2/3-induced actin polymerization on phase-separated Giant Unilamellar Vesicles*

ACS Synthetic Biology - Lopes Dos Santos et al.

Under review

Spatial control of Arp2/3-induced actin polymerization on phase-separated Giant Unilamellar Vesicles

Rogério Lopes dos Santos¹, Michel Malo¹, and Clément Campillo^{*1,2}

¹Université Paris-Saclay, Univ Evry, CY Cergy Paris Université, CNRS, LAMBE, 91025, Evry-Courcouronnes, France.

²Institut Universitaire de France (IUF).

*Corresponding author email: clement.campillo@univ-evry.fr

Abstract

Deciphering the physical mechanisms underlying cell shape changes, while avoiding the cellular interior's complexity, involves the development of controlled basic biomimetic systems that imitate cell functions. In particular, the reconstruction of cytoskeletal dynamics on cell-sized Giant Unilamellar Vesicles (GUVs) has allowed for the reconstituting of some cell-like processes *in vitro*. In fact, such a bottom-up strategy could be the basis for forming protocells able to reorganize or even move autonomously. However, reconstituting the subtle and controlled dynamics of the cytoskeleton-membrane interface *in vitro* remains an experimental challenge. Taking advantage of the lipid-induced segregation of an actin polymerization activator, we present a system that targets actin polymerization on specific domains of phase-separated GUVs. We observe actin networks localized on Lo, Ld, or on both types of domains, and the actin-induced deformation or reorganization of these domains. These results suggest that the system we have developed here could pave the way for future experiments further detailing the interplay between actin dynamics and membrane heterogeneities.

Keywords: Lipid domains, Nucleating promotor factor, Actin network, Giant Unilamellar Vesicles

I. Introduction

Building synthetic cells is one of the major challenges in synthetic biology¹. One capability that synthetic cells need, which is observed in living cells, is the ability to change their shape in response to various internal and external stimuli. In living cells, these shape changes are fuelled by the actin cytoskeleton dynamics that constantly remodel biological membranes for a wide range of biological processes². Inside living cells, Nucleation Promoting Factors (NPFs), such as WASP or WASH, that activate Arp-2/3-induced actin polymerization are often linked to lipid membranes³. Some polymerisation nucleators, such as formin, that form actin bundles in filopodia, for instance, are also linked to lipid membranes. These different actin polymerisation machineries coexist in the cell and compete for a limited pool of actin monomers⁴. Deciphering how actin remodels membranes inside the cell is complicated because hundreds of proteins associated either with actin or with membranes cooperate for these processes^{5,6}. Therefore, minimal biomimetic systems made with artificial membranes and reconstituted actin networks are useful. These systems permit addressing the mechanisms underlying cell shape changes and also forming synthetic cells able to change their shape, move or divide⁷. Various minimal systems allow studying actin effects on reconstituted biological membranes, such as Supported Lipid Bilayers (SLBs)^{8,9}, membrane nanotubes¹⁰⁻¹² or Giant Unilamellar Vesicles (GUVs). Because they are cell-sized and thus allow directly studying membrane remodelling by optical microscopy, GUVs are relevant for building protocells. Many types of actin networks have been reconstituted inside or around GUVs. Actin filaments formed without NPFs as WASP or its VCA domain^{13,14} were coupled to the GUV membrane with or without crosslinkers¹⁵⁻¹⁷. Then, activators of actin polymerization were coupled to the GUV membrane and allowed for the *in vitro* reconstitution of filopodia-like protrusions¹⁸⁻²⁰, actin cortex²¹, blebs^{22,23} and endocytic pits^{18,20}. We recently reviewed these bottom-up reconstitution studies in²⁴. Several articles studied actin polymerization around GUVs, which induces symmetry breaking of the actin gel and the propulsion of the GUVs by an actin "comet", reminiscent of the propulsion of pathogens or endosomes inside the cell. The role of Arp2/3 concentrations²⁵ and NPFs mobility²⁶ on these processes and the detailed forces applied by the actin comet to the GUV^{27,28} were carefully studied.

One key aspect of biological membranes is their compositional heterogeneity which plays a crucial role in cell functions²⁹⁻³¹. Heterogeneous membrane domains dynamically form at the surface of biological membranes and play an important role in cell signalling as they locally concentrate lipids and membrane species in submicrometer areas whose properties differ from the rest of the membrane. The interaction of these domains with the actin cytoskeleton is clearly demonstrated: actin dynamics forms WASH domains at the surface of endosomes³², induces nanodomains

in membrane tubules leading to their scission³³, controls protein clusters formation^{30,34} but the mechanisms by which the cytoskeleton affects lipid domain formation, and stability remains unclear.

A simple model to reconstitute this heterogeneity *in vitro* is phase-separated GUVs³⁵ that form Ld (liquid disordered) and Lo (liquid ordered) domains. Some articles reported the effect of actin or actomyosin on phase-separated SLBs^{8,36-38} or of the prokaryotic tubulin homolog FtsZ on phase-separated GUVs³⁹. So far, only one seminal study has addressed the interplay between lipid domains and actin networks on GUVs⁴⁰. This article showed how the presence of an actin network polymerized on the Ld phase of GUVs affects the transition temperature of their membrane and how the presence of the actin network guides the spatial localization of the domains at the transition. However, there are many open questions on the crosstalk between phase separation in membranes and actin dynamics that call for novel experimental systems coupling phase-separated membranes and actin networks.

Here, we present an approach to target the polymerization of actin networks to specific regions of phase-separated GUVs. Our experimental setup allows the segregation of the same NPF to the two types of membrane domains at the surface of GUVs, thus targeting actin polymerization to Ld, Lo or Ld and Lo domains. We demonstrate this targeted actin polymerization, study the phenotypes of the observed actin-membrane systems, and finally show that actin polymerization reorganizes these domains.

II. Results

Experimental strategy

Our strategy is to use a lipid composition that leads to coexisting Lo and Ld lipid domains on GUVs combined with functionalized lipids that allow the binding of an activator of actin polymerization, or NPF, to trigger Arp2/3 (**Figure 1 A**). A classical lipid composition to prepare phase-separated GUVs is a mixture of DOPC, sphingomyelin, and cholesterol at a molar ratio of 2/2/1 shown to induce lateral lipid separation³⁵. To trigger actin polymerization in the presence of the Arp2/3 complex, we use a construct called "SpVCA" as an NPF. SpVCA comprises two binding tags: streptavidin and histidine, which allow the NPF to bind to either biotinylated or nickel (Ni-NTA) lipids (**Figure 1B,C**).

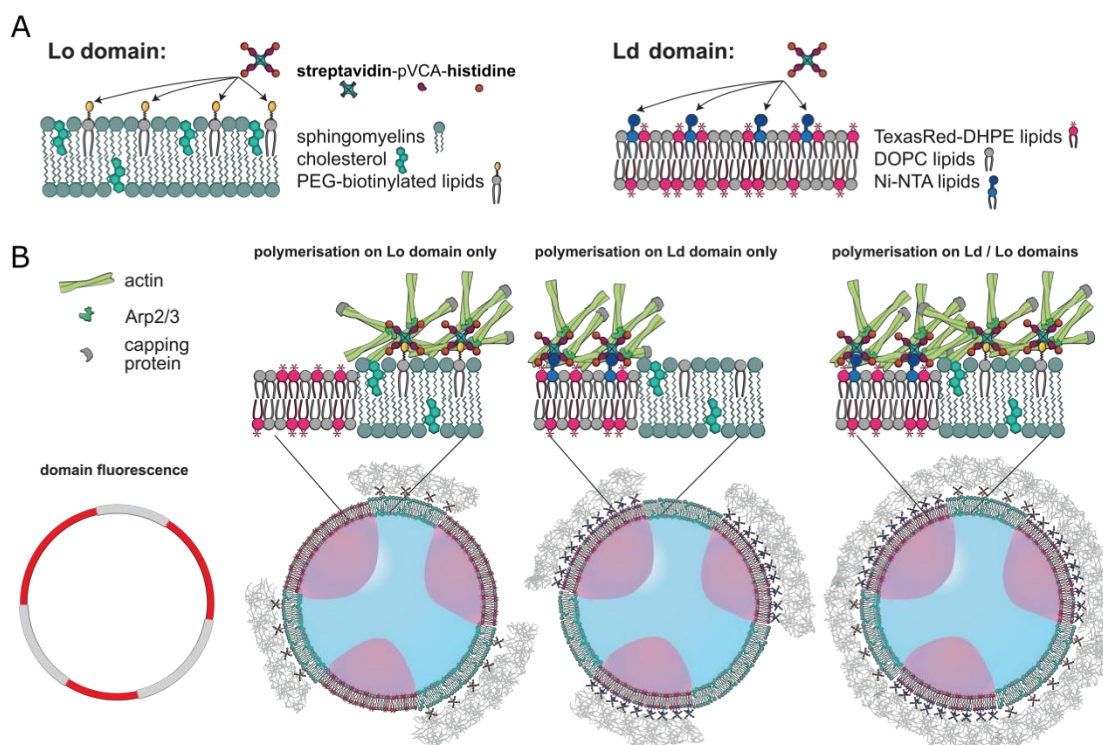


Figure 1: Scheme of the experimental strategy. A: Representation of domains and their composition: Lo domains enriched in sphingomyelin and cholesterol and Ld domains enriched in DOPC and fluorescent TexasRed lipids; segregation of biotinylated and nickel lipids into the Lo and Ld domain, respectively, that allows segregation of SpVCA; The activator of actin polymerization (SpVCA) contains two tags, streptavidin and histidine, allowing binding to biotinylated or nickel lipids, respectively. B: Representation of the polymerization of an Arp2/3 nucleated actin network on Lo, Ld or Lo and Ld domains at the scale of the domains or of a whole GUV.

To begin, we formed GUVs with this lipid composition and confirmed the presence of two or more lipid domains at their surface (**Figure S 1**). The Texas Red fluorescent lipids we use to visualize GUVs are enriched in the Ld domains⁴¹, mainly composed of DOPC³⁵, which appear bright on fluorescent images. In contrast, the Lo domains are enriched with sphingomyelin and cholesterol and appear dark. Then, we assessed the localization of the functionalized lipids. As shown by⁴², Ni-NTA lipids segregate into Ld domains. We tested that biotinylated lipids segregate into the Lo domain (**Figure S 2**).

Therefore, including Ni-NTA lipids in our lipid mixtures should allow us to bind SpVCA and thus target actin polymerization on Ld domains. With PEG-Biotin lipids, actin should polymerize on Lo domains. Combining Ni-NTA and PEG-Biotin lipids should induce polymerization on both types of domains. We will probe this in the following sections. Before presenting these results, we have to clarify an important point on the morphology of the lipid domains observed on our GUVs. We observe two different cases: first, some GUVs present two distinct hemispherical domains and are, therefore, asymmetric. Some other GUVs present multiple domains and thus are mostly symmetric. These differences in GUV morphology stem from differences in GUV

composition: if the lipid mixture we use is fixed, the precise composition of each GUV varies, as shown by^{43,44}. Thus, the size and number of the domains can vary among a GUV population.

Actin polymerization on Ld domains

First, using 1% of Ni-NTA lipids, we tested whether we target actin polymerization on the DOPC-enriched Ld domains. We see in **Figure 2** that Arp2/3 actin networks colocalize with the fluorescent lipids and thus are polymerized on the Ld domains. We observe two types of actin structures: either partial actin shells or elongated actin comets (**Figure 2 C**). The partial shells consist of a few micrometers thick actin networks that emerge from one (**Figure 2 A**) or several (**Figure 2 B**) Ld domains. Comets are more frequently observed than partial shells; we quantified this in **Figure S 3A**. The appearance of an actin shell vs an actin comet depends on the local concentration of the NPFs that can present strong heterogeneities because the intrinsic lipid composition of GUVs itself is heterogeneous among a single preparation, as shown in several studies^{43,44}. Therefore, the polymerization is more efficient on some of the GUVs. At the time when we image the GUVs, low polymerization will induce a shell, whereas more intense polymerization leads to comets. Actin comets are observed classically in experiments where actin gels are grown at the surface of beads⁴⁵, oil droplets^{46,47}, or homogeneous GUVs²⁵⁻²⁸. In these experiments, the comets form because the growth of a symmetric actin shell generates mechanical tension in the actin network. Once a critical stress is reached, the network ruptures and breaks its symmetry, and a comet forms. The mechanisms of symmetry breaking around GUVs and the structure of the actin comets in relation to the Arp2/3 concentration and the interaction between NPFs and actin filaments have been studied in detail in^{25,26}. In our case, comets are not necessarily formed through the symmetry-breaking of the actin gel. Indeed, our GUVs can be asymmetric from the beginning of the experiment, especially in the case of large domains forming two hemispheres. This is also the case for the actin structures formed at their surface. Besides, in the partial shells, we observe membrane nanotubes pulled outwards from the membrane because of actin polymerization dynamics (yellow arrows in **Figure 2**), as observed by²⁰. Note that, in our experiments, the osmolarity of the internal and external buffers are equilibrated, the observation of nanotubes in the actin shell in these conditions agrees with the results of²⁰. The fact that we observe either actin shells or actin comets thus reflects heterogeneity in the efficiency of actin polymerization among GUVs. We believe that this heterogeneity could itself stem from differences in the lipid composition of the GUVs, already observed in other studies^{43,44} and thus of the surface density of the NPFs.

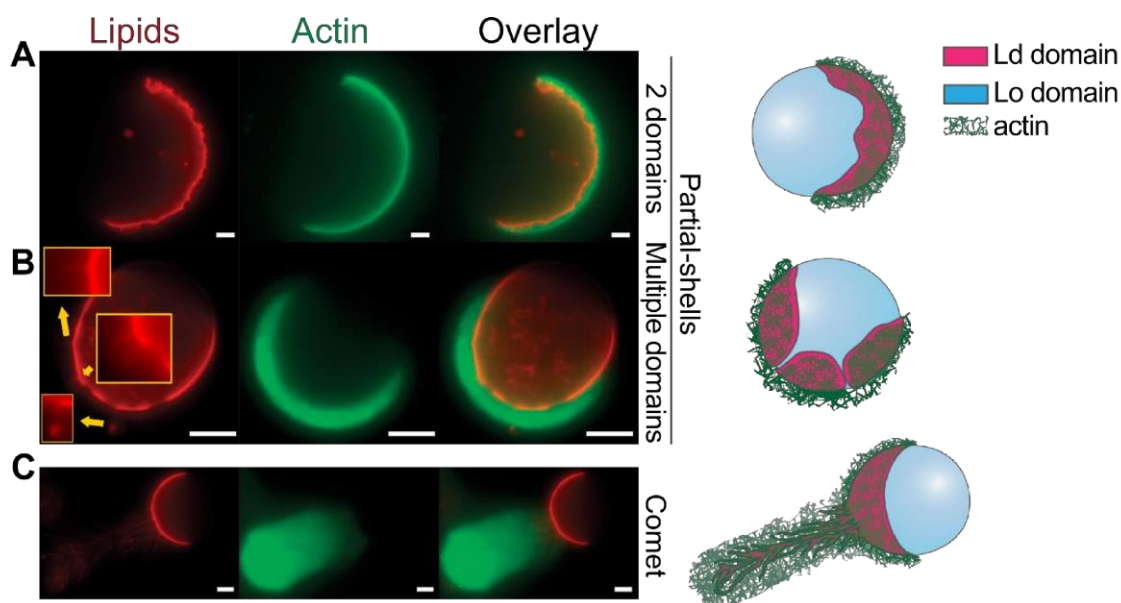


Figure 2: Polymerization of an Arp2/3 actin network on the Ld domains of phase-separated GUVs. The first two panels depict a partial shell of actin polymerized on GUVs presenting one (A) or multiple (B) Ld domains. The last panel (C) shows a comet on a GUV presenting a single large Ld domain connected to the comet. Yellow arrows indicate the presence of membrane tubes. For each row, we present fluorescent images of lipids, actin and their overlay with an illustration of the system. Scale bar = 5 μm .

Actin polymerization on Lo domains

Then, using 0.1% of biotinylated lipids, we assessed if the polymerization was targeted to the Lo domains. We see in **Figure 3** that we observe the formation of an actin network on the region of the GUVs where no lipid fluorescence is visible, revealing Lo domains. To classify the obtained morphologies, we use the same nomenclature as for Ld domains: partial actin shells formed on single or multiple domains (**Figure 3A** and **B**) or actin comets (**Figure 3C**). Compared to the precedent case of polymerization on the Ld domains, where comets were most frequently observed, actin polymerization on Lo domains induces around only 40% of comets and 40% of partial shells (**Figure S 3B**). Note that, as the lipid membrane is not visible in these experiments, the membrane deformations presented in the schematic are only an assumption based on the fact that actin recruitment on the two types of domains looks similar (see below).

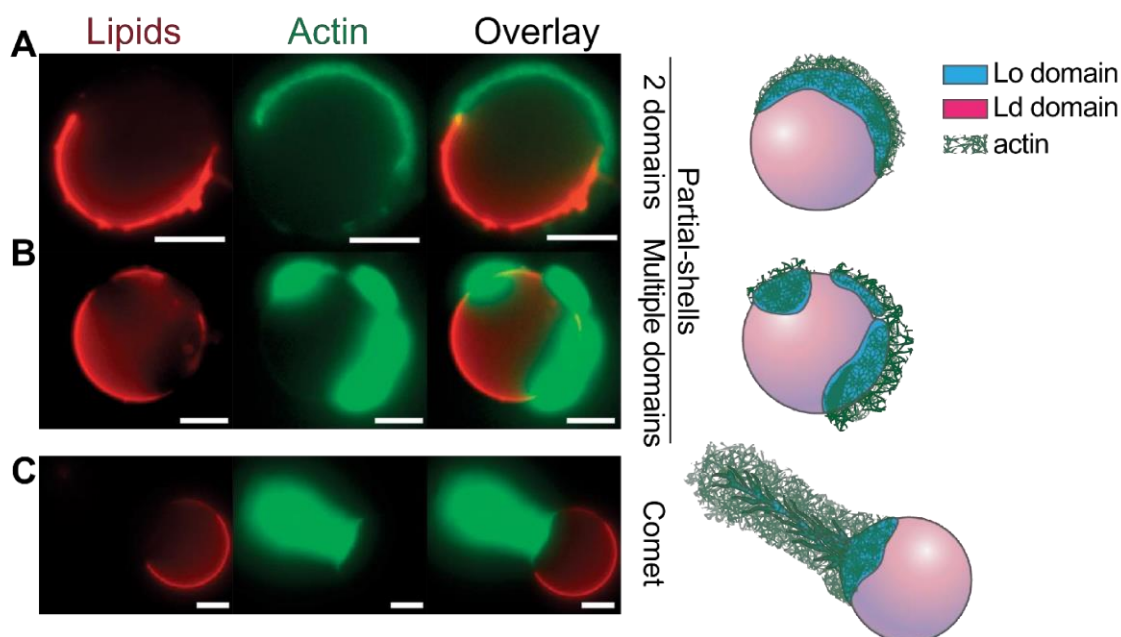


Figure 3: Polymerization of Arp2/3 actin networks on the Lo domains of phase-separated GUVs. The first two panels depict shell-like actin networks polymerized on GUVs presenting one (A) or multiple (B) Lo domains. The last panel (C) shows a comet formed from a Lo domain. For each row, we present fluorescent images of lipid, actin and their overlay with an illustration of the system. Scale bar = 5 μm .

Actin polymerization on both Lo and Ld domains

Finally, when we prepare GUVs with 0.1% biotinylated and 1% Ni-NTA lipids, we simultaneously trigger actin polymerization on both types of domains. (**Figure 4**). Here, actin forms a continuous actin shell surrounding the whole GUV (50 % of cases, quantification in **Figure S 3C**) or a comet on one side of the GUV. In the case of actin shells, we observe that, with the fraction of Ni-NTA and biotinylated lipids that we use, the shells are almost continuous. We have made an estimation of their thickness on Lo and Ld domains from epifluorescence images, which leads to close values ($1 \pm 0.3 \mu\text{m}$ for Ld and $1.2 \pm 0.5 \mu\text{m}$ for Lo, measured on $N = 10$ GUVs) (**Figure 4A** and **B**). Indeed, we have checked that preparing GUVs without domains in the presence of 0.1% biotinylated or 1% Ni-NTA lipids led to similar types of actin structures in our polymerization conditions. This suggests that the efficiency of actin polymerization is the same on Lo and Ld domains, no matter how our NPF is attached to the membrane. Note that there are ten times more Ni-NTA lipids than biotinylated lipids, but on the other hand, the streptavidin-biotin link is much stronger than the Ni-His link, maybe explaining why actin polymerizes similarly from Lo and Ld domains. In the cases of polymerization on Lo or Ld domains only, the GUVs could already be asymmetric before actin polymerization because of lipids segregation. Here, the comets probably emerge

from continuous symmetric actin shells that break their symmetry because of actin-induced forces, as observed on homogeneous GUVs^{27,28}.

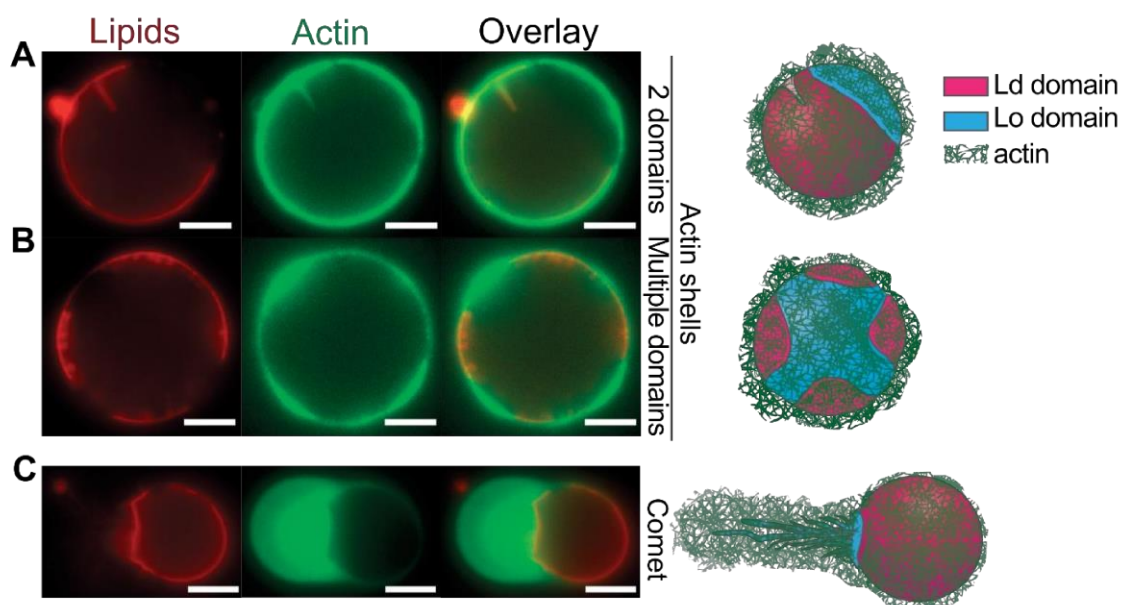


Figure 4: Polymerization of Arp2/3 actin networks on both Ld and Lo domains of phase-separated GUVs. The first two panels depict a shell of an actin network polymerized on GUVs presenting two (A) or multiple (B) domains. The last panel (C) shows a comet. For each row, we present fluorescent images of lipid, actin and their overlay with an illustration of the system. Scale bar = 5 μ m.

Lipid domains rearrangements

As previously stated, there is a close relationship between lipid domains and actin dynamics inside living cells³³, which mechanisms are unclear. Actin dynamics could induce or reorganize domains in cell membranes. Here, we compare the number of domains in our GUVs (two hemispheres vs. multiple domains) before and after actin polymerization (**Figure 5**). As previously, we distinguish the cases of shell-like actin networks and actin comets after polymerization. Figure S4 presents these results without pooling different experiments.

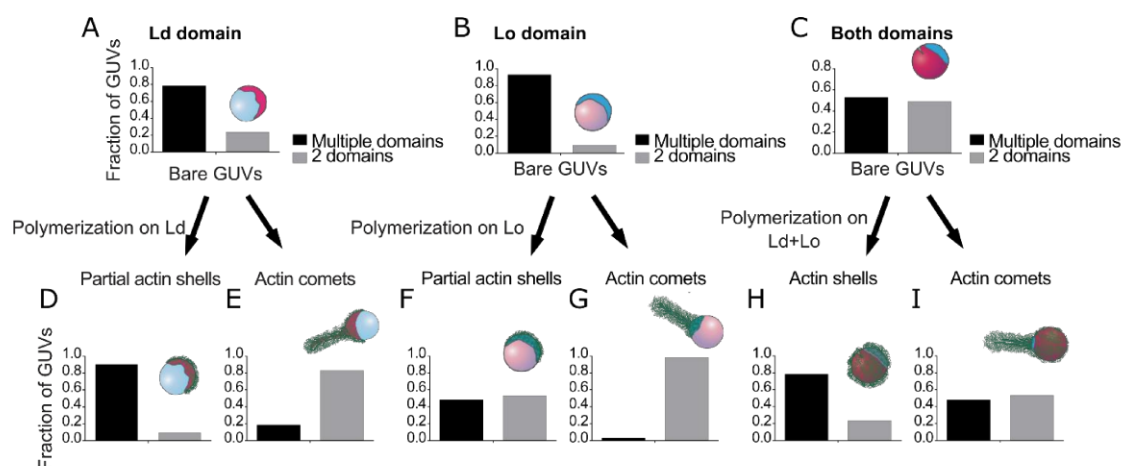


Figure 5: Lipid domains rearrangement by actin polymerization on phase-separated GUVs. In all experiments, we distinguish GUVs with more than two visible domains (multiple domains) and GUVs with only two domains. First row: Number of lipid domains (2 domains vs multiple domains) before actin polymerization on Ld (A), Lo (B) and both Ld and Lo domains (C). Second row: number of lipid domains after actin polymerization on Ld, Lo or both domains, resulting in either partial actin shells (D,F,H) or comets (E,G,I). N=3 experiments for bare GUVs: 80 GUVs before polymerization on Ld domains, 73 GUVs before polymerization on the Lo domain and 52 GUVs before polymerization on both domains. N=3 experiments for actin polymerization on the Ld domains: 21 partial shells and 112 comets; Lo domain: 46 partial shells and 42 comets; and on both domains: 62 partial shells and 38 comets.

The majority of bare GUVs containing Ni-NTA (**Figure 5 A**) or PEG-Biot (**Figure 5 B**) comprise multiple domains before actin polymerization, whereas only 40% of GUVs containing both Ni-NTA and PEG-Biotin form multiple domains (**Figure 5 C**). Interestingly, when actin polymerizes only on Ld or Lo domains and forms actin comets, the repartition of the domains is strongly affected compared to bare GUVs. Indeed, comparing **Figure 5 A** vs **E** and **Figure 5 B** vs **G**, we observe that bare GUVs that had mostly multiple domains before actin polymerization tend to have only two domains when an actin comet is present. We hypothesize that the domains could coalesce under the actin comet. Indeed, in actin comets formed on liquid droplets⁴⁶, the NPFs are transported in the region attached to the comet during its formation. We suspect that, in our case, the same mechanism could induce movement of the domains in this region and, thus, coalescence of adjacent domains. When multiple partial shells of actin are formed (**Figure 5 D** and **F**), the same effect is observed partially in the case of the Lo domains (**Figure 5 F**). Surprisingly, when actin is polymerized on both domains, there is no effect when actin comets form (**Figure 5 C** vs. **I**). In contrast, we observe more domains when partial actin shells form (**Figure 5 C** vs. **H**). A similar effect of NPF domain stabilization was observed by³² in experiments on endosomes; abolishing actin polymerization led to the coalescence of WASH domains. Therefore, in this case, Arp2/3 actin networks also impair the coalescence of membrane domains. Even if the detailed mechanisms by which actin dynamics could favour or impair membrane domains, these observations clearly show that actin polymerization affects the number of domains and

can reorganize them. The dynamics of these processes are beyond the scope of this article.

III. Conclusion

We have developed a biomimetic system to target actin polymerization on specific domains of phase-separated GUVs. We use an NPF that binds to Ni-NTA and biotinylated lipids and thus to Ld and Lo domains, respectively. We demonstrated that this strategy allows triggering actin polymerization on demand on one or both types of domains. We also characterized the morphology of the actin structures induced on hemispherical or multiple domains: after actin polymerization, partial actin shells or actin comets emerge from the desired domain. Compared to the seminal paper by⁴⁰ focused on the effect of an actin network polymerized on the Ld phase on the membrane transition temperature and domain localization, our system allows a larger flexibility in the localization of the actin polymerization and induces a wider diversity in the actin structures and membrane deformations observed. Finally, we observe domain reorganization stemming from actin networks symmetry breaking induced by actin polymerization dynamics on either Ld or Lo domains. The multiple domains present on GUVs before actin polymerization are reorganized and coalesce into two separate hemispheres after actin polymerization.³⁸ observed that the contraction of actomyosin networks pinned on phase-separated SLBs also induced lipid domains reorganization. In this experiment, filaments are preformed, without NPFs, and myosin-induced forces drive domain reorganization. The process we observe differs as the forces driving domain rearrangement solely come from actin polymerization dynamics. A comprehensive description of this rearrangement and its dependence on the mechanics of the lipid membrane, temperature and the actin cocktail composition would require the development of novel tools to trigger the onset of actin polymerization and follow its dynamics. With such experiments, we will follow in detail the dynamics of the symmetry-breaking process, assess if our system follows the same mechanism as homogeneous GUVs^{25,26} and determine if there is a threshold in the density of NPF for symmetry-breaking. In parallel, our work allows many other follow-up experiments. First, using a fluorescent NPF would allow us to directly quantify the density, organization and segregation of NPFs on Lo and Ld domains, in the case of actin shells and actin comets, to compare, in particular, the behaviour of the NPFs in actin comets to existing studies on homogeneous GUVs²⁵. Moreover, using fluorescent Arp2/3, we could quantify the density of branching⁴⁸ and therefore assess in detail the network structure emerging from the different lipid domains. Indeed, this is important to determine if the membrane properties, in particular differences in lipid mobility or membrane mechanics, could affect the structure of the actin network. Finally, we have not assessed the dynamics of these shape changes, as our protocol allows observing the GUVs and actin structures only at a given time. Nevertheless, we can hypothesize that longer polymerization times would increase the fraction of comets vs shells. Such

dynamical experiments would be very interesting, especially including ADF-Cofilin in our actin cocktail to increase the actin turnover to assess its effect on the observed shape changes.

Our results pave the way for studies mimicking biological processes such as endocytosis or intracellular trafficking. Indeed, such cell processes require crosstalk between the cytoskeleton and domains formed in biological membranes⁴⁹. Using phase-separated membranes, we could also build more complicated systems in which different actin activators could coexist on the same membrane, as is the case in cells. For instance, the lamellipodium contains both Arp2/3 and formins that simultaneously activate actin polymerisation at the cell membrane and nucleate different types of networks. With our system, one could investigate how these nucleators cooperate to generate membrane deformations by controlling their localization in adjacent domains on the same membrane. Moreover, localized actin polymerization is required for building protocells in which controlled deformation would be a basis for self-replication or movement⁷.

IV. Methods

Lipids, proteins and buffers. If not specified, all chemicals are purchased from Sigma-Aldrich (St. Louis, Missouri). 1,2-dioleoyl-sn-glycero-3-phosphocholine (referred to as DOPC), N-(dodecanoyl)-sphing-4-enine-1-phosphocholine (sphingomyelin, referred to as SM), cholesterol (referred to as C) from ovine wool, DSPE-PEG (2000)-Biotin (1,2-distearoyl-sn-glycero-3-phosphoethanolamine-N-[biotinyl(polyethylene glycol) 2000]) (PEG-biotin lipids) and 18:1 DGS-NTA(Ni) (1,2-dioleoyl-sn-glycero-3-[(N-(5-amino-1-carboxypentyl) iminodiacetic acid)succinyl] (Ni-NTA) are obtained from Avanti® Polar Lipids, Inc. (Alabaster, AL). Fluorescent lipids are Texas Red™ r-1,2-dihexadecanoylsnglycero-3-phosphoethanolamine triethylammonium salt (Texas-Red™ DHPE) and 4,4-Difluoro-5,7-Dimethyl-4-Bora-3a,4a-Diaza-s-Indacene-3-Pentanoic Acid (BODIPY™ FL C5) from ThermoFisher (Waltham, MA).

Actin from rabbit muscle, porcine Arp2/3 complex and recombinant Human Profilin 1 are purchased from Cytoskeleton (Denver, USA) and used without further purification. Actin-Alexa Fluor™ 488 conjugate from rabbit muscle in solution is from ThermoFisher (Waltham, MA). Streptavidin-pVCA-Histidine (SpVCA-His, where pVCA is the proline-rich domain-verprolin homology-central-acidic sequence from human WASP, starting at amino acid Gln150), and Mouse α 1 β 2 capping protein (CP) are purified by John Manzi and provided by UMR 168, PhysicoChimie Curie.

GUVs internal buffer contains 0.2 M sucrose, 2 mM Tris and is referred to as TPI. The external buffer of GUVs (or actin polymerization buffer), referred to as TPE, contains 95 mM sucrose, 1 mM Tris, 50 mM KCl, 2 mM MgCl₂, 0.1 mM DTT, 0.02 mg/mL β -casein

and 2 mM ATP in Milli Q water. Both buffers are adjusted to pH 7.4 and 220 mOsm as measured with Loeser Osmometer (Typ 16i).

We prepare a solution containing 30 μM monomeric actin with 15% of labelled Alexa Fluor 488 actin conjugate, and then this solution is incubated in G-Buffer (2 mM Tris, 0.2 mM CaCl_2 , 2 mM ATP, 0.2 mM DTT, pH 8.0) overnight at 4°C to ensure actin depolymerization.

Reconstitution of phase-separated GUVs. A ternary lipid mixture is used to achieve membranes with coexisting liquid lipid domains on GUVs. Ternary lipid mixture contains DOPC, cholesterol and sphingomyelin at a molecular ratio of 2/1/2 and is mixed with 0.5% TexasRed lipids, 0.1 % PEG-biotin and/or 1 % NiNTA (GUV). Final lipid mixtures are at 2.5 mg/mL in the organic solvent chloroform/methanol 5:3 (v:v). The electroformation technique adapted from ⁵⁰ is used to prepare GUVs. Briefly, 10 μL of the ternary lipid mixture is spread onto indium tin oxide (ITO)-coated plates and dried by a nitrogen flow. A 1 mm thick PDMS frame is placed between two ITO glass slides (conductive sides facing each other), forming a closed chamber, which is then filled with 400 μL TPI using a 0.75 μm diameter needle syringe. Heated at 60°C, an alternating current is applied (10 Hz, 1 V RMS) to the ITO plates for two hours. Once at room temperature, GUVs form domains.

Polymerization of an actin network on GUVs. GUVs are incubated for 15 min with 350 nM of SpVCA-His, the activator of the Arp2/3 complex, which binds to the biotinylated or nickel lipids of the membrane through the streptavidin or histidine tag, respectively. Actin polymerization starts when SpVCA-His-coated GUVs are placed in a mixture containing a final concentration of 3 μM monomeric actin (15% fluorescently labelled with Alexa Fluor 488), 3 μM profilin, 37 nM Arp2/3 complex and 25 nM CP as in ⁵¹. We leave the GUVs 15 minutes in the actin cocktail for polymerization. Then, the GUVs and actin are diluted two times in the external solution (or TPE). The polymerization is stopped due to the reduction of actin monomers concentration. This allows observation of the polymerized GUVs without further shape changes due to actin polymerization.

Observation and acquisition of images. Fluorescent images are acquired using a Zeiss inverted microscope with a 63x oil-immersion objective to perform epifluorescence microscopy (GFP filter cube, excitation 470 nm, emission 525 nm; Texas red filter cube: excitation 545–580 nm, emission 615 nm). Images are collected by AxioCam MRm camera. For all actin polymerization experiments, the exposure times are 14,6 milliseconds and 30 milliseconds for DHPE-TexasRed (membrane) and Actin-Alexa Fluor™ 488 conjugate (actin network), respectively. The actin shell thickness on GUVs is estimated by drawing a fluorescence intensity profile and measuring the distance between the membrane and actin fluorescence intensity peaks.

Authors information

Rogério Lopes dos Santos, Michel Malo and **Clément Campillo** - Université Paris-Saclay, Univ Evry, CY Cergy Paris Université, CNRS, LAMBE, 91025, Evry-Courcouronnes, France.

Clément Campillo - Institut Universitaire de France (IUF).

Author contributions

C.C. acquired funding. R.L.S. with support from C.C. designed and performed the experiments. M.M. supported data collection.

Notes: The authors declare that they have no competing interests.

Supporting information

Figure S 1: Observation of phase-separated GUVs.

Figure S 2: Biotinylated lipids distribution on a phase-separated GUV.

Figure S 3: Morphology distribution of GUVs upon polymerization of a branched actin network.

Figure S 4: Lipid domains rearrangement upon actin polymerization on phase-separated GUVs (histograms without experiments polling. Each bar represents an independent experiment).

Figure S 5: Zoom from figure 2B of the membrane deformations induced by a partial actin shell.

Acknowledgement

We acknowledge funding from the French Agence Nationale de la Recherche (ANR-18-CE13-0007-01 awarded to C.C.)

We thank Cécile Sykes and Julie Plastino for their help with the proteins and fruitful discussions and acknowledge Agnieszka Kawska at IlluScientia.com for the figure's illustrations.

V. References

- (1) Gallup, O.; Ming, H.; Ellis, T. Ten Future Challenges for Synthetic Biology. *Engineering Biology* **2021**, 5 (3), 51–59. <https://doi.org/10.1049/enb2.12011>.

- (2) Blanchoin, L.; Boujemaa-Paterski, R.; Sykes, C.; Plastino, J. Actin Dynamics, Architecture, and Mechanics in Cell Motility. *Physiological Reviews* **2014**, *94* (1), 235–263. <https://doi.org/10.1152/physrev.00018.2013>.
- (3) Breitsprecher, D.; Goode, B. L. Formins at a Glance. *Journal of Cell Science* **2013**, *126* (1), 1–7. <https://doi.org/10.1242/jcs.107250>.
- (4) Suarez, C.; Kovar, D. R. Internetwork Competition for Monomers Governs Actin Cytoskeleton Organization. *Nat Rev Mol Cell Biol* **2016**, *17* (12), 799–810. <https://doi.org/10.1038/nrm.2016.106>.
- (5) Putra, V. D. L.; Kilian, K. A.; Knothe Tate, M. L. Biomechanical, Biophysical and Biochemical Modulators of Cytoskeletal Remodelling and Emergent Stem Cell Lineage Commitment. *Commun Biol* **2023**, *6* (1), 1–24. <https://doi.org/10.1038/s42003-022-04320-w>.
- (6) Rottner, K.; Faix, J.; Bogdan, S.; Linder, S.; Kerkhoff, E. Actin Assembly Mechanisms at a Glance. *Journal of Cell Science* **2017**, *130* (20), 3427–3435. <https://doi.org/10.1242/jcs.206433>.
- (7) Baldauf, L.; van Buren, L.; Fanalista, F.; Koenderink, G. H. Actomyosin-Driven Division of a Synthetic Cell. *ACS Synth. Biol.* **2022**, *11* (10), 3120–3133. <https://doi.org/10.1021/acssynbio.2c00287>.
- (8) Köster, D. V.; Husain, K.; Iljazi, E.; Bhat, A.; Bieling, P.; Mullins, R. D.; Rao, M.; Mayor, S. Actomyosin Dynamics Drive Local Membrane Component Organization in an in Vitro Active Composite Layer. *PNAS* **2016**, *113* (12), E1645–E1654. <https://doi.org/10.1073/pnas.1514030113>.
- (9) Palani, S.; Ghosh, S.; Ivorra-Molla, E.; Clarke, S.; Suchenko, A.; Balasubramanian, M. K.; Köster, D. V. Calponin-Homology Domain Mediated Bending of Membrane Associated Actin Filaments. *eLife* **2021**, *10*, e61078. <https://doi.org/10.7554/eLife.61078>.
- (10) Allard, A.; Valentino, F.; Sykes, C.; Betz, T.; Campillo, C. Fluctuations of a Membrane Nanotube Covered with an Actin Sleeve. *Phys. Rev. E* **2020**, *102* (5), 052402. <https://doi.org/10.1103/PhysRevE.102.052402>.
- (11) Allard, A.; Bouzid, M.; Betz, T.; Simon, C.; Abou-Ghali, M.; Lemièrè, J.; Valentino, F.; Manzi, J.; Brochard-Wyart, F.; Guevorkian, K.; Plastino, J.; Lenz, M.; Campillo, C.; Sykes, C. Actin Modulates Shape and Mechanics of Tubular Membranes. *Science Advances* **2020**, *6* (17), eaaz3050. <https://doi.org/10.1126/sciadv.aaz3050>.
- (12) Lamour, G.; Allard, A.; Pelta, J.; Labdi, S.; Lenz, M.; Campillo, C. Mapping and Modeling the Nanomechanics of Bare and Protein-Coated Lipid Nanotubes. *Phys. Rev. X* **2020**, *10* (1), 011031. <https://doi.org/10.1103/PhysRevX.10.011031>.
- (13) Helfer, E.; Harlepp, S.; Bourdieu, L.; Robert, J.; MacKintosh, F. C.; Chatenay, D. Microrheology of Biopolymer-Membrane Complexes. *Phys. Rev. Lett.* **2000**, *85* (2), 457–460. <https://doi.org/10.1103/PhysRevLett.85.457>.
- (14) Limozin, L.; Bärmann, M.; Sackmann, E. On the Organization of Self-Assembled Actin Networks in Giant Vesicles. *Eur. Phys. J. E* **2003**, *10* (4), 319–330. <https://doi.org/10.1140/epje/i2002-10118-9>.

- (15) Limozin, L.; Sackmann, E. Polymorphism of Cross-Linked Actin Networks in Giant Vesicles. *Phys. Rev. Lett.* **2002**, *89* (16), 168103. <https://doi.org/10.1103/PhysRevLett.89.168103>.
- (16) Litschel, T.; Kelley, C. F.; Holz, D.; Adeli Koudehi, M.; Vogel, S. K.; Burbaum, L.; Mizuno, N.; Vavylonis, D.; Schwille, P. Reconstitution of Contractile Actomyosin Rings in Vesicles. *Nat Commun* **2021**, *12* (1), 2254. <https://doi.org/10.1038/s41467-021-22422-7>.
- (17) Tsai, F.-C.; Koenderink, G. H. Shape Control of Lipid Bilayer Membranes by Confined Actin Bundles. *Soft Matter* **2015**, *11* (45), 8834–8847. <https://doi.org/10.1039/C5SM01583A>.
- (18) Dürre, K.; Keber, F. C.; Bleicher, P.; Brauns, F.; Cyron, C. J.; Faix, J.; Bausch, A. R. Capping Protein-Controlled Actin Polymerization Shapes Lipid Membranes. *Nat Commun* **2018**, *9* (1), 1630. <https://doi.org/10.1038/s41467-018-03918-1>.
- (19) Liu, A. P.; Richmond, D. L.; Maibaum, L.; Pronk, S.; Geissler, P. L.; Fletcher, D. A. Membrane-Induced Bundling of Actin Filaments. *Nature Physics* **2008**, *4* (10), 789–793. <https://doi.org/10.1038/nphys1071>.
- (20) Simon, C.; Kusters, R.; Caorsi, V.; Allard, A.; Abou-Ghali, M.; Manzi, J.; Di Cicco, A.; Lévy, D.; Lenz, M.; Joanny, J.-F.; Campillo, C.; Plastino, J.; Sens, P.; Sykes, C. Actin Dynamics Drive Cell-like Membrane Deformation. *Nat. Phys.* **2019**, *15* (6), 602–609. <https://doi.org/10.1038/s41567-019-0464-1>.
- (21) Pontani, L.-L.; van der Gucht, J.; Salbreux, G.; Heuvingh, J.; Joanny, J.-F.; Sykes, C. Reconstitution of an Actin Cortex Inside a Liposome. *Biophysical Journal* **2009**, *96* (1), 192–198. <https://doi.org/10.1016/j.bpj.2008.09.029>.
- (22) Bashirzadeh, Y.; Moghimianavval, H.; Liu, A. P. Encapsulated Actomyosin Patterns Drive Cell-like Membrane Shape Changes. *iScience* **2022**, *25* (5), 104236. <https://doi.org/10.1016/j.isci.2022.104236>.
- (23) Loiseau, E.; Schneider, J. A. M.; Keber, F. C.; Pelzl, C.; Massiera, G.; Salbreux, G.; Bausch, A. R. Shape Remodeling and Blebbing of Active Cytoskeletal Vesicles. *Sci. Adv.* **2016**, *2* (4), e1500465. <https://doi.org/10.1126/sciadv.1500465>.
- (24) Lopes dos Santos, R.; Campillo, C. Studying Actin-Induced Cell Shape Changes Using Giant Unilamellar Vesicles and Reconstituted Actin Networks. *Biochemical Society Transactions* **2022**, *50* (5), 1527–1539. <https://doi.org/10.1042/BST20220900>.
- (25) Delatour, V.; Helfer, E.; Didry, D.; Lê, K. H. D.; Gaucher, J.-F.; Carlier, M.-F.; Romet-Lemonne, G. Arp2/3 Controls the Motile Behavior of N-WASP-Functionalized GUVs and Modulates N-WASP Surface Distribution by Mediating Transient Links with Actin Filaments. *Biophysical Journal* **2008**, *94* (12), 4890–4905. <https://doi.org/10.1529/biophysj.107.118653>.
- (26) Delatour, V.; Shekhar, S.; Reymann, A.-C.; Didry, D.; Lê, K. H. D.; Romet-Lemonne, G.; Helfer, E.; Carlier, M.-F. Actin-Based Propulsion of Functionalized Hard versus Fluid Spherical Objects. *New J. Phys.* **2008**, *10* (2), 025001. <https://doi.org/10.1088/1367-2630/10/2/025001>.

- (27) Giardini, P.; Fletcher, D.; Theriot, J. Compression Forces Generated by Actin Comet Tails on Lipid Vesicles. *Proceedings of the National Academy of Sciences of the United States of America* **2003**. <https://doi.org/10.1073/pnas.1031670100>.
- (28) Upadhyaya, A.; Chabot, J. R.; Andreeva, A.; Samadani, A.; Oudenaarden, A. van. Probing Polymerization Forces by Using Actin-Propelled Lipid Vesicles. *PNAS* **2003**, *100* (8), 4521–4526. <https://doi.org/10.1073/pnas.0837027100>.
- (29) Lingwood, D.; Ries, J.; Schwille, P.; Simons, K. Plasma Membranes Are Poised for Activation of Raft Phase Coalescence at Physiological Temperature. *Proceedings of the National Academy of Sciences* **2008**, *105* (29), 10005–10010. <https://doi.org/10.1073/pnas.0804374105>.
- (30) Sezgin, E.; Levental, I.; Mayor, S.; Eggeling, C. The Mystery of Membrane Organization: Composition, Regulation and Roles of Lipid Rafts. *Nat Rev Mol Cell Biol* **2017**, *18* (6), 361–374. <https://doi.org/10.1038/nrm.2017.16>.
- (31) Shelby, S. A.; Castello-Serrano, I.; Wisser, K. C.; Levental, I.; Veatch, S. L. Membrane Phase Separation Drives Responsive Assembly of Receptor Signaling Domains. *Nat Chem Biol* **2023**, 1–9. <https://doi.org/10.1038/s41589-023-01268-8>.
- (32) Derivery, E.; Helfer, E.; Henriot, V.; Gautreau, A. Actin Polymerization Controls the Organization of WASH Domains at the Surface of Endosomes. *PLOS ONE* **2012**, *7* (6), e39774. <https://doi.org/10.1371/journal.pone.0039774>.
- (33) Römer, W.; Pontani, L.-L.; Sorre, B.; Rentero, C.; Berland, L.; Chambon, V.; Lamaze, C.; Bassereau, P.; Sykes, C.; Gaus, K.; Johannes, L. Actin Dynamics Drive Membrane Reorganization and Scission in Clathrin-Independent Endocytosis. *Cell* **2010**, *140* (4), 540–553. <https://doi.org/10.1016/j.cell.2010.01.010>.
- (34) Gowrishankar, K.; Ghosh, S.; Saha, S.; C, R.; Mayor, S.; Rao, M. Active Remodeling of Cortical Actin Regulates Spatiotemporal Organization of Cell Surface Molecules. *Cell* **2012**, *149* (6), 1353–1367. <https://doi.org/10.1016/j.cell.2012.05.008>.
- (35) Veatch, S. L.; Keller, S. L. Separation of Liquid Phases in Giant Vesicles of Ternary Mixtures of Phospholipids and Cholesterol. *Biophysical Journal* **2003**, *85*, 3074–3083.
- (36) Honigsmann, A.; Sadeghi, S.; Keller, J.; Hell, S. W.; Eggeling, C.; Vink, R. A Lipid Bound Actin Meshwork Organizes Liquid Phase Separation in Model Membranes. *eLife* **2014**, *3*, e01671. <https://doi.org/10.7554/eLife.01671>.
- (37) Liebe, N. L.; Mey, I.; Vuong, L.; Shikho, F.; Geil, B.; Janshoff, A.; Steinem, C. Bioinspired Membrane Interfaces: Controlling Actomyosin Architecture and Contractility. *ACS Appl. Mater. Interfaces* **2023**, *15* (9), 11586–11598. <https://doi.org/10.1021/acscami.3c00061>.
- (38) Vogel, S. K.; Greiss, F.; Khmelinskaia, A.; Schwille, P. Control of Lipid Domain Organization by a Biomimetic Contractile Actomyosin Cortex. *eLife* **2017**, *6*, e24350. <https://doi.org/10.7554/eLife.24350>.
- (39) Arumugam, S.; Petrov, E. P.; Schwille, P. Cytoskeletal Pinning Controls Phase Separation in Multicomponent Lipid Membranes. *Biophys J* **2015**, *108* (5), 1104–1113. <https://doi.org/10.1016/j.bpj.2014.12.050>.

- (40) Liu, A. P.; Fletcher, D. A. Actin Polymerization Serves as a Membrane Domain Switch in Model Lipid Bilayers. *Biophysical Journal* **2006**, *91* (11), 4064–4070. <https://doi.org/10.1529/biophysj.106.090852>.
- (41) Baumgart, T.; Hunt, G.; Farkas, E. R.; Webb, W. W.; Feigenson, G. W. Fluorescence Probe Partitioning between Lo/Ld Phases in Lipid Membranes. *Biochim Biophys Acta* **2007**, *1768* (9), 2182–2194. <https://doi.org/10.1016/j.bbamem.2007.05.012>.
- (42) Dürre, K.; Bausch, A. R. Formation of Phase Separated Vesicles by Double Layer CDICE. *Soft Matter* **2019**, *15* (47), 9676–9681. <https://doi.org/10.1039/C8SM02491J>.
- (43) Rinaldin, M.; Fonda, P.; Giomi, L.; Kraft, D. J. Geometric Pinning and Antimixing in Scaffolded Lipid Vesicles. *Nat Commun* **2020**, *11* (1), 4314. <https://doi.org/10.1038/s41467-020-17432-w>.
- (44) Heuvingh, J.; Franco, M.; Chavrier, P.; Sykes, C. ARF1-Mediated Actin Polymerization Produces Movement of Artificial Vesicles. *Proceedings of the National Academy of Sciences* **2007**, *104* (43), 16928–16933. <https://doi.org/10.1073/pnas.0704749104>.
- (45) Bernheim-Groswasser, A.; Wiesner, S.; Golsteyn, R. M.; Carlier, M.-F.; Sykes, C. The Dynamics of Actin-Based Motility Depend on Surface Parameters. *Nature* **2002**, *417* (6886), 308–311. <https://doi.org/10.1038/417308a>.
- (46) Boukellal, H.; Campàs, O.; Joanny, J.-F.; Prost, J.; Sykes, C. Soft Listeria: Actin-Based Propulsion of Liquid Drops. *Phys. Rev. E* **2004**, *69* (6), 061906. <https://doi.org/10.1103/PhysRevE.69.061906>.
- (47) Trichet, L.; Campàs, O.; Sykes, C.; Plastino, J. VASP Governs Actin Dynamics by Modulating Filament Anchoring. *Biophysical Journal* **2007**, *92* (3), 1081–1089. <https://doi.org/10.1529/biophysj.106.091884>.
- (48) Wiesner, S.; Helfer, E.; Didry, D.; Ducouret, G.; Lafuma, F.; Carlier, M.-F.; Pantaloni, D. A Biomimetic Motility Assay Provides Insight into the Mechanism of Actin-Based Motility. *Journal of Cell Biology* **2003**, *160* (3), 387–398. <https://doi.org/10.1083/jcb.200207148>.
- (49) Allard, A.; Lopes dos Santos, R.; Campillo, C. Remodelling of Membrane Tubules by the Actin Cytoskeleton. *Biol. Cell* **2021**, boc.202000148. <https://doi.org/10.1111/boc.202000148>.
- (50) Angelova, M.; Dimitrov, D. S. A Mechanism of Liposome Electroformation. *Progr Colloid Polym Sci* **1988**, *76*, 59–67. <https://doi.org/10.1007/BFb0114171>.
- (51) Carvalho, K.; Tsai, F.-C.; Lees, E.; Voituriez, R.; Koenderink, G. H.; Sykes, C. Cell-Sized Liposomes Reveal How Actomyosin Cortical Tension Drives Shape Change. *PNAS* **2013**, *110* (41), 16456–16461. <https://doi.org/10.1073/pnas.1221524110>.

Supporting information

Phase-separated GUVs

Since our goal is to reconstitute an actin network on the membrane, we have checked that the addition of the lipids that we use to bind NPF does not impair the formation of lipid domains on the membrane. Indeed, in the presence of either PEG-Biotin or NiNTA lipids or both, the formation of lipid domains on GUVs was still observable (**Figure S 1** C, D and E).

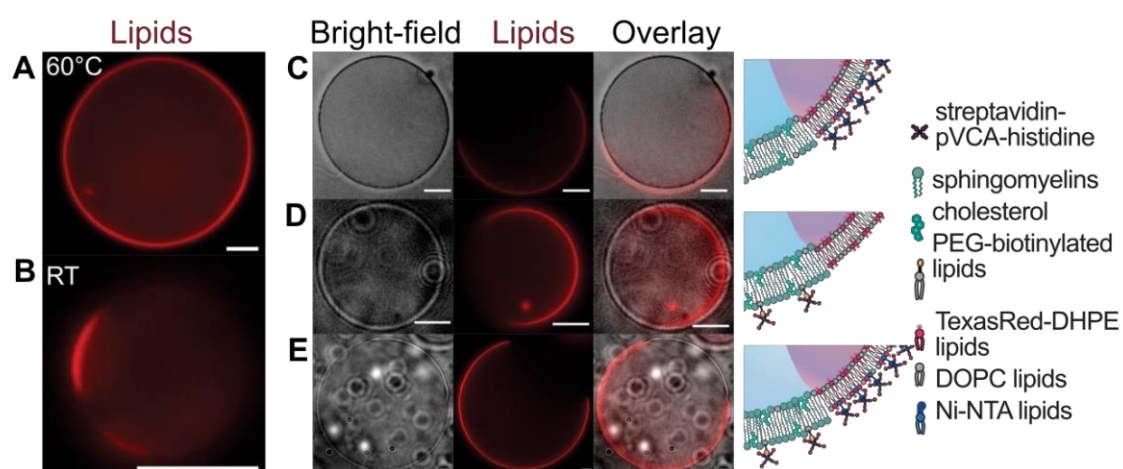


Figure S 1: Observation of phase-separated GUVs. On a temperature-controlled assay: GUVs from the ternary lipid composition showed no domains (A) when the temperature reached 60°C. In contrast, GUVs used for the experiments presented domains (B) at Room Temperature (RT). This is also the case for GUVs comprising lipids conjugated to either biotin (C), Ni-NTA (D), or both (E). Scale bar = 5 μ m.

The next step is to check into which domain the PEG-Biotin and Ni-NTA lipids segregate. In the case of Ni-NTA lipids, (Dürre and Bausch, 2019) showed that they preferentially located into L_d domains. For PEG-Biotin lipids, we marked them using fluorescent Alexa-680 streptavidin on phase-separated GUVs in which Bodipy was used to mark the L_d domain (**Figure S 2**). Indeed, this control experiment shows the segregation of PEG-Biotin lipids into the L_o domain.



Figure S 2: Biotinylated lipids distribution on a phase-separated GUV. From left to right: Lipid membrane marked in green by Bodipy, then Alexa-680 conjugated streptavidin, which bounds to biotinylated lipids segregated to Lo domain as shown on the overlay. Scale bar = 5 μm . The exposure time for Bodipy and Alexa-680-streptavidin is fixed at 100 milliseconds. These acquisition settings were used for all images.

Effect of actin polymerization on different regions of GUVs

Compared to the case of Ld domains, where comets were the most frequently observed actin structure, actin polymerization on Lo domains induces around 40% of partial-shell structures and 40% of comets (**Figure S 3A** and **B**). While polymerization on both domains induces more actin shells (50%) than comets (30%), as observed in **Figure S 3C**.

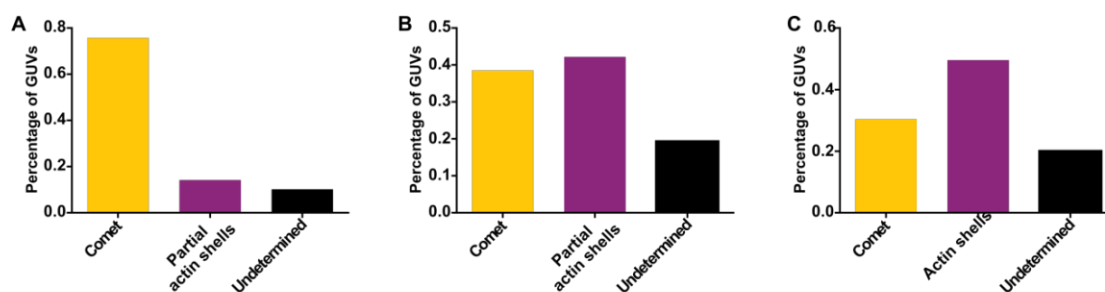


Figure S 3: Morphology distribution of GUVs upon polymerization of a branched actin network. Targeting actin polymerization towards Ld domain (**A**), Lo domain (**B**) or both domains (**C**): Comet represents GUVs with a one-sided elongated actin tail, and partial actin shells represent GUVs with a partially distributed actin network on its surface. $N=4$ independent experiments for a total of 148 GUVs (**A**). $N=3$ independent experiments for 109 GUVs (**B**). In **C**, actin shells represent GUVs with a symmetric actin network on their surface. $N=3$ experiments for 125 GUVs.

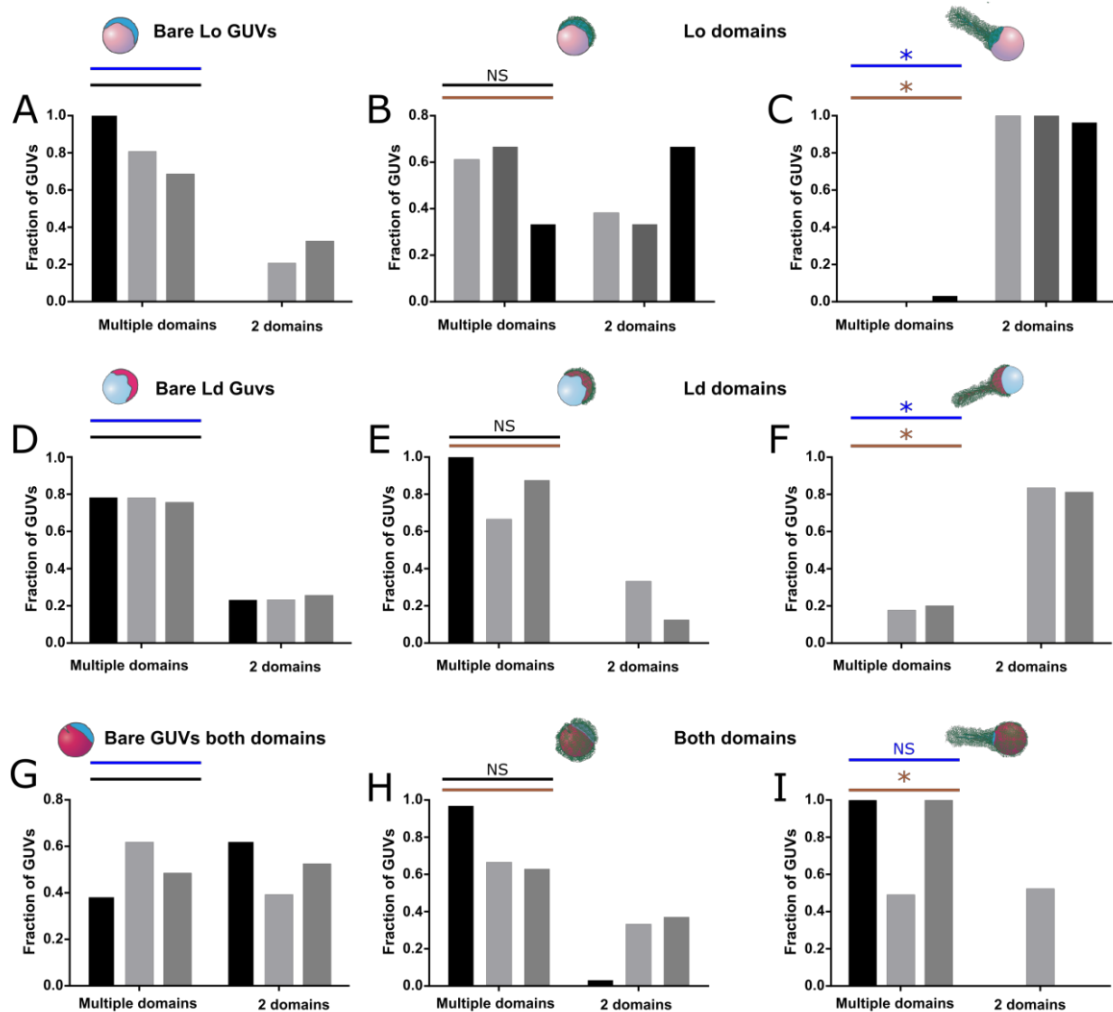


Figure S 4: Lipid domains rearrangement upon actin polymerization on phase-separated GUVs (histograms without experiments pooling. Each bar represents an independent experiment). In all experiments, we separate between GUVs with more than two visible domains (multiple domains) and GUVs with two domains. First row: Number of lipid domains (2 domains vs multiple domains) before actin polymerization on Ld (A), Lo (B) and both domains (C). Second row: number of lipid domains after actin polymerization on Ld, Lo or both domains, resulting in either partial actin shells (D,F,H) or comets (E,G,I). N=3 experiments for bare GUVs: 80 GUVs before polymerization on Ld domains, 73 GUVs before polymerization on the Lo domain and 52 GUVs before polymerization on both domains. N=3 experiments for actin polymerization on the Ld domains: 21 partial shells and 112 comets; Lo domain: 46 partial shells and 42 comets; and on both domains: 62 partial shells and 38 comets. Paired t-test shows non-significant (NS) and significant results ($p < 0.05$ marked by *) when comparing two groups.

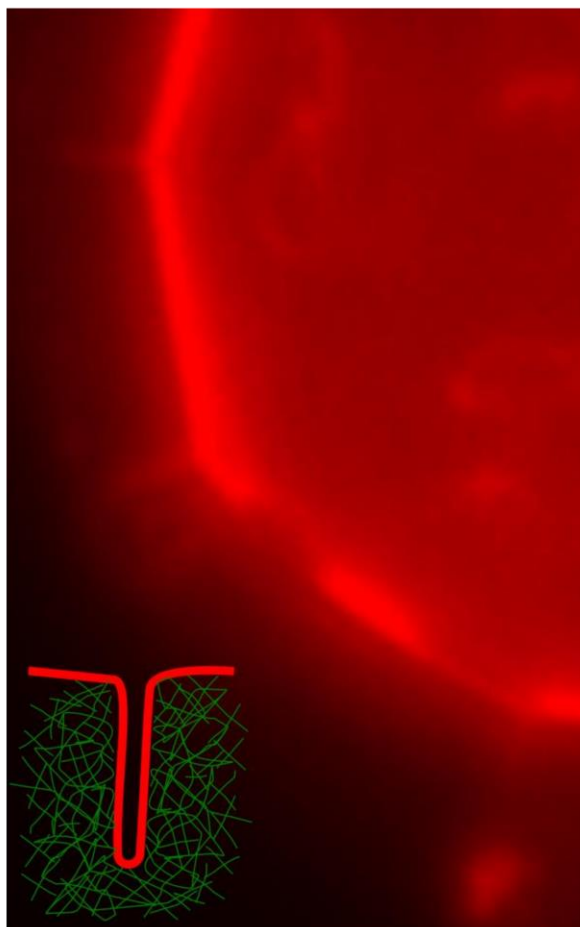


Figure S 5: Zoom from figure 2B of the membrane deformations induced by a partial actin shell: Actin polymerization on the Ld domain induces tubes pulled from the membrane (red). Insert shows the schematic representation of the membrane (red) and actin (green).

4.2.2.2 Additional results on phase-separated GUVs

In this section, we present some results on phase-separated GUVs that are not included in the precedent manuscript but that we discuss in light of the results obtained on homogeneous GUVs (see section 4.2.1).

Polymerisation of a crosslinked actin network on L_d domains

We performed the same experiments as presented in the previous article in the presence of α -actinin and fascin (**Figure 28**), as in the case of homogeneous GUVs (section 4.2.1). Polymerisation in the presence of α -actinin also induces partial shells and comets (**Figure 28 A, B and C**) but favours partial shells compared to the Arp2/3 –only condition (**Figure 29 A**), whereas fascin produces only comets (**Figure 28 D and Figure 29 A**).

As shown in (**Figure 22 B**), most homogeneous DOPC GUVs polymerised with Arp2/3 and α -actinin present lipid nanotubes at their surface. The same tendency appears on phase-separated GUVs. Surprisingly, almost 40% of phase-separated GUVs present spikes under partial shells (**Figure 29 B**), whereas we never observed spikes on homogeneous GUVs. Membrane wrinkling was greatly reduced from almost 80% for homogeneous GUVs (**Figure 22 B**) to 20% for phase-separated GUVs with an α -actinin actin network (**Figure 29 B**). In the presence of fascin, GUVs only form comets (**Figure 29 A**) which are comparable to the comets depicted in **Figure 18** (C and D).

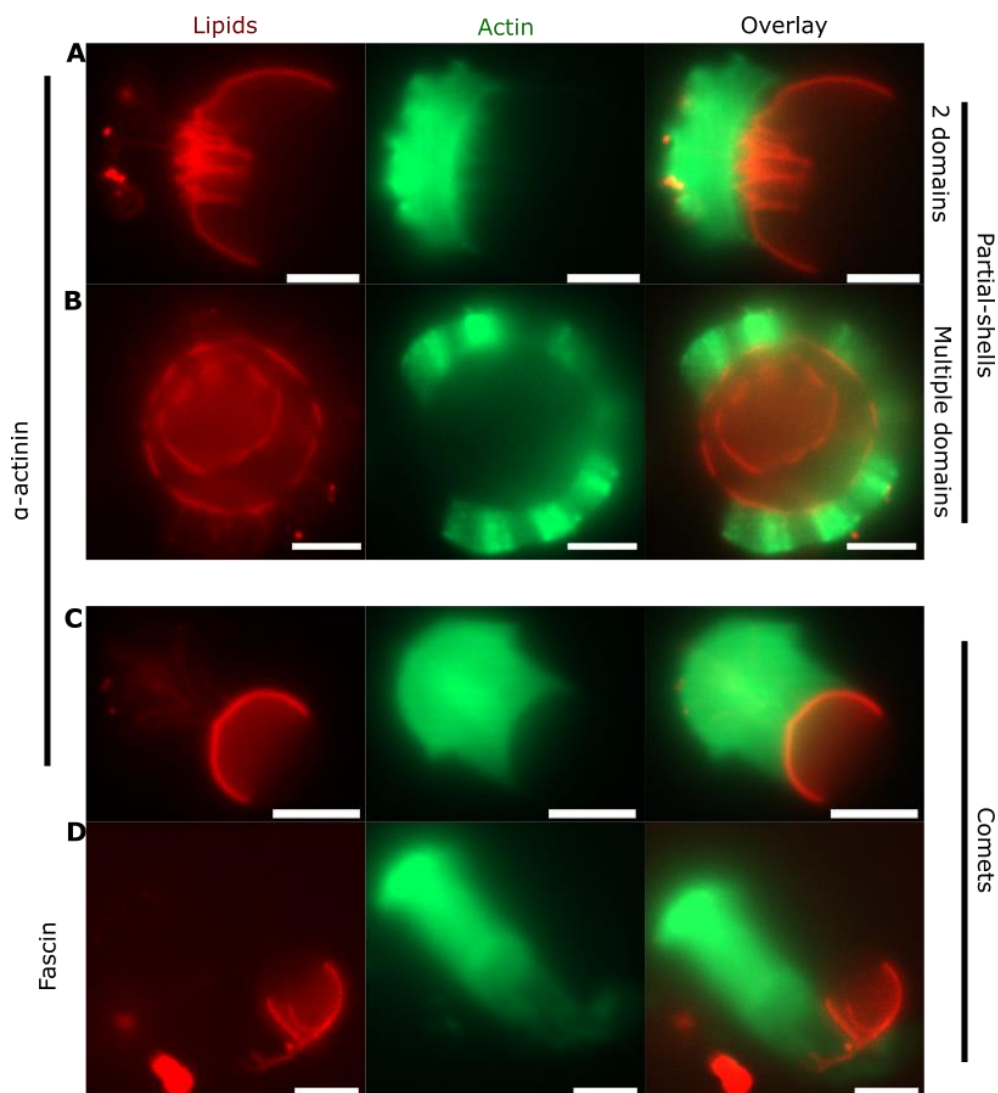


Figure 28: Actin network crosslinked by α -actinin polymerised on the L_d domain of GUVs. The first two panels depict symmetric shells polymerised on GUVs presenting one (A) or multiple (B) L_d domains. Panels C and D show asymmetric shells or comets on GUVs presenting one large L_d domain at the actin side for α -actinin and fascin, respectively. Scale bar 5 μ m.

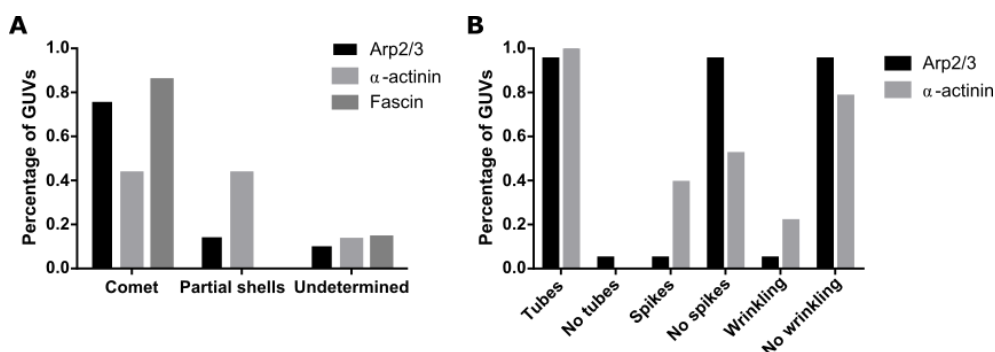


Figure 29: Effect of crosslinked actin networks on L_d domains of phase-separated-GUVs. A: Morphology distribution of phase-separated GUVs with an Arp2/3 actin network in the presence or not of α -actinin or fascin. B: Percentage of GUVs with partial-shell presenting tubes, spikes or wrinkled membranes. $N=4$ experiments for a total of 148 GUVs of Arp2/3; $N=1$ experiment for a total of 53 GUVs of α -actinin. $N=1$ experiment for 14 GUVs of fascin.

Actin polymerisation on both lipid domains

Actin polymerisation on both lipid domains induces symmetric actin shells (55% of GUVs) (**Figure 30 A**). These shell-like actin networks still produce tubes in the observable L_d phase, as in the case of polymerization on the L_d domain alone. Nevertheless, the fraction of GUVs presenting tubes is almost 100% when actin is polymerized on the L_d domain alone, whereas when actin is polymerised on both domains, it is 60%. Interestingly, spikes are observed when actin is polymerised on both domains. However, these GUVs presenting spikes still represent only a small fraction of around 10% as for GUVs polymerised on the L_d domain alone (**Figure 29 B**). Membrane wrinkling appears to be greatly enhanced when polymerising on L_o and L_d domains (**Figure 30 B**). Indeed, 60% of GUVs present wrinkles at their surface, strikingly contrasting with the 10% of GUVs presenting wrinkles with actin polymerisation actin on L_d domains only.

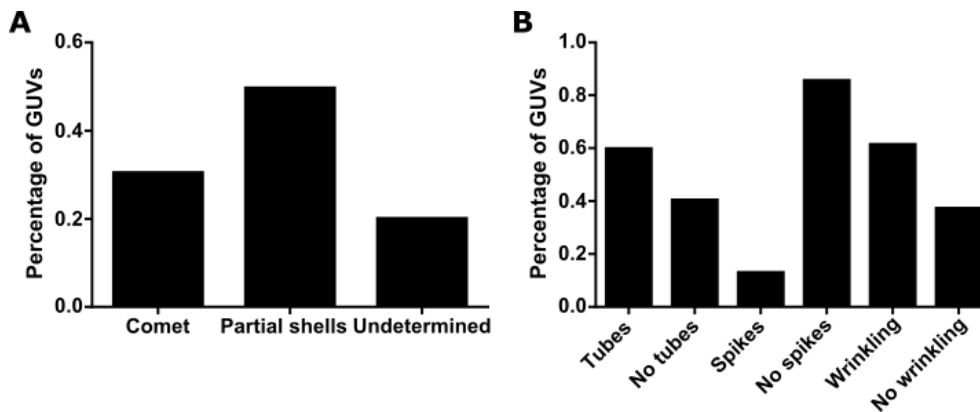


Figure 30: Effect of Arp2/3 actin network polymerised on both L_o and L_d domain of GUVs. A: Morphology distribution of phase-separated GUVs with an Arp2/3 actin network. B: Percentage of GUVs with cortex-like presenting tubes, spikes and wrinkled membranes. $N=3$ experiments for 125 GUVs.

Conclusion

The visible L_d domain of phase-separated GUVs corresponds to a DOPC-enriched domain. Thus, we can compare homogeneous DOPC GUVs and heterogeneous GUVs with actin polymerized on the L_d domain or on both domains.

For the Arp2/3 actin network without crosslinkers, around 10% of phase-separated GUVs with polymerization on the L_d domain present spikes. The same is observed with polymerisation on both L_d and L_o domains. In our experiments, spikes were not observed with polymerisation on DOPC GUVs, which is in accordance with (Simon et al. 2019). Indeed, in this article, spikes were mostly observed when the GUVs were osmotically deflated. Besides, when polymerising on both domains, a striking increase of wrinkling GUVs to 60% is observed when compared to L_d domain polymerised GUVs and DOPC GUVs with 5% and no wrinkling, respectively.

In the case of polymerisation on L_d domains in the presence of α -actinin, the fraction of phase-separated GUVs presenting wrinkling decreases to 20% compared to DOPC GUVs, which is about 80% of GUVs. Moreover, we observe a four times increase in L_d domain

polymerised GUVs presenting spikes (40%) when compared to previous Arp2/3-only network conditions (Arp2/3-only).

Polymerisation in the presence of Fascin on L_d domains induces only comets, which are comparable to the other conditions (DOPC and SM GUVs polymerised with Arp2/3-only or α -actinin; but also with L_o and both domains polymerised with Arp2/3-only).

In summary, on phase-separated GUVs, spikes appear under an actin cortex-like (L_d and $L_d + L_o$ polymerisation). Adding α -actinin enhances spikes formation when polymerising on the L_d domain. Here, the only difference compared to homogeneous GUVs is the actin polymerisation targeted to a specific membrane region. The mechanisms explaining the apparition of spikes only in the presence of membrane domains are undetermined. Spikes were observed by (Simon et al. 2019) only when membrane tension was reduced, but in our case, it is not easy to imagine how the presence of domains could induce such an effect.

4.3 TRACKING ACTIN-INDUCED SHAPE CHANGES ON GUVs

Microfluidic chamber

As a dynamic event, actin polymerisation produces a variety of membrane deformations. As previously shown (**Figure 20**), these deformations depend on the structure of the actin network. It's thought that a symmetric actin network that achieves a critical point of tension upon network growth will result in its symmetry breaking. However, following the symmetry-breaking event in time and space is complicated with our current assay setup because actin polymerisation occurs in an Eppendorf tube before being stopped by diluting actin monomers and placed in an observation chamber without traps. For this reason, we use a microfluidic device containing horseshoe-shaped traps developed by Jacques Fattacioli (**Figure 31**) to start following the dynamics of actin polymerisation on several GUVs (**Figure 33**). The chamber allows for trapping individual GUVs and subsequently adding the actin cocktail while observing GUV remodelling.

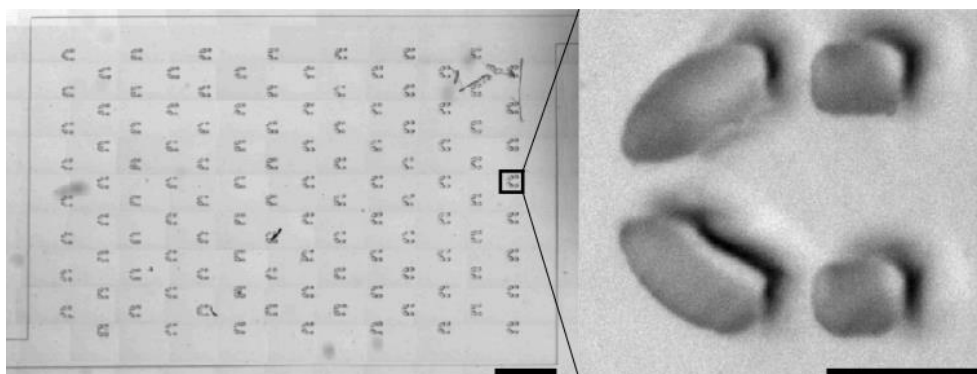


Figure 31: Microfluidic chamber to study the remodelling of GUVs by actin dynamics. With 112 traps to be filled from the right (inlet) to the left (outlet). Scale bar 500 μ m and 50 μ m.

Coating of the microfluidic device

Chamber coating is essential to avoid the adhesion of elements introduced in the chamber. However, not all coating molecules were suitable for our setup. Even if PLL-g-PEG coating was appropriate for bare GUVs only, after injecting the actin mixture, we could see actin adhesion on the chamber surface instead of the GUV surface (**Figure 32**). The same results were obtained with BSA and β -casein. The coating of the microchamber is better with the molecule of PVP. We observe few to no adhesion of GUVs and actin.

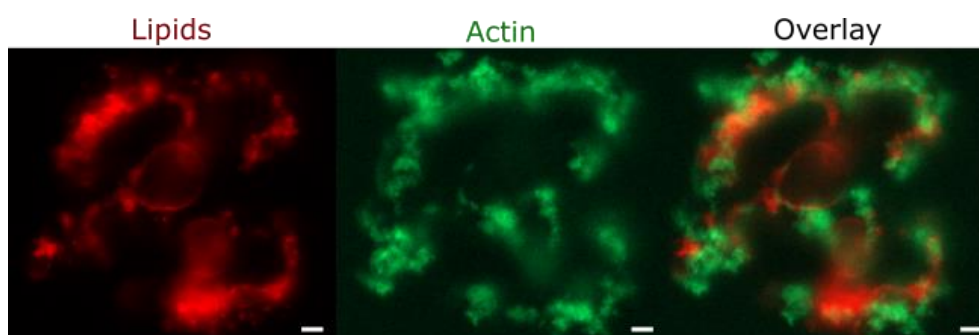


Figure 32: GUVs and actin adhesion to the chamber. The microfluidic device was coated with PLL-g-PEG. From left to right: lipid and actin adhesion can be observed. Scale bar = 10 μ m.

Symmetry breaking event

Finally, I showed we can follow a symmetry-breaking event (**Figure 33**) using the microfluidic chambers coated with PVP. SpVCA preincubation with GUVs outside the chamber before injection and doubling the actin mixture concentration inside the chamber allowed a better ratio of GUVs with actin polymerising. We observe a growing actin network and GUV deformation as a function of time.

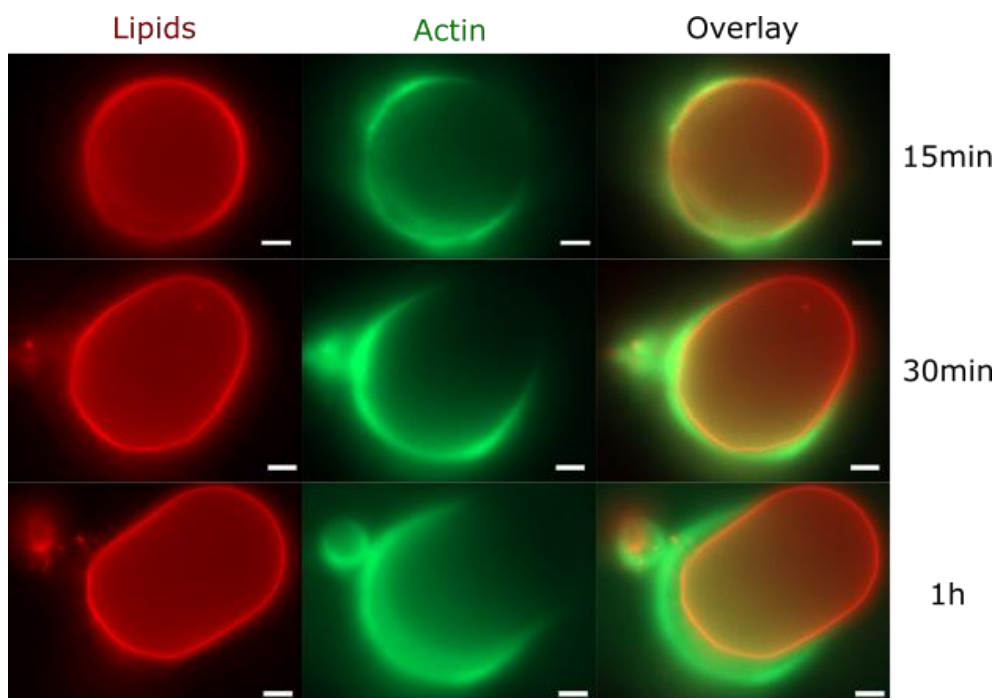


Figure 33: Symmetry breaking event on DOPC GUV. The observation started after 15min of actin polymerisation on the GUV surface. Scale bar = 5 μ m.

However, further optimisation is required. Indeed, from 32 selected GUVs, only 9 GUVs had polymerised actin. Also, a symmetric cortex is yet to be achieved or observed.

5 CONCLUSION AND PERSPECTIVES

The biomimetic systems developed in this thesis allowed us to assess how the interplay between membrane mechanics and the structure of actin networks control the actin-induced shape changes of GUVs. Knowing that biological membranes comprise a very high number of different lipids (van Meer, Voelker, and Feigenson 2008), we used membrane models with different mechanical properties and comprising lipid domains. It has been shown in experiments in living cells that the actin cytoskeleton and membrane domains have subtle interplay (Fritzsche et al. 2017). Besides, we used different types of ABPs, crosslinkers and bundlers to shape the structure of Arp2/3 actin networks (Blanchoin et al. 2014).

So far, only (Liu and Fletcher 2006) explored the influence of the actin network on domain formation in GUVs. The authors demonstrated *in vitro* that the polymerisation of an actin network on GUVs changed the miscibility temperature of their membrane. However, the impact of lipid domains on actin-induced membrane remodelling is still unclear.

Therefore, I have built an *in vitro* system comprising heterogeneous membranes coupled to actin networks. This adds another building block to the formation of biomimetic systems formed by membranes and actin networks to reconstitute cell shape changes.

First, I started by forming phase-separated nanotubes. Using STED microscopy, we demonstrate that membrane nanotubes comprising ternary lipid composition formed lipid domains. Then, we sought to quantify these nanotubes' width and tension values as in (Roy et al. 2020). Here, we formed various attached phase-separated nanotubes by applying a hydrodynamic flow to SLBs. These nanotubes' widths are quantified, and their tension is calculated. The values we obtained are in reasonable agreement with theoretical predictions (M. Heinrich et al. 2010).

AFM can assess the nanomechanical properties of nanotubes. The approach was developed in the laboratory for homogeneous membrane nanotubes, and I showed that the protocol and model

developed by (Lamour et al. 2020) still apply to heterogeneous membrane nanotubes. The advantage of AFM is the ability to directly measure local rigidity. Hence, due to the demonstrated relationship between nanotube height and rigidity, we assessed the morphology and mechanical properties of the L_d and L_o domains of phase-separated nanotubes. A step further for these experiments would be to polymerise actin networks to understand their effect on nanotube remodelling. An interesting approach would be to correlate AFM and STED microscopy. While AFM is a great tool to assess the mechanical properties of materials, it is not suitable for all samples. When a soft material, such as a membrane nanotube, is covered by a harder material, such as an actin network, the membrane properties are not accessible.

Then, using GUVs, I explored the shape changes induced by the polymerisation of actin networks at their surface. Firstly, I sought to change the mechanical properties of their membrane. Experiments with two types of homogeneous (DOPC or SMC) GUVs, highlighted the effect of the membrane composition on the Arp2/3 actin-induced shape changes observed. More precisely, the bending rigidity controls the shape changes induced by actin dynamics. We observed more symmetry breaking for DOPC GUVs, which have a low bending rigidity. SMC GUVs presented more wrinkles and less nanotubes.

I varied the actin structures by introducing α -actinin or fascin. I demonstrate the effect of α -actinin on the actin-induced shape changes. We observe stronger wrinkling in the presence of α -actinin. Fascin induces longer comets and jumps for DOPC GUVs, and abolishes the formation of tubes in the actin shells. For SMC GUVs, we observe no tubes in the shells and peanut shape-like for comets.

A harder membrane seems to impair tube formation and favor wrinkling, especially when the forces induced by actin growth are increased by the presence of a crosslinker. Nevertheless, theoretical modelling is required to understand the detailed mechanisms of these observations.

Finally, I developed a biomimetic system to target actin polymerization on specific domains of phase-separated GUVs. By using an NPF that

binds to Ni-NTA and biotinylated lipids, I demonstrate that the segregation of these lipids into L_d and L_o , respectively, allows us to target actin polymerisation on one or both domains. Such a system allowed the observation of the interplay between actin dynamics and membrane heterogeneities. For instance, actin structures emerge from either hemispherical or multiple domains after actin polymerisation. We observe partial shells and actin comets formed on the desired domain.

Furthermore, we observe domain reorganization due to actin polymerization dynamics on either L_d or L_o domains. The multiple domains present on GUVs are reorganised into two separate hemispheres after actin polymerisation and actin network symmetry breaking. (Vogel et al. 2017) also induced domain reorganisation. However, this was achieved by myosin motor activity on preformed actin filaments bound to phase-separated SLBs.

Although we observe global (formation of comets) or local (tube pulling, wrinkles) deformations and rearrangements of domains, the L_o domains are not fluorescent in our experiments. We sought to use a fluorescent analogue of cholesterol that should segregate to the L_o domains (Garvik et al. 2009), but no fluorescent signal was detected during our experiments. Therefore, a potential actin-induced shape change was not observed, and thus, a suitable dye (Baumgart, Hunt, et al. 2007) should be tested under our experimental conditions. This would allow observation of the L_o domains. Another aspect to be developed in the future is experiments involving different actin networks on the same GUV. For instance, combining Arp2/3 and formins by using our experimental strategy would allow the polymerisation of two types of actin networks on the same GUV. Arp2/3 and formins are known to be implicated in cell membrane deformation, such as the formation of filopodia or lamellipodia (Isogai et al. 2015; Dimchev et al. 2021). Therefore, the polymerisation of Arp2/3 and formin actin networks on the same GUV could highlight the crosstalk between them.

Moreover, in order to optimise all these observations of deformations on GUVs, I started developing a microfluidic device. This device allowed us to trap GUVs and follow actin polymerisation on them. We

observed the symmetry breaking of an actin shell, and further optimisation will allow spatial and temporal following of the actin-induced shape changes on GUVs. Ultimately, controlling when actin polymerisation starts could be achieved by light-activated compounds such as caged-ATP or blebbistatin (Jahnke et al. 2020). However, different ABPs could also be added on demand to the microchamber to mimic specific proteins' chronology and reconstitute certain cell shape changes. Such experiments would pave the way to understanding the interplay between the elements participating in cell shape changes.

6 REFERENCES

- Ahmed, S.N., D.A. Brown, and E. London. 1997. 'On the Origin of Sphingolipid/Cholesterol-Rich Detergent-Insoluble Cell Membranes: Physiological Concentrations of Cholesterol and Sphingolipid Induce Formation of a Detergent-Insoluble, Liquid-Ordered Lipid Phase in Model Membranes'. *Biochemistry* 36 (36): 10944–53. <https://doi.org/10.1021/bi971167g>.
- Alberts, Bruce, Alexander Johnson, Julian Lewis, Martin Raff, Keith Roberts, and Peter Walter. 2008. *Molecular Biology of the Cell: The Problems Book*. Fifth. New York: Garland Science.
- Allain, J.-M., C. Storm, A. Roux, M. Ben Amar, and J.-F. Joanny. 2004. 'Fission of a Multiphase Membrane Tube'. *Physical Review Letters* 93 (15): 158104. <https://doi.org/10.1103/PhysRevLett.93.158104>.
- Allard, A., M. Bouzid, T. Betz, C. Simon, M. Abou-Ghali, J. Lemièrè, F. Valentino, et al. 2020. 'Actin Modulates Shape and Mechanics of Tubular Membranes'. *Science Advances* 6 (17): eaaz3050. <https://doi.org/10.1126/sciadv.aaz3050>.
- Allard, A., F. Valentino, C. Sykes, T. Betz, and C. Campillo. 2020. 'Fluctuations of a Membrane Nanotube Covered with an Actin Sleeve'. *Physical Review E* 102 (5): 052402. <https://doi.org/10.1103/PhysRevE.102.052402>.
- Allard, Antoine, Rogério Lopes dos Santos, and Clément Campillo. 2021. 'Remodelling of Membrane Tubules by the Actin Cytoskeleton'. *Biology of the Cell*, April, boc.202000148. <https://doi.org/10.1111/boc.202000148>.
- Angelova, M., and D. S. Dimitrov. 1988. 'A Mechanism of Liposome Electroformation'. *Trends in Colloid and Interface Science II*, Progress in Colloid & Polymer Science, 76: 59–67. <https://doi.org/10.1007/BFb0114171>.
- Arumugam, Senthil, Eugene P. Petrov, and Petra Schwille. 2015. 'Cytoskeletal Pinning Controls Phase Separation in Multicomponent Lipid Membranes'. *Biophysical Journal* 108 (5): 1104–13. <https://doi.org/10.1016/j.bpj.2014.12.050>.
- Avalos-Padilla, Yunuen, Vasil N. Georgiev, and Rumiana Dimova. 2021. 'ESCRT-III Induces Phase Separation in Model Membranes Prior

- to Budding and Causes Invagination of the Liquid-Ordered Phase'. *Biochimica et Biophysica Acta (BBA) - Biomembranes* 1863 (10): 183689. <https://doi.org/10.1016/j.bbamem.2021.183689>.
- Baldauf, Lucia, Lennard van Buren, Federico Fanalista, and Gijse Hendrika Koenderink. 2022. 'Actomyosin-Driven Division of a Synthetic Cell'. *ACS Synthetic Biology* 11 (10): 3120–33. <https://doi.org/10.1021/acssynbio.2c00287>.
- Bashirzadeh, Yashar, Hossein Moghimianavval, and Allen P. Liu. 2022. 'Encapsulated Actomyosin Patterns Drive Cell-like Membrane Shape Changes'. *iScience* 25 (5): 104236. <https://doi.org/10.1016/j.isci.2022.104236>.
- Baumgart, Tobias, Adam T. Hammond, Prabuddha Sengupta, Samuel T. Hess, David A. Holowka, Barbara A. Baird, and Watt W. Webb. 2007. 'Large-Scale Fluid/Fluid Phase Separation of Proteins and Lipids in Giant Plasma Membrane Vesicles'. *Proceedings of the National Academy of Sciences* 104 (9): 3165–70. <https://doi.org/10.1073/pnas.0611357104>.
- Baumgart, Tobias, Samuel T. Hess, and Watt W. Webb. 2003. 'Imaging Coexisting Fluid Domains in Biomembrane Models Coupling Curvature and Line Tension'. *Nature* 425 (6960): 821–24. <https://doi.org/10.1038/nature02013>.
- Baumgart, Tobias, Geoff Hunt, Elaine R. Farkas, Watt W. Webb, and Gerald W. Feigenson. 2007. 'Fluorescence Probe Partitioning between Lo/Ld Phases in Lipid Membranes'. *Biochimica et Biophysica Acta* 1768 (9): 2182–94. <https://doi.org/10.1016/j.bbamem.2007.05.012>.
- Bernheim-Groswasser, Anne, Sebastian Wiesner, Roy M. Golsteyn, Marie-France Carlier, and Cécile Sykes. 2002. 'The Dynamics of Actin-Based Motility Depend on Surface Parameters'. *Nature* 417 (6886): 308–11. <https://doi.org/10.1038/417308a>.
- Bieling, Peter, Scott D Hansen, Orkun Akin, Tai-De Li, Carl C Hayden, Daniel A Fletcher, and R Dyche Mullins. 2018. 'WH2 and Proline-Rich Domains of WASP-Family Proteins Collaborate to Accelerate Actin Filament Elongation'. *The EMBO Journal* 37 (1): 102–21. <https://doi.org/10.15252/emj.201797039>.
- Biyasheva, Assel, Tatyana Svitkina, Patricia Kunda, Buzz Baum, and Gary Borisy. 2004. 'Cascade Pathway of Filopodia Formation

- Downstream of SCAR'. *Journal of Cell Science* 117 (6): 837–48. <https://doi.org/10.1242/jcs.00921>.
- Blanchoin, Laurent, Rajaa Boujemaa-Paterski, Cécile Sykes, and Julie Plastino. 2014. 'Actin Dynamics, Architecture, and Mechanics in Cell Motility'. *Physiological Reviews* 94 (1): 235–63. <https://doi.org/10.1152/physrev.00018.2013>.
- Bochicchio, D., and L. Monticelli. 2016. 'The Membrane Bending Modulus in Experiments and Simulations'. In *Advances in Biomembranes and Lipid Self-Assembly*, 23:117–43. Elsevier. <https://doi.org/10.1016/bs.abl.2016.01.003>.
- Borghi, N, O Rossier, and F Brochard-Wyart. 2003. 'Hydrodynamic Extrusion of Tubes from Giant Vesicles'. *Europhysics Letters (EPL)* 64 (6): 837–43. <https://doi.org/10.1209/epl/i2003-00321-x>.
- Boukellal, Hakim, Otger Campàs, Jean-François Joanny, Jacques Prost, and Cécile Sykes. 2004. 'Soft Listeria: Actin-Based Propulsion of Liquid Drops'. *Physical Review E* 69 (6): 061906. <https://doi.org/10.1103/PhysRevE.69.061906>.
- Brown, Deborah A., and John K. Rose. 1992. 'Sorting of GPI-Anchored Proteins to Glycolipid-Enriched Membrane Subdomains during Transport to the Apical Cell Surface'. *Cell* 68 (3): 533–44. [https://doi.org/10.1016/0092-8674\(92\)90189-J](https://doi.org/10.1016/0092-8674(92)90189-J).
- Campillo, Clément, Pierre Sens, Darius Köster, Léa-Laetitia Pontani, Daniel Lévy, Patricia Bassereau, Pierre Nassoy, and Cécile Sykes. 2013. 'Unexpected Membrane Dynamics Unveiled by Membrane Nanotube Extrusion'. *Biophysical Journal* 104 (6): 1248–56. <https://doi.org/10.1016/j.bpj.2013.01.051>.
- Canham, P. B. 1970. 'The Minimum Energy of Bending as a Possible Explanation of the Biconcave Shape of the Human Red Blood Cell'. *Journal of Theoretical Biology* 26 (1): 61–81. [https://doi.org/10.1016/S0022-5193\(70\)80032-7](https://doi.org/10.1016/S0022-5193(70)80032-7).
- Carlier, M. F. 1990. 'Actin Polymerization and ATP Hydrolysis'. *Advances in Biophysics* 26: 51–73. [https://doi.org/10.1016/0065-227x\(90\)90007-g](https://doi.org/10.1016/0065-227x(90)90007-g).
- Carlier, M. F., D. Pantaloni, and E. D. Korn. 1986. 'Fluorescence Measurements of the Binding of Cations to High-Affinity and Low-Affinity Sites on ATP-G-Actin'. *The Journal of Biological Chemistry* 261 (23): 10778–84.
- Carvalho, Kevin, Feng-Ching Tsai, Edouard Lees, Raphaël Voituriez,

- Gijsje H. Koenderink, and Cecile Sykes. 2013. 'Cell-Sized Liposomes Reveal How Actomyosin Cortical Tension Drives Shape Change'. *Proceedings of the National Academy of Sciences* 110 (41): 16456–61. <https://doi.org/10.1073/pnas.1221524110>.
- Chakraborty, Saptarshi, Milka Doktorova, Trivikram R. Molugu, Frederick A. Heberle, Haden L. Scott, Boris Dzikovski, Michihiro Nagao, et al. 2020. 'How Cholesterol Stiffens Unsaturated Lipid Membranes'. *Proceedings of the National Academy of Sciences* 117 (36): 21896–905. <https://doi.org/10.1073/pnas.2004807117>.
- Courtemanche, Naomi, and Thomas D. Pollard. 2013. 'Interaction of Profilin with the Barbed End of Actin Filaments'. *Biochemistry* 52 (37): 6456–66. <https://doi.org/10.1021/bi400682n>.
- Cuvelier, Damien, Imre Derényi, Patricia Bassereau, and Pierre Nassoy. 2005. 'Coalescence of Membrane Tethers: Experiments, Theory, and Applications'. *Biophysical Journal* 88 (4): 2714–26. <https://doi.org/10.1529/biophysj.104.056473>.
- Dar, Srishti, Sukrut C Kamerkar, and Thomas J Pucadyil. 2017. 'Use of the Supported Membrane Tube Assay System for Real-Time Analysis of Membrane Fission Reactions'. *Nature Protocols* 12 (2): 390–400. <https://doi.org/10.1038/nprot.2016.173>.
- Delatour, Vincent, Emmanuèle Helfer, Dominique Didry, Kim Hô Diêp Lê, Jean-François Gaucher, Marie-France Carlier, and Guillaume Romet-Lemonne. 2008. 'Arp2/3 Controls the Motile Behavior of N-WASP-Functionalized GUVs and Modulates N-WASP Surface Distribution by Mediating Transient Links with Actin Filaments'. *Biophysical Journal* 94 (12): 4890–4905. <https://doi.org/10.1529/biophysj.107.118653>.
- Delatour, Vincent, Shashank Shekhar, Anne-Cécile Reymann, Dominique Didry, Kim Hô Diêp Lê, Guillaume Romet-Lemonne, Emmanuèle Helfer, and Marie-France Carlier. 2008. 'Actin-Based Propulsion of Functionalized Hard versus Fluid Spherical Objects'. *New Journal of Physics* 10 (2): 025001. <https://doi.org/10.1088/1367-2630/10/2/025001>.
- Delcour, Anne H. 2009. 'Outer Membrane Permeability and Antibiotic Resistance'. *Biochimica et Biophysica Acta (BBA) - Proteins and Proteomics, Mechanisms of Drug Efflux and Strategies to Combat Them*, 1794 (5): 808–16.

- <https://doi.org/10.1016/j.bbapap.2008.11.005>.
- Dimchev, Vanessa, Ines Lahmann, Stefan A. Koestler, Frieda Kage, Georgi Dimchev, Anika Steffen, Theresia E. B. Stradal, Franz Vauti, Hans-Henning Arnold, and Klemens Rottner. 2021. 'Induced Arp2/3 Complex Depletion Increases FMNL2/3 Formin Expression and Filopodia Formation'. *Frontiers in Cell and Developmental Biology* 9. <https://www.frontiersin.org/articles/10.3389/fcell.2021.634708>.
- Djinović-Carugo, Kristina, Paul Young, Mathias Gautel, and Matti Saraste. 1999. 'Molecular Basis for Cross-Linking of Actin Filaments: Structure of the α -Actinin Rod'. *Cell* 98 (4): 537–46. [https://doi.org/10.1016/S0092-8674\(00\)81981-9](https://doi.org/10.1016/S0092-8674(00)81981-9).
- Drury, Jeanie L., and Micah Dembo. 1999. 'Hydrodynamics of Micropipette Aspiration'. *Biophysical Journal* 76 (1): 110–28. [https://doi.org/10.1016/S0006-3495\(99\)77183-3](https://doi.org/10.1016/S0006-3495(99)77183-3).
- Dürre, Katharina, and Andreas R. Bausch. 2019. 'Formation of Phase Separated Vesicles by Double Layer CDICE'. *Soft Matter* 15 (47): 9676–81. <https://doi.org/10.1039/C8SM02491J>.
- Dürre, Katharina, Felix C. Keber, Philip Bleicher, Fridtjof Brauns, Christian J. Cyron, Jan Faix, and Andreas R. Bausch. 2018. 'Capping Protein-Controlled Actin Polymerization Shapes Lipid Membranes'. *Nature Communications* 9 (1): 1630. <https://doi.org/10.1038/s41467-018-03918-1>.
- Eddidin, Michael. 2003. 'Lipids on the Frontier: A Century of Cell-Membrane Bilayers'. *Nature Reviews Molecular Cell Biology* 4 (5): 414–18. <https://doi.org/10.1038/nrm1102>.
- Edwards, Marc, Adam Zwolak, Dorothy A. Schafer, David Sept, Roberto Dominguez, and John A. Cooper. 2014. 'Capping Protein Regulators Fine-Tune Actin Assembly Dynamics'. *Nature Reviews Molecular Cell Biology* 15 (10): 677–89. <https://doi.org/10.1038/nrm3869>.
- Espinoza-Sanchez, Sofia, Lauren Ann Metskas, Steven Z. Chou, Elizabeth Rhoades, and Thomas D. Pollard. 2018. 'Conformational Changes in Arp2/3 Complex Induced by ATP, WASp-VCA, and Actin Filaments'. *Proceedings of the National Academy of Sciences* 115 (37): E8642–51. <https://doi.org/10.1073/pnas.1717594115>.
- Evans, E., and W. Rawicz. 1990. 'Entropy-Driven Tension and Bending

- Elasticity in Condensed-Fluid Membranes'. *Physical Review Letters* 64 (17): 2094–97. <https://doi.org/10.1103/PhysRevLett.64.2094>.
- Evans, Evan, Volkmar Heinrich, Florian Ludwig, and Wieslawa Rawicz. 2003. 'Dynamic Tension Spectroscopy and Strength of Biomembranes'. *Biophysical Journal* 85 (4): 2342–50. [https://doi.org/10.1016/S0006-3495\(03\)74658-X](https://doi.org/10.1016/S0006-3495(03)74658-X).
- Filippov, Andrey, Greger Orädd, and Göran Lindblom. 2003. 'The Effect of Cholesterol on the Lateral Diffusion of Phospholipids in Oriented Bilayers'. *Biophysical Journal* 84 (5): 3079–86.
- Fritzsche, M., D. Li, H. Colin-York, V. T. Chang, E. Moeendarbary, J. H. Felce, E. Sezgin, G. Charras, E. Betzig, and C. Eggeling. 2017. 'Self-Organizing Actin Patterns Shape Membrane Architecture but Not Cell Mechanics'. *Nature Communications* 8 (1): 14347. <https://doi.org/10.1038/ncomms14347>.
- Fujiwara, Ikuko, Shin Takahashi, Hisashi Tadakuma, Takashi Funatsu, and Shin'ichi Ishiwata. 2002. 'Microscopic Analysis of Polymerization Dynamics with Individual Actin Filaments'. *Nature Cell Biology* 4 (9): 666–73. <https://doi.org/10.1038/ncb841>.
- Funk, Johanna, Felipe Merino, Larisa Venkova, Lina Heydenreich, Jan Kierfeld, Pablo Vargas, Stefan Raunser, Matthieu Piel, and Peter Bieling. 2019. 'Profilin and Formin Constitute a Pacemaker System for Robust Actin Filament Growth'. Edited by Pekka Lappalainen, Anna Akhmanova, and Pekka Lappalainen. *eLife* 8 (October): e50963. <https://doi.org/10.7554/eLife.50963>.
- Gallop, Jennifer L, Christine C Jao, Helen M Kent, P Jonathan G Butler, Philip R Evans, Ralf Langen, and Harvey T McMahon. 2006. 'Mechanism of Endophilin N-BAR Domain-Mediated Membrane Curvature'. *The EMBO Journal* 25 (12): 2898–2910. <https://doi.org/10.1038/sj.emboj.7601174>.
- Gallup, Olivia, Hia Ming, and Tom Ellis. 2021. 'Ten Future Challenges for Synthetic Biology'. *Engineering Biology* 5 (3): 51–59. <https://doi.org/10.1049/enb2.12011>.
- Gardel, M. L., J. H. Shin, F. C. MacKintosh, L. Mahadevan, P. A. Matsudaira, and D. A. Weitz. 2004. 'Scaling of F-Actin Network Rheology to Probe Single Filament Elasticity and Dynamics'. *Physical Review Letters* 93 (18): 188102.

- <https://doi.org/10.1103/PhysRevLett.93.188102>.
- Gardel, Margaret L., Karen E. Kasza, Clifford P. Brangwynne, Jiayu Liu, and David A. Weitz. 2008. 'Chapter 19: Mechanical Response of Cytoskeletal Networks'. *Methods in Cell Biology* 89: 487–519. [https://doi.org/10.1016/S0091-679X\(08\)00619-5](https://doi.org/10.1016/S0091-679X(08)00619-5).
- Garvik, Olav, Peter Benediktson, Adam Cohen Simonsen, John Hjort Ipsen, and Daniel Wüstner. 2009. 'The Fluorescent Cholesterol Analog Dehydroergosterol Induces Liquid-Ordered Domains in Model Membranes'. *Chemistry and Physics of Lipids* 159 (2): 114–18. <https://doi.org/10.1016/j.chemphyslip.2009.03.002>.
- Gauthier, Nils C., Thomas A. Masters, and Michael P. Sheetz. 2012. 'Mechanical Feedback between Membrane Tension and Dynamics'. *Trends in Cell Biology* 22 (10): 527–35. <https://doi.org/10.1016/j.tcb.2012.07.005>.
- Giardini, P., D. Fletcher, and J. Theriot. 2003. 'Compression Forces Generated by Actin Comet Tails on Lipid Vesicles'. *Proceedings of the National Academy of Sciences of the United States of America*. <https://doi.org/10.1073/pnas.1031670100>.
- Girard, Philippe. 2004. 'Membranes hors d'équilibre: échanges et transport actif'.
- Goldschmidt-Clermont, P J, L M Machesky, S K Doberstein, and T D Pollard. 1991. 'Mechanism of the Interaction of Human Platelet Profilin with Actin.' *Journal of Cell Biology* 113 (5): 1081–89. <https://doi.org/10.1083/jcb.113.5.1081>.
- Gucht, Jasper van der, Ewa Paluch, Julie Plastino, and Cécile Sykes. 2005. 'Stress Release Drives Symmetry Breaking for Actin-Based Movement'. *Proceedings of the National Academy of Sciences of the United States of America* 102 (22): 7847–52. <https://doi.org/10.1073/pnas.0502121102>.
- Häckl, W., U. Seifert, and E. Sackmann. 1997. 'Effects of Fully and Partially Solubilized Amphiphiles on Bilayer Bending Stiffness and Temperature Dependence of the Effective Tension of Giant Vesicles'. *Journal de Physique II* 7 (8): 1141–57. <https://doi.org/10.1051/jp2:1997177>.
- Hac-Wydro, Katarzyna, and Paweł Wydro. 2007. 'The Influence of Fatty Acids on Model Cholesterol/Phospholipid Membranes'. *Chemistry and Physics of Lipids* 150 (1): 66–81. <https://doi.org/10.1016/j.chemphyslip.2007.06.213>.

- Hampton, Cheri M., Dianne W. Taylor, and Kenneth A. Taylor. 2007. 'Novel Structures for Alpha-Actinin:F-Actin Interactions and Their Implications for Actin-Membrane Attachment and Tension Sensing in the Cytoskeleton'. *Journal of Molecular Biology* 368 (1): 92–104. <https://doi.org/10.1016/j.jmb.2007.01.071>.
- Hao, Mingming, Sushmita Mukherjee, and Frederick R. Maxfield. 2001. 'Cholesterol Depletion Induces Large Scale Domain Segregation in Living Cell Membranes'. *Proceedings of the National Academy of Sciences* 98 (23): 13072–77. <https://doi.org/10.1073/pnas.231377398>.
- Heinrich, M., A. Tian, C. Esposito, and T. Baumgart. 2010. 'Dynamic Sorting of Lipids and Proteins in Membrane Tubes with a Moving Phase Boundary'. *Proceedings of the National Academy of Sciences* 107 (16): 7208–13. <https://doi.org/10.1073/pnas.0913997107>.
- Heinrich, Volkmar, and Richard E. Waugh. 1996. 'A Piconewton Force Transducer and Its Application to Measurement of the Bending Stiffness of Phospholipid Membranes'. *Annals of Biomedical Engineering* 24 (5): 595–605. <https://doi.org/10.1007/BF02684228>.
- Helfer, E., S. Harlepp, L. Bourdieu, J. Robert, F. C. MacKintosh, and D. Chatenay. 2000. 'Microrheology of Biopolymer-Membrane Complexes'. *Physical Review Letters* 85 (2): 457–60. <https://doi.org/10.1103/PhysRevLett.85.457>.
- Helfrich, W. 1973. 'Elastic Properties of Lipid Bilayers: Theory and Possible Experiments'. *Zeitschrift Für Naturforschung C* 28 (11–12): 693–703. <https://doi.org/10.1515/znc-1973-11-1209>.
- Hochmuth, R.M., H.C. Wiles, E.A. Evans, and J.T. McCown. 1982. 'Extensional Flow of Erythrocyte Membrane from Cell Body to Elastic Tether. II. Experiment'. *Biophysical Journal* 39 (1): 83–89. [https://doi.org/10.1016/S0006-3495\(82\)84493-7](https://doi.org/10.1016/S0006-3495(82)84493-7).
- Honigsmann, Alf, Sina Sadeghi, Jan Keller, Stefan W Hell, Christian Eggeling, and Richard Vink. 2014. 'A Lipid Bound Actin Meshwork Organizes Liquid Phase Separation in Model Membranes'. *ELife* 3 (March): e01671. <https://doi.org/10.7554/eLife.01671>.
- Horger, Kim S., Daniel J. Estes, Ricardo Capone, and Michael Mayer.

2009. 'Films of Agarose Enable Rapid Formation of Giant Liposomes in Solutions of Physiologic Ionic Strength'. *Journal of the American Chemical Society* 131 (5): 1810–19. <https://doi.org/10.1021/ja805625u>.
- Imam, Zachary I., and George D. Bachand. 2019. 'Multicomponent and Multiphase Lipid Nanotubes Formed by Gliding Microtubule-Kinesin Motility and Phase-Separated Giant Unilamellar Vesicles'. *Langmuir*, November. <https://doi.org/10.1021/acs.langmuir.9b02637>.
- Isambert, Hervé, Pascal Venier, Anthony C. Maggs, Abdelatif Fattoum, Ridha Kassab, Dominique Pantaloni, and Marie-France Carlier. 1995. 'Flexibility of Actin Filaments Derived from Thermal Fluctuations: EFFECT OF BOUND NUCLEOTIDE, PHALLOIDIN, AND MUSCLE REGULATORY PROTEINS *'. *Journal of Biological Chemistry* 270 (19): 11437–44. <https://doi.org/10.1074/jbc.270.19.11437>.
- Isogai, Tadamoto, Rob van der Kammen, Daniela Leyton-Puig, Katarzyna M. Kedziora, Kees Jalink, and Metello Innocenti. 2015. 'Initiation of Lamellipodia and Ruffles Involves Cooperation between MDia1 and the Arp2/3 Complex'. *Journal of Cell Science* 128 (20): 3796–3810. <https://doi.org/10.1242/jcs.176768>.
- Israelachvili, Jacob N. 2011. 'Soft and Biological Structures'. In *Intermolecular and Surface Forces*, 535–76. Elsevier. <https://doi.org/10.1016/B978-0-12-375182-9.10020-X>.
- Iwasa, Janet H., and R. Dyche Mullins. 2007. 'Spatial and Temporal Relationships between Actin-Filament Nucleation, Capping, and Disassembly'. *Current Biology* 17 (5): 395–406. <https://doi.org/10.1016/j.cub.2007.02.012>.
- Jahnke, Kevin, Stefan J. Maurer, Cornelia Weber, Jochen Estebano Hernandez Bücher, Andreas Schoenit, Elisa D'Este, Elisabetta Ada Cavalcanti-Adam, and Kerstin Göpfrich. 2022. 'Actomyosin-Assisted Pulling of Lipid Nanotubes from Lipid Vesicles and Cells'. *Nano Letters*, January. <https://doi.org/10.1021/acs.nanolett.1c04254>.
- Jahnke, Kevin, Marian Weiss, Cornelia Weber, Ilia Platzman, Kerstin Göpfrich, and Joachim P. Spatz. 2020. 'Engineering Light-Responsive Contractile Actomyosin Networks with DNA

- Nanotechnology'. *Advanced Biosystems* 4 (9): 2000102. <https://doi.org/10.1002/adbi.202000102>.
- Kabsch, W, H G Mannherz, and D Suck. 1985. 'Three-Dimensional Structure of the Complex of Actin and DNase I at 4.5 Å Resolution.' *The EMBO Journal* 4 (8): 2113–18.
- Kabsch, Wolfgang, Hans Mannherz, Dietrich Suck, Emil Pai, and Kenneth Holmes. 1990. 'Atomic Structure of the Actin: DNase I Complex'. *Nature* 347 (October): 37–44. <https://doi.org/10.1038/347037a0>.
- Kawska, A., K. Carvalho, J. Manzi, R. Boujemaa-Paterski, L. Blanchoin, J.-L. Martiel, and C. Sykes. 2012. 'How Actin Network Dynamics Control the Onset of Actin-Based Motility'. *Proceedings of the National Academy of Sciences* 109 (36): 14440–45. <https://doi.org/10.1073/pnas.1117096109>.
- Köster, Darius Vasco, Kabir Husain, Elda Iljazi, Abrar Bhat, Peter Bieling, R. Dyche Mullins, Madan Rao, and Satyajit Mayor. 2016. 'Actomyosin Dynamics Drive Local Membrane Component Organization in an in Vitro Active Composite Layer'. *Proceedings of the National Academy of Sciences* 113 (12): E1645–54. <https://doi.org/10.1073/pnas.1514030113>.
- Koster, Gerbrand, Martijn VanDuijn, Bas Hofs, and Marileen Dogterom. 2003. 'Membrane Tube Formation from Giant Vesicles by Dynamic Association of Motor Proteins'. *Proceedings of the National Academy of Sciences* 100 (26): 15583–88. <https://doi.org/10.1073/pnas.2531786100>.
- Kroy, Klaus, and Erwin Frey. 1996. 'Force-Extension Relation and Plateau Modulus for Wormlike Chains'. *Physical Review Letters* 77 (2): 306–9. <https://doi.org/10.1103/PhysRevLett.77.306>.
- Kulkarni, Rakesh, Erik A. C. Wiemer, and Wen Chang. 2022. 'Role of Lipid Rafts in Pathogen-Host Interaction - A Mini Review'. *Frontiers in Immunology* 12. <https://www.frontiersin.org/articles/10.3389/fimmu.2021.815020>.
- Kusters, Remy, Camille Simon, Rogério Lopes Dos Santos, Valentina Caorsi, Sangsong Wu, Jean-Francois Joanny, Pierre Sens, and Cecile Sykes. 2019. 'Actin Shells Control Buckling and Wrinkling of Biomembranes'. *BioRxiv*, September, 781153. <https://doi.org/10.1101/781153>.

- Kwik, Jeanne, Sarah Boyle, David Fooksman, Leonid Margolis, Michael P. Sheetz, and Michael Edidin. 2003. 'Membrane Cholesterol, Lateral Mobility, and the Phosphatidylinositol 4,5-Bisphosphate-Dependent Organization of Cell Actin'. *Proceedings of the National Academy of Sciences* 100 (24): 13964–69. <https://doi.org/10.1073/pnas.2336102100>.
- Lamour, Guillaume, Antoine Allard, Juan Pelta, Sid Labdi, Martin Lenz, and Clément Campillo. 2020. 'Mapping and Modeling the Nanomechanics of Bare and Protein-Coated Lipid Nanotubes'. *Physical Review X* 10 (1): 011031. <https://doi.org/10.1103/PhysRevX.10.011031>.
- Liebe, Nils L., Ingo Mey, Loan Vuong, Fadi Shikho, Burkhard Geil, Andreas Janshoff, and Claudia Steinem. 2023. 'Bioinspired Membrane Interfaces: Controlling Actomyosin Architecture and Contractility'. *ACS Applied Materials & Interfaces* 15 (9): 11586–98. <https://doi.org/10.1021/acsami.3c00061>.
- Lieber, Arnon D., Shlomit Yehudai-Resheff, Erin L. Barnhart, Julie A. Theriot, and Kinneret Keren. 2013. 'Membrane Tension in Rapidly Moving Cells Is Determined by Cytoskeletal Forces'. *Current Biology* 23 (15): 1409–17. <https://doi.org/10.1016/j.cub.2013.05.063>.
- Limozin, L., M. Bärmann, and E. Sackmann. 2003. 'On the Organization of Self-Assembled Actin Networks in Giant Vesicles'. *The European Physical Journal E* 10 (4): 319–30. <https://doi.org/10.1140/epje/i2002-10118-9>.
- Limozin, Laurent, and Erich Sackmann. 2002. 'Polymorphism of Cross-Linked Actin Networks in Giant Vesicles'. *Physical Review Letters* 89 (16): 168103. <https://doi.org/10.1103/PhysRevLett.89.168103>.
- Lingwood, D., J. Ries, P. Schwille, and K. Simons. 2008. 'Plasma Membranes Are Poised for Activation of Raft Phase Coalescence at Physiological Temperature'. *Proceedings of the National Academy of Sciences* 105 (29): 10005–10. <https://doi.org/10.1073/pnas.0804374105>.
- Litschel, Thomas, Charlotte F. Kelley, Danielle Holz, Maral Adeli Koudehi, Sven K. Vogel, Laura Burbaum, Naoko Mizuno, Dimitrios Vavylonis, and Petra Schwille. 2021. 'Reconstitution of Contractile Actomyosin Rings in Vesicles'. *Nature*

- Communications* 12 (1): 2254. <https://doi.org/10.1038/s41467-021-22422-7>.
- Liu, Allen P., and Daniel A. Fletcher. 2006. 'Actin Polymerization Serves as a Membrane Domain Switch in Model Lipid Bilayers'. *Biophysical Journal* 91 (11): 4064–70. <https://doi.org/10.1529/biophysj.106.090852>.
- Liu, Allen P., David L. Richmond, Lutz Maibaum, Sander Pronk, Phillip L. Geissler, and Daniel A. Fletcher. 2008a. 'Membrane-Induced Bundling of Actin Filaments'. *Nature Physics* 4 (10): 789–93. <https://doi.org/10.1038/nphys1071>.
- . 2008b. 'Membrane-Induced Bundling of Actin Filaments'. *Nature Physics* 4 (10): 789–93. <https://doi.org/10.1038/nphys1071>.
- Loiseau, Etienne, Jochen A. M. Schneider, Felix C. Keber, Carina Pelzl, Gladys Massiera, Guillaume Salbreux, and Andreas R. Bausch. 2016. 'Shape Remodeling and Blebbing of Active Cytoskeletal Vesicles'. *Science Advances* 2 (4): e1500465. <https://doi.org/10.1126/sciadv.1500465>.
- Loisel, Thomas P., Rajaa Boujemaa, Dominique Pantaloni, and Marie-France Carlier. 1999. 'Reconstitution of Actin-Based Motility of Listeria and Shigella Using Pure Proteins'. *Nature* 401 (6753): 613–16. <https://doi.org/10.1038/44183>.
- Lopes dos Santos, Rogério, and Clément Campillo. 2022. 'Studying Actin-Induced Cell Shape Changes Using Giant Unilamellar Vesicles and Reconstituted Actin Networks'. *Biochemical Society Transactions* 50 (5): 1527–39. <https://doi.org/10.1042/BST20220900>.
- Machesky, Laura M., Simon J. Atkinson, Christophe Ampe, Joel Vandekerckhove, and Thomas D. Pollard. 1994. 'Purification of a Cortical Complex Containing Two Unconventional Actins from Acanthamoeba by Affinity Chromatography on Profilin-Agarose'. *The Journal of Cell Biology* 127 (1): 107–15.
- Machesky, Laura M., R. Dyche Mullins, Henry N. Higgs, Donald A. Kaiser, Laurent Blanchoin, Robin C. May, Margaret E. Hall, and Thomas D. Pollard. 1999. 'Scar, a WASp-Related Protein, Activates Nucleation of Actin Filaments by the Arp2/3 Complex'. *Proceedings of the National Academy of Sciences* 96 (7): 3739–44. <https://doi.org/10.1073/pnas.96.7.3739>.

- Marsh, Derek. 2006. 'Elastic Curvature Constants of Lipid Monolayers and Bilayers'. *Chemistry and Physics of Lipids* 144 (2): 146–59. <https://doi.org/10.1016/j.chemphyslip.2006.08.004>.
- Maruyama, Koscak, and Setsuro Ebashi. 1965. 'α-Actinin, a New Structural Protein from Striated Muscle'. *The Journal of Biochemistry* 58 (1): 13–19.
- McConnell, Harden M., and Roger D. Kornberg. 1971. 'Inside-Outside Transitions of Phospholipids in Vesicle Membranes'. *Biochemistry* 10 (7): 1111–20. <https://doi.org/10.1021/bi00783a003>.
- McCullough, Brannon R., Laurent Blanchoin, Jean-Louis Martiel, and Enrique M. De La Cruz. 2008. 'Cofilin Increases the Bending Flexibility of Actin Filaments: Implications for Severing and Cell Mechanics'. *Journal of Molecular Biology* 381 (3): 550–58. <https://doi.org/10.1016/j.jmb.2008.05.055>.
- Meer, Gerrit van, Dennis R. Voelker, and Gerald W. Feigenson. 2008. 'Membrane Lipids: Where They Are and How They Behave'. *Nature Reviews. Molecular Cell Biology* 9 (2): 112–24. <https://doi.org/10.1038/nrm2330>.
- Mesarec, Luka, Mitja Drab, Samo Penič, Veronika Kralj-Iglič, and Aleš Iglič. 2021. 'On the Role of Curved Membrane Nanodomains and Passive and Active Skeleton Forces in the Determination of Cell Shape and Membrane Budding'. *International Journal of Molecular Sciences* 22 (5): 2348. <https://doi.org/10.3390/ijms22052348>.
- Meyer, Rudolf K, and Ueli Aebi. 1990. 'Bundling of Actin Filaments by Ct-Actinin Depends on Its Molecular Length'. *The Journal of Cell Biology* 110: 12.
- Mingeot-Leclercq, Marie-Paule, Magali Deleu, Robert Brasseur, and Yves F Dufrêne. 2008. 'Atomic Force Microscopy of Supported Lipid Bilayers'. *Nature Protocols* 3 (10): 1654–59. <https://doi.org/10.1038/nprot.2008.149>.
- Mogilner, A., and B. Rubinstein. 2005. 'The Physics of Filopodial Protrusion'. *Biophysical Journal* 89 (2): 782–95. <https://doi.org/10.1529/biophysj.104.056515>.
- Moore, P B, C F Lopez, and M L Klein. 2001. 'Dynamical Properties of a Hydrated Lipid Bilayer from a Multinano-second Molecular Dynamics Simulation.' *Biophysical Journal* 81 (5): 2484–94.

- Mullins, R. Dyche, John A. Heuser, and Thomas D. Pollard. 1998. 'The Interaction of Arp2/3 Complex with Actin: Nucleation, High Affinity Pointed End Capping, and Formation of Branching Networks of Filaments'. *Proceedings of the National Academy of Sciences* 95 (11): 6181–86. <https://doi.org/10.1073/pnas.95.11.6181>.
- Nichol, J. A., and O. F. Hutter. 1996. 'Tensile Strength and Dilatational Elasticity of Giant Sarcolemmal Vesicles Shed from Rabbit Muscle'. *The Journal of Physiology* 493 (Pt 1) (Pt 1): 187–98. <https://doi.org/10.1113/jphysiol.1996.sp021374>.
- Nicolson, Garth L. 2014. 'The Fluid—Mosaic Model of Membrane Structure: Still Relevant to Understanding the Structure, Function and Dynamics of Biological Membranes after More than 40years'. *Biochimica et Biophysica Acta (BBA) - Biomembranes*, Membrane Structure and Function: Relevance in the Cell's Physiology, Pathology and Therapy, 1838 (6): 1451–66. <https://doi.org/10.1016/j.bbamem.2013.10.019>.
- Nicolson, Garth L., and Gonzalo Ferreira de Mattos. 2021. 'A Brief Introduction to Some Aspects of the Fluid–Mosaic Model of Cell Membrane Structure and Its Importance in Membrane Lipid Replacement'. *Membranes* 11 (12): 947. <https://doi.org/10.3390/membranes11120947>.
- Niemelä, Perttu, Marja T. Hyvönen, and Ilpo Vattulainen. 2004. 'Structure and Dynamics of Sphingomyelin Bilayer: Insight Gained through Systematic Comparison to Phosphatidylcholine'. *Biophysical Journal* 87 (5): 2976–89. <https://doi.org/10.1529/biophysj.104.048702>.
- Noireaux, V., R.M. Golsteyn, E. Friederich, J. Prost, C. Antony, D. Louvard, and C. Sykes. 2000. 'Growing an Actin Gel on Spherical Surfaces'. *Biophysical Journal* 78 (3): 1643–54. [https://doi.org/10.1016/S0006-3495\(00\)76716-6](https://doi.org/10.1016/S0006-3495(00)76716-6).
- Palani, Saravanan, Sayantika Ghosh, Esther Ivorra-Molla, Scott Clarke, Andrejus Suchenko, Mohan K Balasubramanian, and Darius Vasco Köster. 2021. 'Calponin-Homology Domain Mediated Bending of Membrane Associated Actin Filaments'. Edited by Pekka Lappalainen. *ELife* 10 (July): e61078. <https://doi.org/10.7554/eLife.61078>.
- Pautot, Sophie, Barbara J. Frisken, and D. A. Weitz. 2003. 'Production

- of Unilamellar Vesicles Using an Inverted Emulsion'. *Langmuir* 19 (7): 2870–79. <https://doi.org/10.1021/la026100v>.
- Peter, Brian J., Helen M. Kent, Ian G. Mills, Yvonne Vallis, P. Jonathan G. Butler, Philip R. Evans, and Harvey T. McMahon. 2004. 'BAR Domains as Sensors of Membrane Curvature: The Amphiphysin BAR Structure'. *Science (New York, N.Y.)* 303 (5657): 495–99. <https://doi.org/10.1126/science.1092586>.
- Picas, Laura, Felix Rico, and Simon Scheuring. 2012. 'Direct Measurement of the Mechanical Properties of Lipid Phases in Supported Bilayers'. *Biophysical Journal* 102 (1): L01–3. <https://doi.org/10.1016/j.bpj.2011.11.4001>.
- Pollard, T D. 1986. 'Rate Constants for the Reactions of ATP- and ADP-Actin with the Ends of Actin Filaments.' *Journal of Cell Biology* 103 (6): 2747–54. <https://doi.org/10.1083/jcb.103.6.2747>.
- Pollard, Thomas D. 2016. 'Actin and Actin-Binding Proteins'. *Cold Spring Harbor Perspectives in Biology* 8 (8). <https://doi.org/10.1101/cshperspect.a018226>.
- Pollard, Thomas D., Laurent Blanchoin, and R. Dyche Mullins. 2000. 'Molecular Mechanisms Controlling Actin Filament Dynamics in Nonmuscle Cells'. *Annual Review of Biophysics and Biomolecular Structure* 29 (1): 545–76. <https://doi.org/10.1146/annurev.biophys.29.1.545>.
- Pontani, Léa-Laetitia, Jasper van der Gucht, Guillaume Salbreux, Julien Heuvingh, Jean-François Joanny, and Cécile Sykes. 2009. 'Reconstitution of an Actin Cortex Inside a Liposome'. *Biophysical Journal* 96 (1): 192–98. <https://doi.org/10.1016/j.bpj.2008.09.029>.
- Putra, Vina D. L., Kristopher A. Kilian, and Melissa L. Knothe Tate. 2023. 'Biomechanical, Biophysical and Biochemical Modulators of Cytoskeletal Remodelling and Emergent Stem Cell Lineage Commitment'. *Communications Biology* 6 (1): 1–24. <https://doi.org/10.1038/s42003-022-04320-w>.
- Rawicz, W, K C Olbrich, T McIntosh, D Needham, and E Evans. 2000. 'Effect of Chain Length and Unsaturation on Elasticity of Lipid Bilayers.' *Biophysical Journal* 79 (1): 328–39.
- Rinaldin, Melissa, Piermarco Fonda, Luca Giomi, and Daniela J. Kraft. 2020. 'Geometric Pinning and Antimixing in Scaffolded Lipid Vesicles'. *Nature Communications* 11 (1): 4314.

- <https://doi.org/10.1038/s41467-020-17432-w>.
- Römer, Winfried, Léa-Laetitia Pontani, Benoît Sorre, Carles Rentero, Ludwig Berland, Valérie Chambon, Christophe Lamaze, et al. 2010. 'Actin Dynamics Drive Membrane Reorganization and Scission in Clathrin-Independent Endocytosis'. *Cell* 140 (4): 540–53. <https://doi.org/10.1016/j.cell.2010.01.010>.
- Rossier, O., D. Cuvelier, N. Borghi, P. H. Puech, I. Derényi, A. Buguin, P. Nassoy, and F. Brochard-Wyart. 2003. 'Giant Vesicles under Flows: Extrusion and Retraction of Tubes'. *Langmuir* 19 (3): 575–84. <https://doi.org/10.1021/la026236t>.
- Rothberg, K G, Y S Ying, B A Kamen, and R G Anderson. 1990. 'Cholesterol Controls the Clustering of the Glycophospholipid-Anchored Membrane Receptor for 5-Methyltetrahydrofolate.' *Journal of Cell Biology* 111 (6): 2931–38. <https://doi.org/10.1083/jcb.111.6.2931>.
- Rottner, Klemens, Jan Faix, Sven Bogdan, Stefan Linder, and Eugen Kerkhoff. 2017. 'Actin Assembly Mechanisms at a Glance'. *Journal of Cell Science* 130 (20): 3427–35. <https://doi.org/10.1242/jcs.206433>.
- Rotty, Jeremy D., Congying Wu, and James E. Bear. 2013. 'New Insights into the Regulation and Cellular Functions of the ARP2/3 Complex'. *Nature Reviews Molecular Cell Biology* 14 (1): 7–12. <https://doi.org/10.1038/nrm3492>.
- Rouiller, Isabelle, Xiao-Ping Xu, Kurt J. Amann, Coumaran Egile, Stephan Nickell, Daniela Nicastro, Rong Li, Thomas D. Pollard, Niels Volkmann, and Dorit Hanein. 2008. 'The Structural Basis of Actin Filament Branching by the Arp2/3 Complex'. *Journal of Cell Biology* 180 (5): 887–95. <https://doi.org/10.1083/jcb.200709092>.
- Roux, Aurélien. 2013. 'The Physics of Membrane Tubes: Soft Templates for Studying Cellular Membranes'. *Soft Matter* 9 (29): 6726. <https://doi.org/10.1039/c3sm50514f>.
- Roux, Aurélien, Giovanni Cappello, Jean Cartaud, Jacques Prost, Bruno Goud, and Patricia Bassereau. 2002. 'A Minimal System Allowing Tubulation with Molecular Motors Pulling on Giant Liposomes'. *Proceedings of the National Academy of Sciences* 99 (8): 5394–99. <https://doi.org/10.1073/pnas.082107299>.
- Roux, Aurélien, Damien Cuvelier, Pierre Nassoy, Jacques Prost, Patricia

- Bassereau, and Bruno Goud. 2005. 'Role of Curvature and Phase Transition in Lipid Sorting and Fission of Membrane Tubules'. *The EMBO Journal* 24 (8): 1537–45. <https://doi.org/10.1038/sj.emboj.7600631>.
- Roy, Debjit, Jan Steinkühler, Ziliang Zhao, Reinhard Lipowsky, and Rumiana Dimova. 2020. 'Mechanical Tension of Biomembranes Can Be Measured by Super Resolution (STED) Microscopy of Force-Induced Nanotubes'. *Nano Letters* 20 (5): 3185–91. <https://doi.org/10.1021/acs.nanolett.9b05232>.
- Schafer, D A, P B Jennings, and J A Cooper. 1996. 'Dynamics of Capping Protein and Actin Assembly in Vitro: Uncapping Barbed Ends by Polyphosphoinositides.' *Journal of Cell Biology* 135 (1): 169–79. <https://doi.org/10.1083/jcb.135.1.169>.
- Sezgin, Erdinc, Ilya Levental, Satyajit Mayor, and Christian Eggeling. 2017. 'The Mystery of Membrane Organization: Composition, Regulation and Roles of Lipid Rafts'. *Nature Reviews Molecular Cell Biology* 18 (6): 361–74. <https://doi.org/10.1038/nrm.2017.16>.
- Shelby, Sarah A., Ivan Castello-Serrano, Kathleen C. Wisser, Ilya Levental, and Sarah L. Veatch. 2021. 'Membrane Phase Separation Drives Organization at B Cell Receptor Clusters'. bioRxiv. <https://doi.org/10.1101/2021.05.12.443834>.
- . 2023. 'Membrane Phase Separation Drives Responsive Assembly of Receptor Signaling Domains'. *Nature Chemical Biology*, March, 1–9. <https://doi.org/10.1038/s41589-023-01268-8>.
- Silvius, John R. 2003. 'Role of Cholesterol in Lipid Raft Formation: Lessons from Lipid Model Systems'. *Biochimica et Biophysica Acta (BBA) - Biomembranes* 1610 (2): 174–83. [https://doi.org/10.1016/S0005-2736\(03\)00016-6](https://doi.org/10.1016/S0005-2736(03)00016-6).
- Silvius, John R., Denis del Giudice, and Michel Lafleur. 1996. 'Cholesterol at Different Bilayer Concentrations Can Promote or Antagonize Lateral Segregation of Phospholipids of Differing Acyl Chain Length'. *Biochemistry* 35 (48): 15198–208. <https://doi.org/10.1021/bi9615506>.
- Simon, Camille, Valentina Caorsi, Clément Campillo, and Cécile Sykes. 2018. 'Interplay between Membrane Tension and the Actin Cytoskeleton Determines Shape Changes'. *Physical Biology* 15

- (6): 065004. <https://doi.org/10.1088/1478-3975/aad1ab>.
- Simon, Camille, Rémy Kusters, Valentina Caorsi, Antoine Allard, Majdouline Abou-Ghali, John Manzi, Aurélie Di Cicco, et al. 2019. 'Actin Dynamics Drive Cell-like Membrane Deformation'. *Nature Physics* 15 (6): 602–9. <https://doi.org/10.1038/s41567-019-0464-1>.
- Simons, K., and D. Toomre. 2000. 'Lipid Rafts and Signal Transduction'. *Nature Reviews Molecular Cell Biology* 1 (1): 31–39. <https://doi.org/10.1038/35036052>.
- Simons, Kai, and Elina Ikonen. 1997. 'Functional Rafts in Cell Membranes' 387.
- Singer, S. J., and Garth L. Nicolson. 1972. 'The Fluid Mosaic Model of the Structure of Cell Membranes'. *Science* 175 (4023): 720–31. <https://doi.org/10.1126/science.175.4023.720>.
- Sorre, B., A. Callan-Jones, J.-B. Manneville, P. Nassoy, J.-F. Joanny, J. Prost, B. Goud, and P. Bassereau. 2009. 'Curvature-Driven Lipid Sorting Needs Proximity to a Demixing Point and Is Aided by Proteins'. *Proceedings of the National Academy of Sciences* 106 (14): 5622–26. <https://doi.org/10.1073/pnas.0811243106>.
- Surma, Michal A., Christian Klose, Robin W. Klemm, Christer S. Ejsing, and Kai Simons. 2011. 'Generic Sorting of Raft Lipids into Secretory Vesicles in Yeast'. *Traffic* 12 (9): 1139–47. <https://doi.org/10.1111/j.1600-0854.2011.01221.x>.
- Ti, Shih-Chieh, Christopher T. Jurgenson, Bradley J. Nolen, and Thomas D. Pollard. 2011. 'Structural and Biochemical Characterization of Two Binding Sites for Nucleation-Promoting Factor WASp-VCA on Arp2/3 Complex'. *Proceedings of the National Academy of Sciences* 108 (33): E463–71. <https://doi.org/10.1073/pnas.1100125108>.
- Titushkin, Igor, and Michael Cho. 2006. 'Distinct Membrane Mechanical Properties of Human Mesenchymal Stem Cells Determined Using Laser Optical Tweezers'. *Biophysical Journal* 90 (7): 2582–91. <https://doi.org/10.1529/biophysj.105.073775>.
- Tristram-Nagle, S, H I Petrache, and J F Nagle. 1998. 'Structure and Interactions of Fully Hydrated Dioleoylphosphatidylcholine Bilayers'. *Biophysical Journal* 75 (2): 917–25.
- Tsai, Feng-Ching, and Gijssje Hendrika Koenderink. 2015. 'Shape Control of Lipid Bilayer Membranes by Confined Actin Bundles'.

- Soft Matter* 11 (45): 8834–47.
<https://doi.org/10.1039/C5SM01583A>.
- Tseng, Yiider, Elena Fedorov, J. Michael McCaffery, Steven C Almo, and Denis Wirtz. 2001. 'Micromechanics and Ultrastructure of Actin Filament Networks Crosslinked by Human Fascin: A Comparison with α -Actinin'. *Journal of Molecular Biology* 310 (2): 351–66. <https://doi.org/10.1006/jmbi.2001.4716>.
- Upadhyaya, Arpita, Jeffrey R. Chabot, Albina Andreeva, Azadeh Samadani, and Alexander van Oudenaarden. 2003. 'Probing Polymerization Forces by Using Actin-Propelled Lipid Vesicles'. *Proceedings of the National Academy of Sciences* 100 (8): 4521–26. <https://doi.org/10.1073/pnas.0837027100>.
- Veatch, Sarah L, and Sarah L Keller. 2003. 'Separation of Liquid Phases in Giant Vesicles of Ternary Mixtures of Phospholipids and Cholesterol'. *Biophysical Journal* 85 (November): 3074–83.
- Vignjevic, Danijela, Shin-ichiro Kojima, Yvonne Aratyn, Oana Danciu, Tatyana Svitkina, and Gary G. Borisy. 2006. 'Role of Fascin in Filopodial Protrusion'. *Journal of Cell Biology* 174 (6): 863–75. <https://doi.org/10.1083/jcb.200603013>.
- Vogel, Sven Kenjiro, Ferdinand Greiss, Alena Khmelinskaia, and Petra Schwille. 2017. 'Control of Lipid Domain Organization by a Biomimetic Contractile Actomyosin Cortex'. *ELife* 6 (May): e24350. <https://doi.org/10.7554/eLife.24350>.
- Waugh, R E. 1982. 'Surface Viscosity Measurements from Large Bilayer Vesicle Tether Formation. I. Analysis.' *Biophysical Journal* 38 (1): 19–27.
- Wegner, Albrecht. 1976. 'Head to Tail Polymerization of Actin'. *Journal of Molecular Biology* 108 (1): 139–50. [https://doi.org/10.1016/S0022-2836\(76\)80100-3](https://doi.org/10.1016/S0022-2836(76)80100-3).
- Winkler, Jörg, Heinrich Lünsdorf, and Brigitte M. Jockusch. 1997. 'Flexibility and Fine Structure of Smooth-Muscle α -Actinin'. *European Journal of Biochemistry* 248 (1): 193–99. <https://doi.org/10.1111/j.1432-1033.1997.00193.x>.
- Yuan, Jing, Steven M. Hira, Geoffrey F. Strouse, and Linda S. Hirst. 2008. 'Lipid Bilayer Discs and Banded Tubules: Photoinduced Lipid Sorting in Ternary Mixtures'. *Journal of the American Chemical Society* 130 (6): 2067–72. <https://doi.org/10.1021/ja710305c>.
- Zigmond, Sally H. 1998. 'Actin Cytoskeleton: The Arp2/3 Complex Gets

to the Point'. *Current Biology* 8 (18): R654–57.
[https://doi.org/10.1016/S0960-9822\(07\)00415-0](https://doi.org/10.1016/S0960-9822(07)00415-0).

Synthèse:

Les cellules adaptent constamment leur forme pour réaliser des processus biologiques tels que la migration, le trafic intracellulaire et la division. De tels processus nécessitent le remodelage actif des membranes cellulaires, alimenté par la dynamique du cytosquelette d'actine (Blanchoin et al. 2014).

Évaluer les mécanismes de remodelage membranaire par le cytosquelette d'actine dans une cellule est très difficile à cause de la nature très complexe des cellules. En effet, de nombreux types de protéines sont impliqués dans ces processus. Par conséquent, les systèmes biomimétiques reconstitués sont utiles car ils présentent l'avantage d'un environnement biochimiquement contrôlé. Ils permettent de contrôler et d'ajuster les propriétés biophysiques à la fois des membranes et des réseaux d'actine reconstitués. Cette approche *in vitro* est basée sur la conception ascendante en complexité de systèmes biomimétiques pour comprendre le rôle de chaque élément de la machinerie biologique et leur interaction sur les changements de forme cellulaire.

Dans ce travail, mon objectif est de construire des systèmes biomimétiques comprenant des membranes lipidiques séparées par phases et des réseaux d'actine. En effet, la membrane cellulaire est hautement hétérogène, et ces hétérogénéités interagissent avec le cytosquelette d'actine (Fritzsche et al. 2017). Cependant, les membranes utilisées dans les études biomimétiques sont, dans la plupart des cas, homogènes. Seuls Liu et Fletcher (2006) ont utilisé des vésicules unilamellaires géantes hétérogènes contenant des domaines lipidiques. Ils ont montré que le réseau d'actine affecte la formation et l'organisation des domaines lipidiques sur les GUVs. Ce résultat suggère que les cellules contrôlent l'organisation des membranes en adaptant leur cytosquelette d'actine. Néanmoins, l'effet des hétérogénéités membranaires sur le remodelage membranaire par l'actine reste flou.

Ce manuscrit est organisé comme suit. Dans la section 2, j'introduis le contexte de mon travail : je décris brièvement les propriétés des membranes biologiques et du cytosquelette d'actine, telles qu'observées dans les situations biologiques et dans les systèmes biomimétiques reconstitués. Je montre comment les membranes lipidiques reconstituées, telles que les vésicules unilamellaires géantes (GUVs), les bicouches lipidiques supportées (SLBs) ou les nanotubes membranaires, associées à des techniques telles que l'aspiration par micropipette (Rawicz et al. 2000), les pincettes optiques (A. Allard, Valentino, et al. 2020) et la microscopie à force atomique (AFM) (Lamour et al. 2020), donnent accès aux propriétés physiques des membranes reconstituées. De plus, je montre les effets des réseaux d'actine reconstitués sur ces modèles de membrane, permettant de reproduire certaines des modifications de forme observées in vivo. En particulier, j'ai participé à deux articles de revue résumant la littérature scientifique sur les GUVs reconstituées interagissant avec les réseaux d'actine (Lopes dos Santos et Campillo 2022) et le remodelage des nanotubes membranaires par l'actine in vivo et in vitro (Antoine Allard, Lopes dos Santos, et Campillo 2021).

La section 3 présente tous les matériaux et méthodes utilisés pour ce travail : notamment la préparation de systèmes de membranes reconstituées couplées à des réseaux d'actine et les techniques d'observation que j'ai utilisées, telles que la STED, l'AFM et la microscopie à fluorescence.

Enfin, dans la section 4, je présente et discute mes résultats. Tout d'abord, j'ai étudié les mécanismes et la morphologie des nanotubes séparés par phases avec l'AFM. Ensuite, j'ai étudié sur les GUVs comment la composition membranaire et la structure du réseau d'actine affectent le remodelage membranaire par l'actine. De plus, j'ai développé un système basé sur les GUVs avec des domaines lipidiques permettant un contrôle spatial du site de polymérisation de l'actine, offrant ainsi un nouveau degré de contrôle sur ces systèmes biomimétiques.

Titre : Approches biomimétiques des changements de formes cellulaires : Impact des propriétés de la membrane et des réseaux d'actine

Mots clés : Domaines lipidiques, Réseau d'actine, Vésicules Unilamellaires Géantes, Nanotubes de membrane.

Résumé : Les processus biologiques tels que la migration, le trafic intracellulaire et la division nécessitent un remodelage des membranes cellulaires. Ces changements de forme reposent sur l'action du cytosquelette d'actine qui polymérise à la surface de ces membranes. Les mécanismes physiques de déformation des membranes par l'actine restent à élucider. Pour ce faire, j'utilise un système minimal *in vitro* dont la composition et l'environnement biochimique sont contrôlés. J'utilise deux modèles membranaires : des nanotubes, dont je sonde par AFM les propriétés mécaniques, et des GUVs sur lesquels je reconstitue des réseaux d'actine. Je montre l'effet de la composition membranaire et de la structure du réseau sur les déformations de membranes induites par l'actine. Enfin, j'ai développé un système basé sur des GUVs comportant des domaines lipidiques permettant de contrôler le site de polymérisation d'actine, permettant un nouveau degré de contrôle sur ces systèmes biomimétiques.

Title : Biomimetic approaches of cell shape changes: Impact of membrane and actin network properties .

Keywords : Lipid domains, Actin network, Giant Unilamellar Vesicles, Membrane nanotubes.

Abstract : Biological processes such as migration, intracellular trafficking, and division require remodelling of cell membranes. These shape changes are based on the action of the actin cytoskeleton, which polymerizes on the surface of these membranes. The physical mechanisms of membrane deformation by actin remain to be elucidated. To do this, I use a minimal *in vitro* system whose composition and biochemical environment are controlled. I use two membrane models: nanotubes, whose mechanical properties I probe by AFM and GUVs on which I reconstitute the actin network. I show the effect of membrane composition and network structure on actin-induced membrane deformations. Finally, I developed a system based on GUVs with lipid domains to control the site of actin polymerization, allowing a new degree of control over these biomimetic systems.